

**DEVELOPMENT OF CANCER DIAGNOSTICS USING
NANOPARTICLES AND AMPHIPHILIC POLYMERS**

A Dissertation
Presented to
The Academic Faculty

by

Matthew N. Rhyner

In Partial Fulfillment
of the Requirements for the Degree
Doctor of Philosophy in the
Wallace H. Coulter Department of Biomedical Engineering

Georgia Institute of Technology
May 2008

Copyright 2008 by Matthew N. Rhyner

DEVELOPMENT OF CANCER DIAGNOSTICS USING NANOPARTICLES AND AMPHIPHILIC POLYMERS

Approved by:

Dr. Shuming Nie, Advisor
School of Biomedical Engineering
Georgia Institute of Technology

Dr. Niren Murthy
School of Biomedical Engineering
Georgia Institute of Technology

Dr. Mark Prausnitz
School of Chemical and Biological
Engineering
Georgia Institute of Technology

Dr. Leland Chung
School of Medicine
Emory University

Dr. Gang Bao
School of Biomedical Engineering
Georgia Institute of Technology

Date Approved: December 6th, 2007

To my Family: Corinne, Charlie, Mom, and Dad.

ACKNOWLEDGEMENTS

While a PhD dissertation is largely an individual effort, its successful culmination depends on the help, support, and understanding of many others. I have been lucky and grateful to be surrounded by mentors, friends, and family that have helped me grow intellectually, professionally, and personally over the past several years. I am eternally grateful for all you have given me.

Mentors

First, I would like to thank the professional mentors that have advised me during my career at Georgia Tech. In particular, I would like to thank Dr. Shuming Nie for giving me the support, guidance, freedom, and structure that was invaluable throughout graduate school. Every time I would worry or feel stuck, Shuming would provide a new approach or way of looking at a problem that would settle my nerves and allow me to move forward. I have learned a tremendous amount from you both about nanotechnology and the way the world works. Thanks for believing in me and giving me opportunities to prove myself. I hope that we can remain friends and colleagues over the next several decades.

Next, I would like to thank Dr. Marie Thursby and Dr. Carolyn Davis of the TI:GER program. Your support of our team has opened new doors for me, and helped me discover a passion that I was unaware of before joining your program. In addition, you made the long hours and hard work fun, interesting, and enriching. I am very lucky to have two dedicated, creative, and unique mentors enlighten me about technology commercialization.

Finally, there have been many other mentors that have had an impact on my development in a variety of ways: Dr. Lee Herron—your help on the TIGON project was

invaluable. I hope that I will be working with you in the future. Dr. Barbara Boyan—thanks for the opportunities to teach. I learned a tremendous amount working for you, and am very grateful for your help with the policy forum. Dr. Robert Nerem—thanks for supporting the seminar series and giving me opportunities to speak. I am glad to have a connection to you through the Renaissance Weekends, and hope to see at one sometime soon.

Labmates

Next, I would like to thank every one of the graduate students, postdocs, and core facility personnel that I worked with during graduate school. In particular, Andrew Smith deserves praise for being the best quantum dot expert the world has ever seen. Without your help, I would still be working on my proposal. I am sure you are going to become a famous professor, following in the footsteps of our illustrious advisor. Undergrads beware. I am also glad to count you among my close friends. Next, I would like to thank Amit Agrawal and Tushar Sathe for their friendship, support, and collaborations. I really enjoyed working with you, and learned a tremendous amount from each of you, both about science and India. Finally, to the newer group members, particularly Brad Kairdolf and Mike Mancini: you have been great sources of practical and experimental help. Your existence in lab has made last few years more fun, easier, and more productive. I know you both will be successful in whatever future endeavors you pursue. Thanks to the postdocs Aaron Mohs, Ximei Qian, Gang Ruan, Debatosh Majumdar, and Hongwei Duan for fruitful and fun discussion about the tiny objects we've all been studying so intently. Also, thanks to Drs. Hong Yi and Hui Mao for endless experimental help as I pursued this project.

Finally, to the administrators Michelle Denney, Ryan Jowers, Michelle Bluman. Nothing would function at all without your responsiveness, great attitudes, and kindness.

Classmates

One of the best parts about the BME department is the great people spread throughout it. I was very lucky to have some smart, outgoing classmates. Our friendship over the years has made graduate school more fun than I would have thought possible. I hope that we can remain friends and colleagues for years to come. In particular, the following current or future doctors are particularly important: Sean Sullivan, Craig Duvall, Scott Robinson, John Wilson, Adam Higgins, and Heather Bara. I will refrain from describing our (mis)adventures in any great detail here, but will say that I am glad to have you as close friends, and look forward to continuing our friendships over the coming years. I am excited to see what the future holds for you all.

Family

I must thank my family for all the love and support they have provided me. To my mom and dad: you have always lent an ear at times of trouble and guided me through many difficult situations personally and professionally. Without your nurturing, I would not be here in the first place, so you deserve enormous credit for all that has transpired. To my beautiful and brilliant fiancé, Corinne: I am so happy that you are in my life and we have a bright future together. Without your support and kind ear, none of this would be possible. I am very excited about spending our lives together, and look forward to supporting you as you complete your own PhD dissertation. What would life be like if I hadn't taught astronomy for a summer? To Charlie, my brother: I have loved watching you develop and mature throughout your collegiate years. I am glad you decided to attend Emory, and that we have spent so much time together. I know you have a fulfilling and happy future ahead of you, and I am excited to see where your many talents will lead you. Finally, I must make mention of my deceased grandparents:

Doc, Gam, Grandma, and Grandpa. Each of you taught me invaluable lessons in the ways of the world, and how to be a good person. Though you have been gone for some time, I think of you each often, and feel blessed to have known you.

TABLE OF CONTENTS

	<u>PAGE</u>
ACKNOWLEDGEMENTS	IV
LIST OF TABLES	XII
LIST OF FIGURES	XIII
LIST OF SYMBOLS AND ABBREVIATIONS	XVI
SUMMARY	XX
1. NANOTECHNOLOGY IN CANCER THERAPY AND DIAGNOSIS	1
1.1 ABSTRACT	1
1.2 INTRODUCTION	1
Cancer is the second leading cause of death in the United States	2
1.3 THE GENETIC ORIGINS OF CANCER	3
Disturbances in Growth and Antigrowth Signaling	4
Apoptotic Escape and Enhanced Replication Potential	5
Tumors Generate New Blood Vessels	6
Cancerous Cells Metastasize	6
Physiological Characteristics	7
1.4 THE PROMISE OF NANOTECHNOLOGY	8
In Vitro Diagnostics	8
<i>In Vivo</i> Diagnostics	9
Improved Therapies	9
1.6 DISSERTATION STRUCTURE	10
1.5 CONCLUSIONS	11
2. QUANTUM DOTS FOR BIOLOGY AND MEDICINE	12

2.1 ABSTRACT	12
2.2 INTRODUCTION	12
2.3 SEMICONDUCTOR QDs	14
2.4 STRATEGIES FOR BIONFUNCTIONALIZATION	17
Solution Based Assays	18
Cell Labeling and Studying Cellular Dynamics	21
Animal Imaging	24
2.5 Challenges, Opportunities, and Future Perspectives	26
2.6 CONCLUSION	28
3. SYNTHESIS AND CHARACTERIZATION OF OPTICAL MICELLAR PROBES	29
3.1 ABSTRACT	29
3.2 INTRODUCTION	29
3.3 METHODS	32
3.4 RESULTS AND DISCUSSION	36
Development of Procedure	44
Design of Polymers	46
Separations and Scale-up	48
Multicolor Probes	49
3.6 CONCLUSIONS	50
4. SYNTHESIS AND CHARACTERIZATION OF OPTOMAGNETIC MICELLAR PROBES	51
4.1 ABSTRACT	51
4.2 INTRODUCTION	51
4.3 METHODS	57
4.4 RESULTS AND DISCUSSION	58
T1 Imaging	58

T2 Imaging	59
Iron Oxide Nanoparticle Concentration	61
4.5 CONCLUSION	63
5. PERFORMANCE OF MICELLAR PROBES IN CHEMICAL AND BIOLOGICAL CONDITIONS	65
5.1 ABSTRACT	65
5.2 INTRODUCTION	65
5.3 MATERIALS AND METHODS	68
5.4 RESULTS AND DISCUSSION	70
Photooxidation	70
Acid Etching	72
Chemical Oxidation	73
Stability in Cell Culture	74
Comparisons of Polyacrylic acid coatings and PMMA-PEO Micelles	75
5.5 Conclusions	82
6. ADDITION OF FUNCTIONAL GROUPS ON MICELLAR PROBE SURFACE	84
6.1 ABSTRACT	84
6.2 INTRODUCTION	84
6.3 METHODS	87
6.4 RESULTS AND DISCUSSION	90
Conjugation to Folic Acid	94
6.5 CONCLUSIONS	95
7. EVALUATION OF NANOPARTICLE BINDING KINETICS USING SURFACE PLASMON RESONANCE	97
7.1 ABSTRACT	97
7.2 INTRODUCTION	97

Bead Based assays	99
Fluorescent Polarization	100
Differential Scanning Calorimetry (DSC)	100
Isothermal Titration Calorimetry (ITC)	101
Surface Plasmon Resonance (SPR)	101
SPR for studying nanoparticle binding	102
7.3 METHODS	103
7.4 RESULTS AND DISCUSSION	105
7.5 CONCLUSIONS	117
8. FUTURE DIRECTIONS	118
8.1 ABSTRACT	118
8.2 SUMMARY	118
8.3 FUTURE DIRECTIONS FOR DISSERTATION TECHNOLOGY	120
Fundamental Physical Studies	120
Engineering of the Synthetic Procedure	121
Bioapplication Studies	122
8.5 CONCLUSIONS	124
APPENDIX A: TIGON NANOSTRATEGIES EXECUTIVE SUMMARY	125
A.1 ABSTRACT	125
A.2 EXECUTIVE SUMMARY	125
REFERENCES	128
CURRICULUM VITAE	146

LIST OF TABLES

	<u>PAGE</u>
Table 4.1: Summary of ICP spectroscopy results from UGA Chemical Analysis Lab	62
Table 7.1: Comparison of techniques used for assessing biological binding events	99
Table 7.2: Sampling of cancer-related binding partners known to exhibit multivalency.	106
Table A.1. TIGON Nanostrategies Revenues and Profits Through Year 5 (\$)	127

LIST OF FIGURES

	<u>PAGE</u>
Figure 1.1: Decline in death rates due to the top 4 mortality causes in the US over the past 54 years.	2
Figure 1.2: The normal apoptotic signaling pathway.	5
Figure 1.3: The process of cancer metastasis.	7
Figure 1.4: Polymeric micelles are one example of nanoparticles that can be used to improve the efficacy of currently available chemotherapeutics.	10
Figure 2.1: Illustration of two general QD functionalization strategies for cancer-related studies.	15
Figure 2.2: Photon count data collected from QDs bound to two different versions of RSV.	19
Figure 2.3: Fluorescence image of single QDs and aggregates in the cytoplasm of live fibroblast cells.	23
Figure 2.4: Combined x-ray and fluorescent image of QDs injected into the hindquarters of a mouse.	26
Figure 3.1: Our general approach to creation of size and composition tunable micellar probes.	30
Figure 3.2: TEM and DLS data comparing the size and structure of single and multiple QD micelles.	35
Figure 3.3: Fluorescent images and spectral data of micelle encapsulated QDs (100: 1 feeding ratio).	38
Figure 3.4: TEM micrographs of products from ultracentrifugation.	40
Figure 3.5: Chromatograms and TEMs of micelles separated using FPLC.	41
Figure 3.6: Fluorescent spectra and micrographs of multicolor micellar probes.	43
Figure 3.7: Examples of encapsulation methods investigated for this thesis.	45
Figure 3.8: Amphiphilic polymers used to encapsulate hydrophobic nanoparticles in literature.	47
Figure 3.9: TEM images demonstrating the difference between the crude reaction product (A) and purified, concentrated micelles (B)	48
Figure 3.10: The two main interactions that dictate the stable assembly of the micellar probes.	49

Figure 4.1: Illustration of the creation of MRI signals.	52
Figure 4.2: Dual-modal imaging using QD-based probes as the fluorescent reagent.	55
Figure 4.3: Ideal optomagnetic probe.	56
Figure 4.4: MRI scanner results of resolve-AI loaded micelles.	58
Figure 4.5: Fluorescent and magnetic resonance characterization data for optomagnetic probes.	60
Figure 4.6: DLS and TEM data for optomagnetic probes.	61
Figure 5.1: Photooxidation of QDs dissolved in borate buffer.	71
Figure 5.2: Acid-induced etching of QDs.	72
Figure 5.3: Hydrogen peroxide-mediated degradation of QDs in borate buffer.	73
Figure 5.4: Stability of QD coatings in cell culture at 37 °C, visualized via bright field and confocal fluorescence micrograph overlays, focused near the cell centers.	75
Figure 5.5: FPLC chromatograms comparing various nanoparticle coatings.	77
Figure 4.6: Fluorescent micrographs comparing micelle encapsulated QDs with carboxylated QDs.	78
Figure 5.7 : Agarose gel electrophoresis of sample with and without incubation with plasma.	80
Figure 5.8: Fluorescent micrographs of QD samples incubated with granulocytes for 24 hours.	82
Figure 6.1: Design of targeted micelles developed in this chapter.	86
Figure 6.2: Polymers used for the two approaches in this chapter.	87
Figure 6.3: GPC data demonstrating the synthesis of PMMA-PEO-SH model polymer.	90
Figure 6.4: FPLC Chromatograms of various polymer samples.	92
Figure 6.5: Fluorescamine assay demonstrating existence of free amines.	93
Figure 6.5 Chromatograms of conjugated and non-conjugated micelles.	94
Figure 7.1: Comparison of conjugation of model anti-beta2-microglobulin to CM5.	107
Figure 7.2: Example of sandwich assay using BIACORE.	108
Figure 7.3: Antibodies binding to the alpha5beta3 protein.	110
Figure 7.4: RGDs binding to alpha5beta3 integrin.	111

Figure 7.5: Multiple, sequential injections of QD-streptavidin followed by injections of a mixture of RGDbiotin and QD streptavidin. 112

Figure 7.6: Sensitivity of the SPR system to different target ligand immobilization levels. 114

Figure 7.7: Sequential injections of targeting molecule and QD-streptavidin. 115

Figure 7.8: Folic acid binding to the folate binding protein shows a strong, reproducible, and reversible response while non-targeted micelles exhibit no non-specific binding to the folate binding protein. 116

LIST OF SYMBOLS AND ABBREVIATIONS

k_B	Boltzmann constant ($1.3806503 \times 10^{-23} \text{m}^2 \text{kg s}^{-2} \text{K}^{-1}$)
K	Particle anisotropy constant
V	Particle Volume
T	Temperature
F_m	Magnetic Force
M	Magnetic Dipole
B	Magnetic Induction
M	Magnetization
X	Magnetic Susceptibility
H	Magnetic Field Strength
$^{\circ}\text{C}$	Degree Celsius
BSA	Bovine Serum Albumin
CCD	Charge-Coupled Device
CdSe	Cadmium Selenide
DAPI	4',6-Diamidino-2-Phenylindole
DCC	Dicyclohexylcarbodiimide
DHLA	Dihydrolipoic Acid
DLS	Dynamic Light Scattering
DMF	Dimethyl Formamide
EDC	1-Ethyl-3-(3-Dimethylaminopropyl) Carbodiimide
EDTA	Ethylenediamine Tetraacetic Acid
ELISA	Enzyme Linked Immunosorbent Assay
EMEM	Eagle's Modified Essential Medium
EPR	Enhanced Permeability and Retention

FACS	Fluorescence Activated Cell Sorting
FDA	Food and Drug Administration
Fe ₂ O ₃	Iron(III) Oxide (Ferrite)
Fe ₃ O ₄	Iron (II,III) Oxide (Magnetite)
FISH	Fluorescence In Situ Hybridization
FPLC	Fast Protein Liquid Chromatography
HPLC	High Performance Liquid Chromatography
Gd-DTPA	Gadopentic Acid
GPC	Gel Permeation Chromatography
GPI	Glycosylphosphatidylinositol
HER2	Human Epidermal growth factor Receptor 2
ICP-MS	Inductively Coupled Plasma – Mass Spectroscopy
IHC	Immunohistochemistry
IR	Infrared
M	Molar
MALDI-TOF	Matrix-Assisted Laser Desorption/Ionization – Time of Flight
MNP	Magnetic Nanoparticle
MPA	Mercaptopropionic Acid
MRI	Magnetic Resonance Imaging
MW	Molecular Weight
NaCl	Sodium Chloride
NCI	National Cancer Institute
NHS	N-hydroxysuccinimide
NIH	National Institute of Health
NIR	Near Infrared
NMR	Nuclear Magnetic Resonance

ODA	Octyldecylamine
ODE	Octyldecylethylene
PCR	Polymerase Chain Reaction
PAA	Poly(acrylic acid)
PBS	Phosphate Buffered Saline
PEI	Poly(ethylene imine)
PEG	Poly(ethylene glycol)
PEO	Poly(ethylene oxide)
PET	Positron Emission Tomography
PMAO	Poly(maleic anhydride alt-1-octadecene)
PMMA	Poly(methyl methacrylate)
PMT	Photomultiplier Tube
QD	Quantum Dot
QD-COOH	Carboxylated Quantum Dot
QD-OH	Hydroxyl modified Quantum Dot
QY	Quantum Yield
RES	Reticuloendothelial System
RI	Refractive Index
R_L	SPR Response from Bound Ligand
R_M	Maximum SPR Response
RNAi	Ribonucleic Acid Interference
RSV	Respiratory Syncytial Virus
RT-PCR	Real-Time Polymerase Chain Reaction
SDS	Sodium Dodecyl Sulfate
S_M	Stoichiometric Ratio
SNR	Signal to Noise Ratio

SPR	Surface Plasmon Resonance
TBE	Tris-Borate-EDTA Buffer
tbutMA	Poly(t-butylmethacrylate)
TDA	Tetradecylamine
TEM	Transmission Electron Microscopy
THF	Tetrahydrofuran
TMR	Tetramethyl Rhodamine
TNF	Tumor Necrosis Factor
TOPO	Trioctylphosphine oxide
UV	Ultraviolet
Vis	Visible Wavelengths
ZnS	Zinc Sulfide

SUMMARY

This dissertation presents a new class of cancer diagnostic agents composed of quantum dots, magnetic nanoparticles, and amphiphilic polymers. The central hypothesis is that biocompatible, amphiphilic block copolymers can be used to create multinanoparticle micellar probes with imaging capabilities and surface properties optimized for applications in cancer diagnostics. To test this hypothesis, we investigated a number of different block copolymer structures and synthetic procedures. We found that use of a poly(methyl methacrylate)-poly(ethylene oxide) polymer in conjunction with a dialysis-based procedure produced uniform probes with excellent imaging properties. We also found that the probes formed using these materials and methods were surprisingly stable, even after incubation in whole human blood for 24 hrs at 37°C. As a corollary, we hypothesized that modified polymer structures could be used to introduce functional groups for use in linking the micellar probes to biological molecules. To test this hypothesis, we used a modified version of our synthetic procedure and utilized a novel method for studying nanoparticle binding to biological molecules in real time. We found that active amine groups could be added to the polymer shell using these methods, and that surface plasmon resonance could be used for studying nanoparticle binding.

In sum, this dissertation makes several contributions to the field of cancer nanotechnology. First, we provide a new encapsulation procedure and nanostructure that has promising physical and biological properties. Secondly, we provide general strategies that can be used for future nanoprobe development. Finally, we demonstrate the capability of a new method for quantitative study of probe binding characteristics. Together, these contributions drive the field of cancer nanotechnology forward by providing a deeper understanding of the relationship between surface design and behavior in biological systems.

CHAPTER 1

NANOTECHNOLOGY IN CANCER THERAPY AND DIAGNOSIS

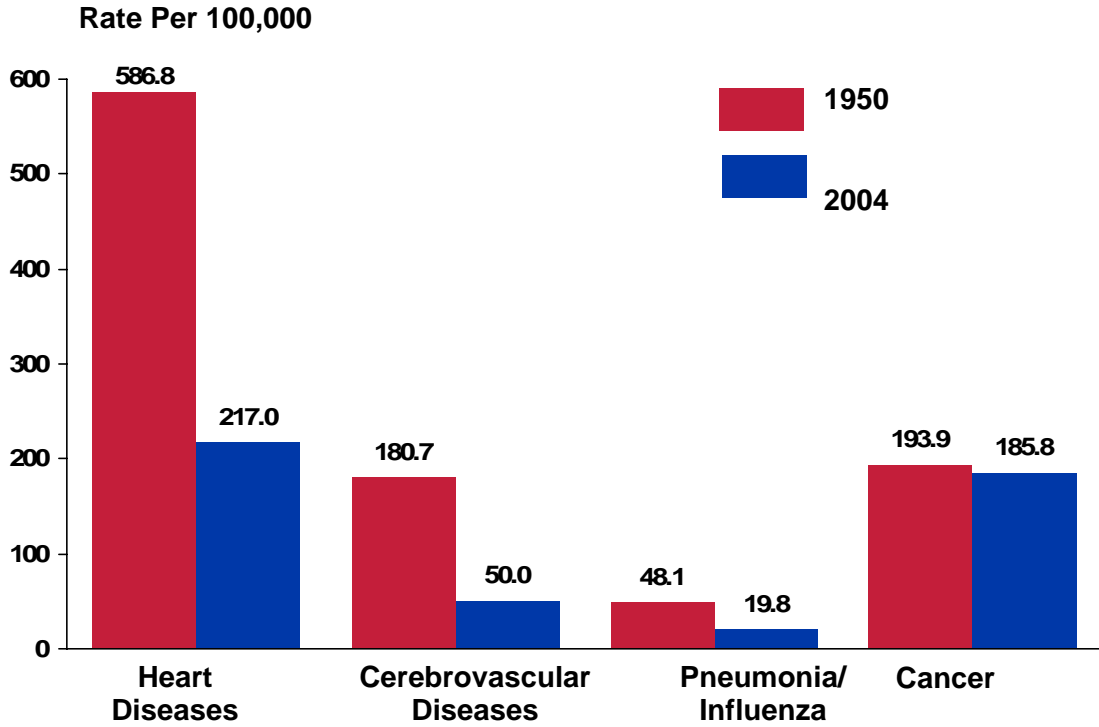
1.1 ABSTRACT

Nanotechnology can be generally defined as the engineering and design of materials that have at least one dimension between 1 and 100 nm in size. It is an emerging discipline that is finding application in a variety of research fields and industrial applications. While nanotechnology has been explored in a wide array of biomedical applications, the greatest interest and efforts have focused on cancer diagnosis and therapy. In this introductory chapter, we explore the reasoning behind this focus on cancer nanotechnology. In so doing, we present the molecular and gross physical properties that make cancer susceptible to nanoscale devices, and some of the areas in which nanoparticles are most likely to make the greatest impact. Finally, we present the overall structure of the dissertation, briefly summarizing each chapter.

1.2 INTRODUCTION

The main advantage of nanotechnology is the ability to utilize the special properties that materials possess when they have nanoscale dimensions. These properties can include physical, chemical, electrical, or biological characteristics that are not available when the material is in the bulk state. Further, the ability to engineer these particles on such a small scale allows them to interact in special ways with biological systems, as they are roughly the size of many native proteins. Recently, key stakeholders from the government, academia, and industry have been driving the rapid development of nanotechnology for the diagnosis and treatment of cancer [1-3]. To understand why such great interest has been focused on cancer nanotechnology, we characteristics.

Cancer is the second leading cause of death in the United States



* Age-adjusted to 2000 US standard population.

Figure 1.1: Decline in death rates due to the top 4 mortality causes in the US over the past 54 years [4].

Cancer is a leading cause of mortality in the United States, only outpaced by cardiovascular disease. In 2007, the American Cancer Society estimated that 1.4 million new cases of cancer would be discovered and 560,000 lives would be lost to the disease [4]. Figure 1.1 shows that while the death rate due to other common killers has dropped precipitously over the past 50 years, there has been relatively little progress in battling

cancer deaths. Since 2002, there has been some decline in death caused by cancer, but this is mostly due to prevention, yearly screening, and vast decline in smoking amongst Americans rather than improved diagnosis and treatment techniques. Indeed, despite the exponential increase in our understanding in the molecular underpinnings and pathophysiology of cancer over the last decade, relatively few new treatment options have been developed. The major treatment routes still include surgery to remove diseased tissue followed by intense radiation treatment. These harsh treatments typically leave patients weak and disfigured. Further, despite efficacy in removing primary tumors, these treatments also fail to prevent or remove metastases, which are responsible for over 90% of the deaths due to cancer each year [5, 6].

Responding to this challenge, in 2004, the National Cancer Institute (NCI) stated its goal as the “elimination of death and suffering due to cancer by the year 2015.” A major component of this goal is the development of new and improved diagnostic and therapeutic agents using nanotechnology [2]. Thus, a primary reason to focus on nanotechnology applications in cancer as opposed to other disease areas is it still remains one of our deadliest killers, and relatively little progress has been made in reversing that trend.

1.3 THE GENETIC ORIGINS OF CANCER

Cancer begins as an accumulation of genetic replication errors in victims. These errors are oftentimes caused by the existence of external toxins in the body (such as nicotine, particulates, etc), but can also occur without environmental stimuli. It has been estimated that as many as 5 distinct mutations must occur in concert for cancerous disease to develop [7, 8]. Further, the evolution of benign mutations into malignant disease can take years or decades. However, most malignant cancers share a series of

genetic and pathophysiological traits that we will briefly discuss, pointing towards what is known about the molecular entities involved in each disease process. It is this series of shared characteristics that makes nanotechnology a promising approach for oncology applications.

Disturbances in Growth and Antigrowth Signaling

Growth signaling is a highly regulated process that involves several complex molecular systems in normal cells. Normally, growth signals are either secreted from nearby cells or taken up from the extracellular matrix. However, in malignant cells, growth signals are either self-made, or the cells have developed mutated control mechanisms for growth regulation. Many common growth factor receptors have been implicated in cancer development, including: the epidermal growth factor receptor [9], insulin-like growth factor receptor [10], the platelet derived growth factor receptor [11], fibroblast growth factor receptor [12], nerve growth factor receptor [13], and the vascular endothelial growth factor receptor [14], amongst others.

Similar to growth signaling, normal cells frequently receive antigrowth signals that help to regulate their lifecycle. However, in cancerous cells, the receptors for these signals may be mutated or the systems that these receptors control may be malfunctioning. A common mutation is the down regulation of thrombospondin-1 or interferon beta [15]. Abnormalities in the expression of these antigrowth factors can set of a series of genetic events that lead to dramatic tumor growth.

Apoptotic Escape and Enhanced Replication Potential

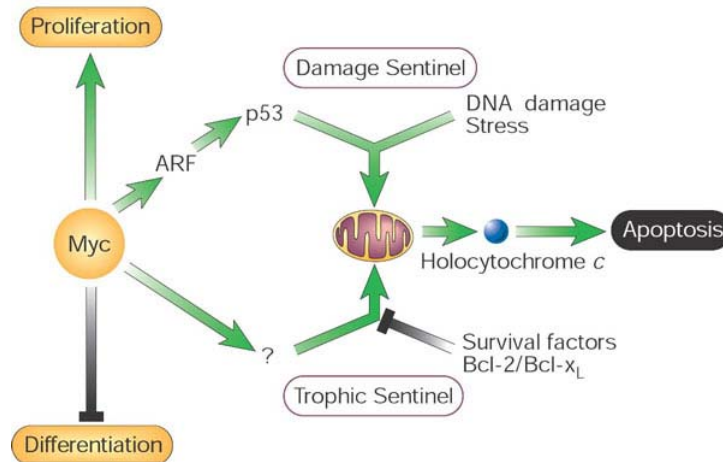


Figure 1.2: The normal apoptotic signaling pathway. In many tumors, the protein p53 is mutated or downregulated, leading to increased tumor longevity [16].

In tandem with abnormal extracellular signaling pathways, cancer cells also have mutated internal pathways. For example, cancers have been shown to effectively avoid the apoptotic pathways, shown in Figure 1.2, that lead normal cells to die. These pathways typically monitor the external and internal environment of the cell, and cause it to die if there are significant abnormalities. However, in cancerous cells, this signaling never occurs, or is greatly disturbed. For example, a common mutation identified in this pathway is the p53 signaling molecule, which is frequently missing in cancerous cells [17, 18]. Loss of this protein prevents the cell from entering the apoptotic pathway, despite significant mutations in the cells' genome.

In addition to avoiding death, cancer cells also gain the ability to replicate almost limitlessly. DNA telomeres are sequences located at the end of each DNA molecule that regulate the number of times a cell can divide by shortening each time a chromosome is split. In cancer, cells either have mutated DNA telomerases, which allow the telomere

length to remain constant by synthesizing new telomere fragments or have developed methods of maintaining telomere length in chromosomal splitting through sequence exchange [19]. This consistent telomere length has led to significant tumor growth in *in vivo* models.

Tumors Generate New Blood Vessels

To feed tumor growth, cancer cells have developed methods for initiating and sustaining angiogenesis. These angiogenic blood vessels have unique properties compared to the well established normal vasculature. For example, they often have relatively high proportions of proliferating endothelial cells, increased tortuosity, a deficiency in pericytes and an aberrant basal membrane formation [20, 21]. These angiogenic pathways are thought to be regulated by various mediators such as vascular endothelium growth factor, bradykinin, nitric oxide, prostaglandins, and matrix metalloproteinases [22, 23]. Further work has shown that different antiangiogenic factors are effective at treating tumors by starving them of blood supply [24].

Cancerous Cells Metastasize

A unique and deadly feature of cancer is the ability of the disease to spread to new regions of the body. In normal tissues, cells are coded for certain organs throughout the body, and are quickly destroyed if they somehow escape to the wrong location. In tumors, cancer cells develop a series of mutations that makes them resistant to immune destruction and able to migrate and establish residency at new sites within the body [25-28]. Figure 1.3 shows a schematic representation of this process. The metastatic cells must penetrate the basement membrane of their home tissue environment, travel through the circulatory system, penetrate the surface membranes of their new tissue environment, and then establish new blood vessels to generate growth.

While the process is still poorly understood, progress has been made in several areas, including understanding the role integrins play in the home and new tissues [14, 29, 30].

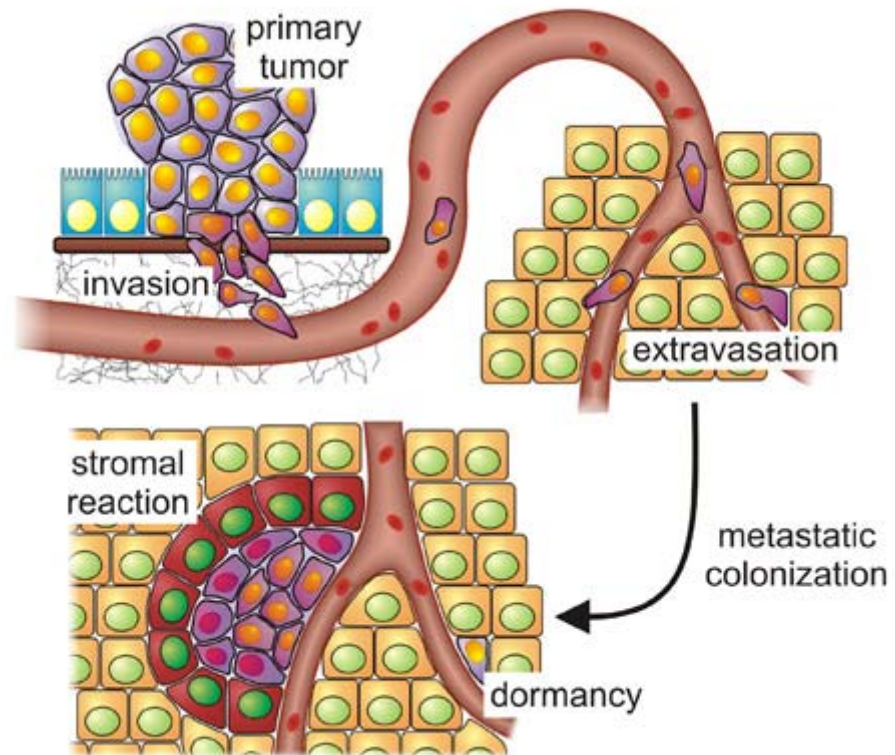


Figure 1.3: The process of cancer metastasis. Metastasis occurs in three main stages: primary tumor invasion of the blood vessels, extravasation to distal disease sites, and colonization of those distant sites [31].

Physiological Characteristics

These molecular changes give rise to the gross physiological characteristics of cancer, which include abnormal cell shape, clustered tumors with necrotic cores, and leaky tumor vasculature. The tumor interstitial compartment is predominantly composed of a collagen and elastic fiber network. The interstitium, unlike most tissues, has a high interstitial pressure leading to an outward convective flow. Further, tumors

also lack lymphatic networks [20, 21, 32, 33]. These physiological and molecular differences create barriers to the diagnosis and therapy of cancer. First, there exists drug resistance at the cellular level due to the enhanced survival mechanisms of cancerous cells. Secondly, the physiological properties described create barriers to delivery of therapies and contrast agents. Add to this the fact that most tumors and metastases start as very small cancerous lesions with few outward markers until the disease has progressed significantly, and the daunting problems facing oncologists become apparent, and help explain the relative lack of progress in treating cancer.

1.4 THE PROMISE OF NANOTECHNOLOGY

The promise of nanotechnology is that by engineering multifunctional therapeutic and diagnostic probes that are thousands of times smaller than cancer cells themselves, researchers hope to overcome some of the physiological and molecular barriers that make cancer difficult to treat and detect. There are several specific areas in which different types of nanoparticles are hoped to impact clinical treatment and identification of cancer.

In Vitro Diagnostics

In the broad area of in vitro diagnostics, nanoparticles have been making significant impacts in several applications, including: intracellular molecular imaging, molecular profiling, and highly sensitive solution assays. For each application, different nanoparticle-based strategies are used, but each relies on the special properties of nanoparticle probes to improve their efficacy. One famous example includes the development of “bio-bar” codes for attomolar detection of prostate specific antigen using gold nanoparticles [34, 35]. In our group, work has focused on detecting very rare circulating tumor cells using magnetic and optical nanoparticles.

***In Vivo* Diagnostics**

In vivo cancer diagnostics based on nanoparticles is a relatively new area. In this field, nanoparticles with contrast properties, such as magnetic nanoparticle (MNP) for magnetic resonance imaging, quantum dots (QDs) for optical imaging, or Raman active nanoparticles for Raman spectroscopy are used to detect cancerous lesions at an earlier stage than available with traditional contrast agents. For example, Gao and co-workers recently demonstrated sensitive tumor detection using biofunctionalized QDs [36]. Others have effectively demonstrated the utility of MNPs in *in vivo* applications [37-39], and new work in our laboratory has shown highly sensitive Raman active nanoparticles can also be used for tumor detection. Because the rest of this thesis focuses on the development of polymeric micelles for *in vivo* applications, we present a more detailed review of this subject in Chapter 3.

Improved Therapies

The final general area where nanotechnology is expected to make an impact is in cancer therapy [40]. In this field, two main strategies are pursued: in the first, nanoparticles themselves are used as therapeutic agents, usually by acting as thermal conduits to ablate cancerous lesions [41, 42]. In the second, and more popular strategy, currently available cancer drugs are modified by incorporation into a nanostructure [33, 43-51]. This strategy allows higher therapeutic doses without inducing patient toxicity, which is the limiting factor in current chemotherapies. In this thesis, we have used elements of this approach to design passively and actively targeted micellar probes for the delivery of *in vivo* imaging agents. Figure 1.4 shows a drug delivery nanoparticle which encapsulates hydrophobic compounds on the interior of biocompatible micellar structures. Using this strategy, circulation lifetimes and biocompatibility can be greatly improved. It is this general approach that we take in the remainder of the thesis to

create a new class of nanoparticle imaging agents.

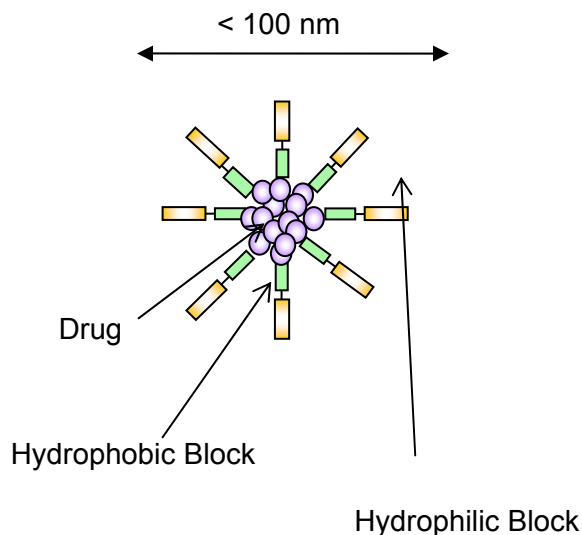


Figure 1.4: Polymeric micelles are one example of nanoparticles that can be used to improve the efficacy of currently available chemotherapeutics.

1.5 DISSERTATION STRUCTURE

This dissertation focuses on the development of a new class of nanotechnology-based probes for cancer diagnostics. Each chapter focuses on a certain developmental aspect of these probes, and discusses the approaches in detail. Here, we briefly describe each chapter.

Chapter 1- This chapter describes the broad scope of cancer nanotechnology in order to give the reader an understanding of this dissertation's place in the field.

Chapter 2- This chapter gives an in-depth description and analysis of one particular class of nanoparticles, QDs, and details advances in functionalizing these nanoparticles for biological applications.

Chapter 3- This chapter presents a detailed description and analysis of a new functionalization procedure we developed for converting QDs into biological probes.

Chapter 4- Here we extend the functionalization procedure to incorporate multiple classes of imaging agents into our newly developed probes.

Chapter 5- This chapter investigates the performance of our new functionalization strategy in stringent biological and chemical conditions, and compares the new technology to previously existing coatings.

Chapter 6- In this chapter, we investigate methods for adding functional groups to the surface of our micellar probes.

Chapter 7- Here we demonstrate the utility of surface plasmon resonance technology in the study of nanoparticle binding, and describe how this technique could be used to improve nanoparticle surface design.

Chapter 8- We present several suggested areas for future development, both of the specific technologies presented in this dissertation and for cancer nanotechnology in general.

1.6 CONCLUSIONS

In this chapter, we have presented the broad scope of cancer nanotechnology, and explained the reasons why it is a rapidly growing research area. Cancer has several molecular and physiological characteristics that pose problems for traditional therapies and diagnostics, but may be amenable to approaches utilizing nanoparticles. Nanotechnology can be applied in a diverse set of clinical situations, but the main areas include *in vitro* and *in vivo* diagnostics and therapeutics. Within these fields, this thesis focuses on the development of nanoparticle based *in vivo* diagnostics.

CHAPTER 2

QUANTUM DOTS FOR BIOLOGY AND MEDICINE

2.1 ABSTRACT

In this chapter, we focus on the development of semiconductor QDs, one particular type of nanotechnology. QDs are crystalline particles under 10 nm in diameter that are being rapidly developed for cancer research and diagnosis. In contrast to traditional organic dyes and fluorescent proteins, QD's small size endows them with superior optical and electronic properties including resistance to photobleaching, size tunable emission wavelengths, enhanced brightness, and significant multiplexing capacity. Major advances have shown QDs to be useful in a variety of oncology-related applications, including: solution-phase studies for multiplexed and highly sensitive analyte detection, living cell studies for understanding receptor dynamics and signaling over long time scales, and whole-animal *in vivo* studies for ultrasensitive disease detection. For each application, QDs must be specially tailored by modulating the particles' surface properties to enhance stability, retain brightness, and add targeting functions. Here we discuss the advancement of QDs in oncology-related settings while highlighting the surface strategies used and offering insight on how these strategies affect end use applications.

2.2 INTRODUCTION

Recent advances in molecular biology and imaging technology have revolutionized cancer detection and diagnosis. Simultaneously, fluorescent probe development in basic biological labs has unlocked new understanding about intracellular dynamics and protein cascades that cause cancer. While these considerable achievements have led us quite far, several problems exist with the current state of the

art. For example, most clinical imaging techniques can only detect tumors that have already reached 1 mL in volume. A malignant tumor of this size already contains 1 billion cancer cells, and has a high chance of metastasizing to distal sites within the body. In research labs, commonly used fluorophores such as organic dyes and fluorescent proteins can yield some information about molecular events, but are difficult to work with and lack true multiplexing capability. Conversely, nanoparticles such as semiconductor QDs offer tremendous advantages as compared to the current state of the art due to their small size and unique emission properties. QDs are 2-9 nm in size, or roughly 10,000 times smaller than an average tumor cell, offering hope of detecting much smaller disease sites. Their emission properties include size-tunable emission wavelengths throughout the visible spectrum and into the infrared, broad absorption peaks, high photostability and brightness, and narrow emission peaks [52, 53]. In addition to size and emission advantages, QDs have many points of control that allow them to be tailored to applications of interest. In recent years, researchers throughout the world have capitalized on these unique properties to develop applications critical for cancer research and diagnosis.

QD-based bioanalytical applications have been developed in three important areas: (1) solution-based detection, (2) analyte tracking in cells, and (3) *in vivo* imaging in whole animals. For each application, QD surfaces must be modified to endow desired properties. There exist two broad modification strategies: (1) directly modifying the QD surface for attachment to biorecognition molecules (also referred to as ligand exchange) or (2) over coating QDs with polymers to enhance biocompatibility [54-56]. In the following, we briefly discuss the novel properties of QDs and then focus on the three types of bioanalytical assays, emphasizing how different surface strategies have enabled or hindered QDs end use application.

2.3 SEMICONDUCTOR QDs

QDs are crystalline semiconductors between 2 and 9 nm in size that have been studied for over twenty years, only recently having made the jump into biomedicine. The moniker “quantum dot” refers only to the special confinement of electrons within this small size range. Researchers have developed many different types of “quantum” materials, includes wells, holes, rods, and planes, all with different states of electron confinement [57]. There is a rich array of production methods available, from photolithography on circuit boards to synthesis as colloidal solutions. The QDs produced in colloidal solutions are the most useful for bioapplications and are what most interdisciplinary researchers refer to when using the phrase “quantum dot.”

The highest quality QDs are composites of two semiconductors that have overlapping electronic band gaps. The most common QD structure for bioapplications is a CdSe core with a thin, protective shell of ZnS. However, many other types of QDs exist, including CdS cores with no protective shell, PbSe, and even HgTe [58-60]. Colloidal QDs are produced using either surfactant micelles, coprecipitation, or high temperature organic solvent synthesis routes. We have extensively shown that the best QDs are produced using the high temperature technique [61-63]. This synthesis leaves QDs with a surface monolayer coating of nonpolar coordinating ligands, meaning the final QDs are highly hydrophobic and must be transferred into aqueous solutions before use in bioapplications. There are many transfer processes to choose from, and this step represents the first point of control for designing QDs for cancer research

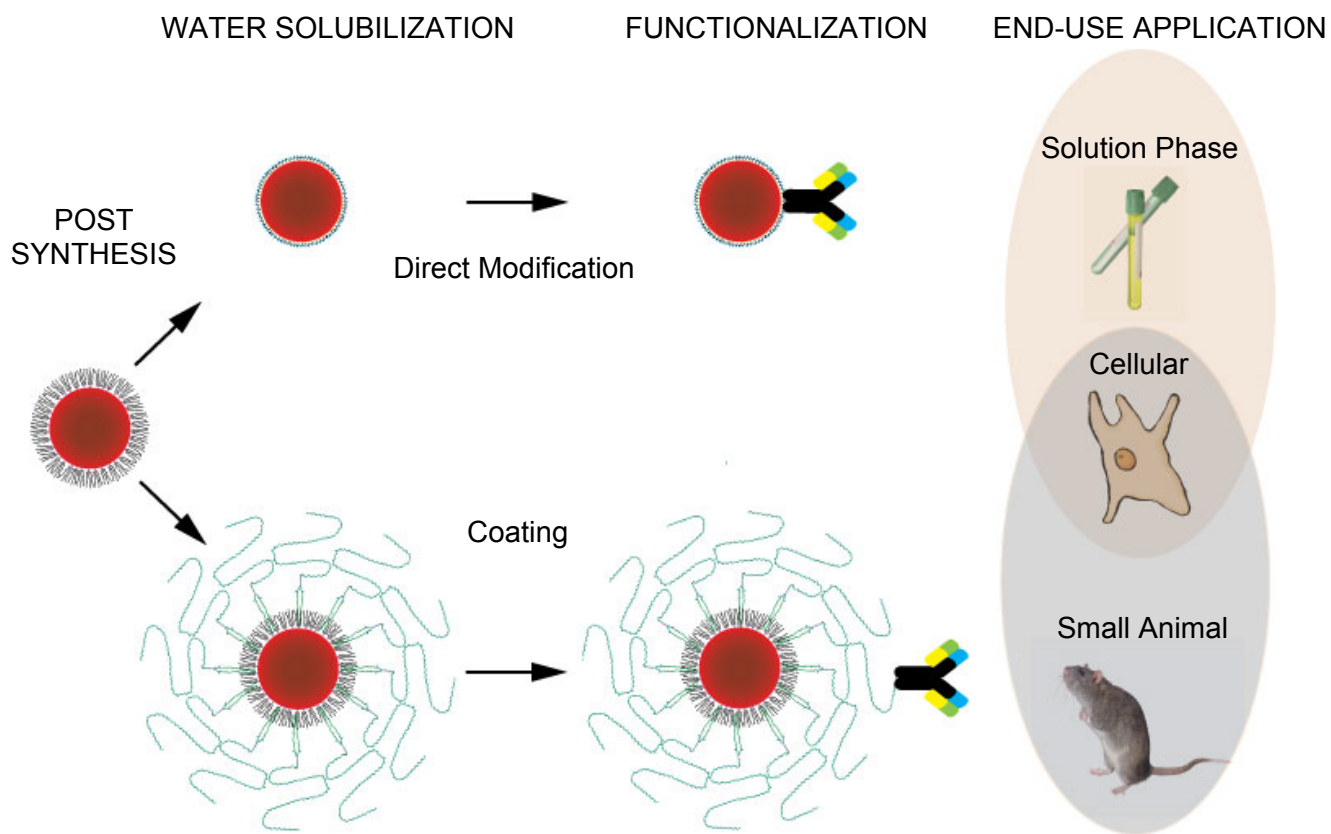


Figure 2.1: Illustration of two general QD functionalization strategies for cancer-related studies. Post synthesis QDs are highly hydrophobic and must be water solubilized, either through direct modification (ligand exchange) or coating. In general, directly modified QDs are better suited for solution phase studies while coated QDs are more useful in *in vivo* investigations (here drawn as an antibody). Next, the QDs are linked to functional biomolecules and applied to the system of interest.

and diagnosis. Figure 2.1 shows the general steps required to functionalize QDs for these applications and the different applications which each surface strategy is best suited for.

Once appropriately modified, colloiddally prepared CdSe/ZnS make excellent contrast agents because of their unique spectral properties. The first and most dramatic property is their size-tunable emission. Due to the unique confinement of electrons within such a small semiconductor, the physical size has a great effect on the energy of the electronic process that produces photons. Therefore, by adjusting the nanoparticle diameter, it is possible to vary the emission wavelength of QDs. CdSe/ZnS QDs that are ~2 nm in diameter produce a blue emission while QDS ~7 nm in diameter emit red light [64]. Researchers have even pushed the emission wavelength into the near infrared, to take advantage of low background in biological tissues at these wavelengths [65].

Another important property is the broad QD stokes shift, which allows excitation at one wavelength and observable emission at much longer wavelengths. In conjunction with QD's broad absorption peaks and narrow emission peaks, this property allows multiplexed applications, where one excitation wavelength causes simultaneous detectable emission of several QD colors without special equipment. Another important spectral property is QD's long term photostability. A huge problem with traditional organic fluorophores is their short term stability under bright excitation light. This causes imaging to become a very involved process, where every camera and microscope setting must be perfectly aligned prior to image capture, and fluorophores can still only be observed for a few seconds. Long term photostability allows investigators to image the same area repeatedly until they are satisfied with the results. Further, it opens the possibility of studies investigating the dynamics of cellular protein expression and exchange over time, without changing samples, fluorophores, or microscope settings. For this myriad of reasons, QDs have become the focus of intensive research and design work by clinicians, chemists, engineers, and others interested in understanding cancer and developing the next generation of cancer detection systems.

2.4 STRATEGIES FOR BIONFUNCTIONALIZATION

A substantial amount of research has focused on modifying QD surfaces for use in oncological systems. The choice between direct modification and coating approaches largely depends on the end QD use. Direct modification was the first approach used for functionalizing QDs, exchanging hydrophobic coordinating ligands for mercaptoacetic acid and silica [66]. This approach is well suited for simple targeting of fixed cell surface markers or solution based assays, due to simple, fast procedures, and small final probe size. Unfortunately, it becomes less attractive for living systems, as there are often biocompatibility issues. Another general problem with modification strategies is a drop in quality in fluorescent properties. QD surface ligands are specially designed to retain exceptional photoluminescence, and any modification can lead to defects and loss in quantum yield (QY). Despite these issues, direct modification remains a viable and useful approach for many investigations, as recent work has demonstrated [67].

Coating strategies have been developed as an alternative in response to these challenges. One primary superiority is the ability to solubilize and functionalize QDs without dramatically changing their emission properties. In fact, commercially available QDs (from Quantum Dot Corporation) use a modified poly(acrylic acid) (PAA) polymer to coat the surface, in a fashion similar to published work [68]. In addition, nanoparticle biocompatibility can be enhanced by introducing specialized polymer chains or non-reactive moieties to the nanoparticle surface. Further, coating allows multiple types of ligands to be attached to a single QD surface, for example, targeting, anti-immune, and possibly drugs [36].

Both direct conjugation and coating have achieved success in some specialized applications, but better designs are required before QDs will be used as a day-in, day-out diagnostic tool for cancer research and diagnosis. Here we review the two design strategies, analyzing their strengths and weaknesses based on three different

applications of interest: cellular labeling and dynamics, solution based assays, and *in vivo* imaging. We also provide insight and examples of how these strategies could be improved.

Solution Based Assays

Direct modification is the dominant method used for solution based assays. Several groups have used the technique to develop sensitive, advanced detection techniques that could be adopted for cancer detection. For example, one group has developed multiple immunoassays based on replacing QD surface ligands with a charged polymer known as DHLA [69-72]. The most interesting applications include a method for studying protein attachment to nanoparticle surfaces, detecting up to four toxins in a “sandwich immunoassay”, and finally as an “immunochromatography” reagent that could detect both large and small molecule targets [71-75]. While impressive, analyte detection is only one area where QDs will have an impact in solution phase studies. For example, DNA telomerization and synthesis via PCR have been observed and studies have even demonstrated potential as photosensitizing agents in photodynamic therapy [76-78]. However, the most exciting example of a solution phase study has been the use of QDs and other nanoparticles to detect single proteins, DNA, and viruses in a flowing fluid. This approach allowed single molecules to be detected from target concentrations as low as 20-30 fM. The direct conjugation of targeting ligands to the QD surface prevented the need for further derivitization of these ligands, thus enhancing the sensitivity of the approach [67].

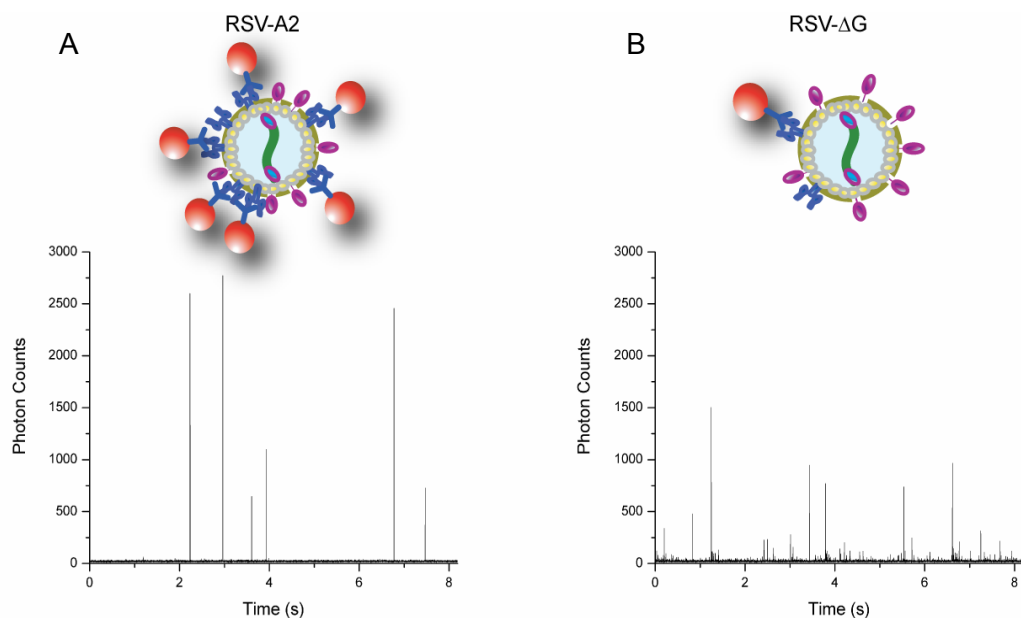


Figure 2.2: Photon count data collected from QDs bound to two different versions of RSV. The probes detect small differences in viral surface protein expression. In (A), more QD probes bind to a virus that has greater F and G protein expression on its surface, leading to higher photon counts and indicating increased infectivity. In (B), a reduction in F and G protein expression leads to reduced binding and lower photon counts. The data was obtained with a Single Photon Avalanche Detector and integrated over 1 ms interval. (Agrawal and Nie, unpublished data)

Figure 2.2 shows that this approach can even be used to analyze miniscule differences in protein expression between two strains of the Respiratory Syncytial Virus (RSV), the leading cause of respiratory tract infection in the infants and the immune compromised. In this work, two strains of RSV (wild type- A2 and G-attachment protein mutant Δ G) were used to probe F-protein concentration directly on the viral particle surface, which is correlated with infectivity [79]. QDs conjugated with monoclonal

antibody for F protein were allowed to incubate with different strains of the virus and the solution was allowed to flow through a capillary running over a fixed-point confocal microscope equipped with a photon counter. It was found that RSV- Δ G strain has reduced expression of F-attachment protein as well as reduced G-protein expression. It is possible that the lower level of F protein expression by RSV- Δ G compared to RSV-A2 may be associated with altered gene expression levels linked to changes in the gene end termination signal that precedes the F protein gene, as changes in this region may affect downstream gene expression levels [80]. This study is but one example of how QD probes can be developed for understanding subtle changes in cancer gene expression that will have a dramatic impact on patient outcome.

Because direct modification has been so adept with solution based assays, there has been little incentive to introduce coated QDs. However, there are some examples of quality work using these techniques. For example, one group demonstrated that commercially available QDs could be attached to targeting oligonucleotides for the simultaneous detection of three different synthetic sequences derived from anthrax related genes using colocalization studies [81]. Others have demonstrated a novel assay using coated QDs to study actin filament sliding in an in vitro model, and even microtubule motor protein movement [82, 83]. In a bellwether study, one group demonstrated that QDs coated with a special triblock copolymer could screen siRNA libraries for the most effective RNAi sequence [84].

Perhaps the most useful application has been the advent of QD western blot technology. The original work showed a significant enhancement of sensitivity (picogram vs microgram) with existing imaging systems and no significant changes to protocol [85]. Later, others further verified this by QD-blotting several telomere related proteins. In this application, QD-activated probes have the potential to achieve widespread use, as long as costs can be controlled [86].

In the future, a solution based cancer marker assay developed from the work presented here could be a vital and regular tool used by clinical oncologists.

Cell Labeling and Studying Cellular Dynamics

While solution assays are useful for fast cancer blood marker detection, cell labeling and cellular dynamics offer new detailed information on the disease's progression and development. In this area, the use of directly modified QDs and coated QDs has been roughly equal, but commercially available coated QDs are quickly becoming a preferred strategy, allowing retention of optical properties while improving cellular biocompatibility.

In the earliest cellular work, highly specific targeting ligands were linked directly to modified QD surfaces and used for a variety of studies including fluorescence in situ hybridization, binding to serotonin transporter proteins, and long term visualization in Hela mammalian cells [87-89]. Unfortunately, non-specific binding related to an incomplete surface coating caused significant problems in these investigations. In another cell-membrane receptor study, researchers directly coated QDs with peptides inspired from naturally occurring detoxifying peptides in bacteria. This allowed them to stain GPI anchored avidin-CD14 chimeric membrane proteins. Unfortunately, as is often the case with surface modified QDs, the QY was low [90]. In a critical cancer-related application, an anti-p glycoprotein antibody was attached to QD surfaces and was subsequently used for detection of the protein in MCF7 breast adenocarcinoma cells [91]. This protein is a key player in multidrug resistance, and understanding its function will lead to new, more potent chemotherapies. Finally, in a futuristic study, QDs and siRNA were combined to study the function of T-cadherin in cell-cell communication. The directly modified QDs allowed researchers to accurately monitor which cells were

properly transfected with siRNA [84]. Studies such as these have highlighted both the strengths and weaknesses of the direct modification approach.

While directly modified QDs are somewhat waning in interest for cellular use, the easy availability of coated QDs has prompted an explosion in their use. One example is the use of biotin-streptavidin linked peptides and subsequent endocytosis to label cells for fluorescent assisted cell sorting (FACS) [92]. Others have used QDs to study size-dependent endocytosis, activation of neuronal receptors, and internalization of cationic peptides in long-term studies [93-95]. These investigations showed that coated QDs are effective probes for studying signal transduction pathways, and although receptor binding is affected, the long-term capabilities of QDs make them ideal for these investigations.

In more applied studies, QDs were encapsulated in phospholipid micelles with surface PEG coatings by a simple evaporation method. The solubilized QDs were loaded into frog oocytes and this allowed researchers to trace the lineage of cells during embryogenesis all the way to the tadpole level [96]. In another breakthrough, scientists observed diffusion dynamics of neuronal glycine receptors and subsequent diffusion to synapses [97]. By using coated QDs, they obviated the low-QY problems that plagued similar studies with directly modified QDs [90]. Multiplexed assays using polymer coated and peptide conjugated QDs to “barcode” cells, could detect up to 10 different codes [98]. In addition, an impressive breakthrough was recently published where coated QDs were used along with two photon excitation laser scanning microscopy to create 3D reconstructions of human aortas and atherosclerotic plaques, yielding dramatic images for easy diagnosis by clinicians [99].

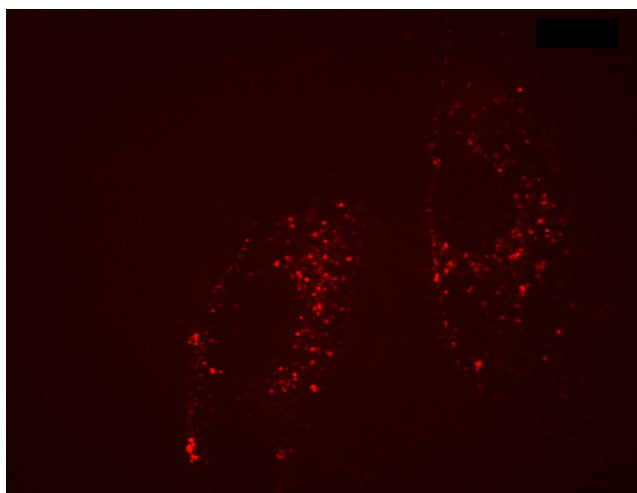


Figure 2.3: Fluorescence image of single QDs and aggregates in the cytoplasm of live fibroblast cells. QD blinking was readily observed in these cells along with uniform distribution of QDs throughout the cell. Commercially available QDs were delivered to cells by creating transient pores in the cell membrane. This image was taken 6 hours after delivery with no loss in fluorescence or increase in aggregation. The image was obtained with a spinning disk confocal microscope with the focal plane at the center of the cells.

While any of these techniques could easily be modified for cancer-related investigations, there have been several studies specifically addressing cancer dynamics. In a series of important cancer-related developments, QD polymer-streptavidin conjugates were used to show that transmembrane proteins erb2 (also known as Her2) and erb1, but not erb3 form heterodimers as a first step in a receptor tyrosine kinase signaling pathway [100]. Earlier, a team showed that similar polymer coated QDs could stain the Her2 marker in fixed and unfixed cells along with tubulin [101]. They used this to monitor the effect of phalloidin on microtubules. This technique also demonstrated significant improvement as compared to earlier work which had utilized a direct

conjugation strategy [66]. Others used silica coated QDs to monitor cell migration and division in a long term study greatly simplified by QDs. They were able to observe marked (and expected) differences between metastatic and non-metastatic cell lines [102].

All of these studies show how QDs interact with the cell surface, but very few demonstrate real time imaging in living cells. Recently, QDs were used to track individual microtubule motors as they traversed the cytoskeleton in live cells [103]. However, these QDs were largely aggregated, making the probe size very large and non-uniform. Figure 2.3 shows a dramatic example of coated QDs used for intracellular imaging. Using a protein that transiently forms pores in the cell membrane we were able to observe single QDs in the milieu. Delivery methods such as these, which can reproducibly introduce single QDs intracellularly, will be necessary to truly study cancer-related events and mutations.

Animal Imaging

The holy grail of cancer nanotechnology is to be able to sensitively and specifically target tiny disease sites within a whole organism. Of course, this is hugely more complicated than either solution or cellular studies. In these applications, coated QDs can have several advantages as opposed to a direct conjugation scheme. Nonetheless, there has been limited progress in using direct strategies *in vivo*. For instance, one group used peptide conjugated QDs to target lung tissues, tumor blood vessels, and lymphatic conduits. They also showed the usefulness of attaching a PEG coating to the surface of nanoparticles to reduce uptake by the reticuloendothelial system [38]. An exciting advance was the demonstration of near-infrared QDs as intrasurgery guides for sentinel lymph node resection both in small mice and larger pigs [104, 105]. Unfortunately, these QDs had very low QY, meaning improvements must be

made before this becomes a widely accepted surgical method. Finally, a group showed that metastatic tumor cell extravasation could be tracked by using QDs and fluorescence emission-scanning microscopy after tissue resection [106]. While these studies are promising, the true potential of QD-based animal studies will probably require high QY near infrared QDs coated with well designed polymers.

While the field awaits high QY near infrared QDs, a few important steps have been taken with coated QDs. The major and most impressive work in this category successfully used a decorated triblock polymer coating to both passively and actively target tumors in a whole mouse. This work demonstrated high specificity, although spectral processing was needed due to the wavelength of QDs used [54]. In other novel work, blood vessels were imaged up to 100 μm deep using two photon excitation and 550 nm dots [107]. While not a true "*in vivo*" study, cells pre-loaded QDs and injected into a mice were located in the kidney, liver, spleen, and lung (after resection) [108]. Finally, a group used the PEG-conjugated lipid encapsulation method to distinguish tumor vessels from both the perivascular cells and the extra cellular matrix while studying probes' size-dependent access to tumors [109]. Taken together, these studies reveal tremendous potential for *in vivo* studies using QDs. As the march of QD emission wavelengths continues well past 800 nm, these investigations will become much more impressive.

As an example of what lies in the future, Figure 2.4 shows combined x-ray and fluorescent images of high-quality, deep-red QDs injected into a mouse. The very low background and high QY create dramatic, easy-to-read images that will yield vital information for oncologists. Pioneering studies such as these will offer insight into cancer progression in animal models, and hold promise for direct clinical use if significant hurdles can be overcome.

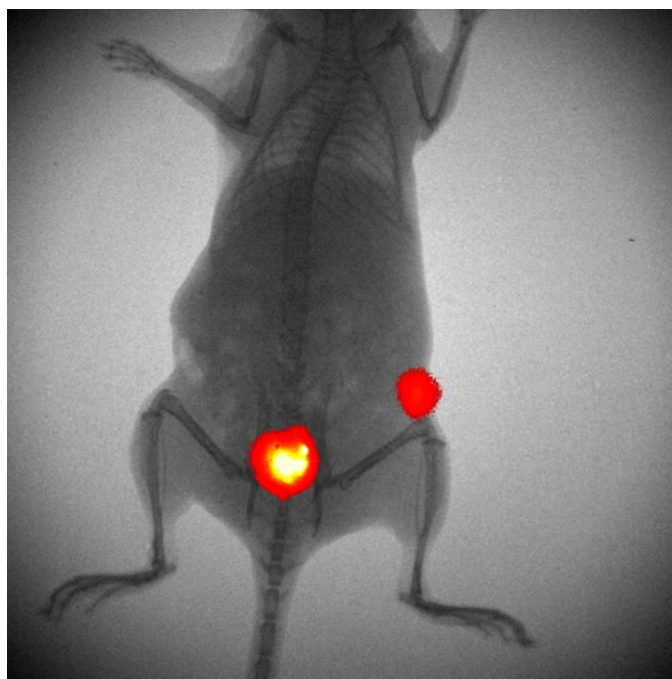


Figure 2.4: Combined x-ray and fluorescent image of QDs injected into the hindquarters of a mouse. These high QY, deep red QDs are easily detectable above background. The images were captured sequentially with a Kodak *in vivo* Image Station.

2.5 Challenges, Opportunities, and Future Perspectives

It is clear from the preceding discussion that the utility of QDs in biological and medical settings is highly dependent upon the quality of the surface design strategy. However, the importance of surface design is not limited to utility issues. It is becoming clear that surface properties also play a major role in shaping QD toxicity profiles. In particular, two studies point out that the type of QD used, its preparation method, and most importantly the surface coating all determine the biocompatibility of QDs [110,

111]. Observed cytotoxicity likely arises from free radical generation caused by the cadmium oxide ion, and is exacerbated by oxidation and weak surface coating protection [112]. We anticipate that through improved understanding of the interaction between QD surface coatings and cadmium oxide ion concentration and further studies of the cytotoxic effect, QDs will overcome this limitation.

As coating strategies become more en vogue, investigators will have to become more intelligent about their designs. Systematic studies of the interaction between QD hydrophobic surface ligands and hydrophobic polymer chains will allow us to design coatings that bind tightly and easily to QDs while retaining their excellent fluorescent properties will be necessary. It will also be important to determine an optimum coating thickness, one that is thick enough to protect the QD from oxidation, but also not so thick that advantages from the small QD size are lost. Further systematic studies modulating the number and type of hydrophilic functional groups on the outer surface of the polymer coat will reduce non-specific absorption and enable attachment to biomolecules of choice. This, combined with advances in biochemistry and molecular biology, should lead to impressive targeting applications at the cellular and whole animal level.

Futuristic applications will develop from an understanding of QD surface interactions. For example, therapeutic molecules that are linked through coating molecules to targeted QDs will allow oncologists to both administer chemotherapy and monitor recovery in real time without waiting months to see if a drug has been effective.

Combined optomagnetic probes will be one of the first new devices that appear. Already, researchers have made advances in combining gadolinium with a phospholipid micelle surface strategy [113]. Future work will use QDs linked by customized polymers to both gadolinium and MNPs to provide surgeons with a pre-surgery MRI image of a cancer site and fluorescent “runway lights” during surgery to guide them into very

specific disease sites, all with one contrast agent. Later in this thesis, we present work towards this goal.

Ultimately, advances in QD nanotechnology in solution based assays, cellular studies, and *in vivo* imaging will lead to personalized and predictive medicine where each therapeutic approach is tailored to every patient's particular disease profile.

2.6 CONCLUSION

Because of the significant advantages of the coating approach in terms of retaining QD optical properties, preventing adsorption of biological molecules, and enhancing circulation lifetimes, we chose to focus on this approach for the development of *in vivo* imaging agents in this dissertation work. In the next chapter, we present our detailed coating strategy, and spend the remainder of the thesis exploring extensions and performance of this coating approach.

CHAPTER 3

SYNTHESIS AND CHARACTERIZATION OF OPTICAL MICELLAR PROBES

3.1 ABSTRACT

The focus of this chapter is on the development of synthetic procedures for encapsulation of nanoparticles in biocompatible block copolymer micelles. The major result presented is a facile method of synthesis based on dialysis which allows control over micellar size between the single nanoparticle regime and multinanoparticle micellar structures. In addition, we present different purification procedures that can be used to concentrate the micelles and prepare them for applications in blood profiling, *in vivo* imaging, and other bioassays. Finally, we present DLS, TEM, fluorescent and UV/Vis spectroscopy, and fluorescent microscopy data in support of our results.

3.2 INTRODUCTION

The synthesis of high quality, monodisperse crystalline nanomaterials such as QDs and MNPs in organic solutions has reached near perfection over the past two decades [59, 114-117]. With many of the basic chemical questions answered, attention has turned to finding significant applications for these materials. The most promising applications lie in the fields of biomedical science and clinical technology. The dramatic growth of these fields in recent years has highlighted the need for superior technologies for detection, treatment, and analysis. Systems that incorporate unique nanomaterials and are specially designed for biological applications will provide new, powerful tools to medical researchers [52, 55, 118, 119]. Design inspiration for such systems can be culled from the field of polymeric drug delivery, which focuses on improving the therapeutic index of anticancer compounds [40, 120]. Specifically, polymeric micelles formed from biocompatible amphiphilic diblock copolymers have been developed to

entrap and deliver hydrophobic chemotherapeutic agents such as Taxol [121, 122].

These micellar systems rely on entropic forces in aqueous solution to drive self-assembly of polymer chains around a hydrophobic core of drugs.

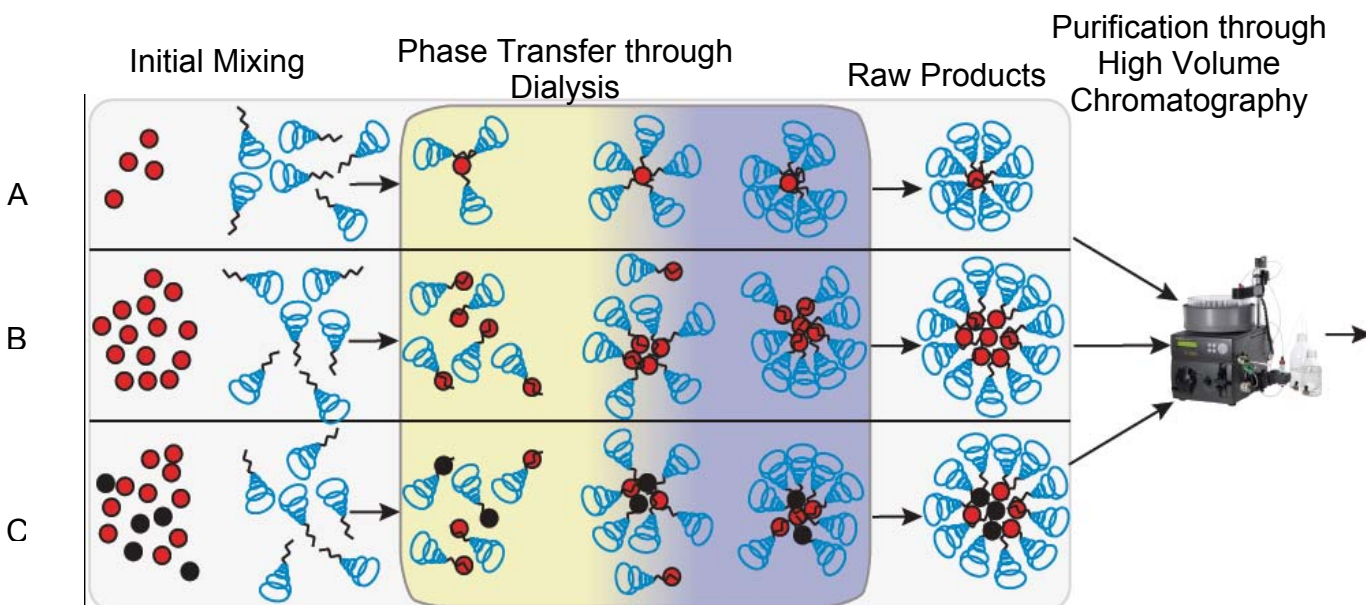


Figure 3.1: Our general approach to creation of size and composition tunable

micellar probes. In A, high polymer:QD ratios produce singly encapsulated nanoparticle probes. In (B) lower polymer:QD ratios produce multinanoparticle probes, and in (C)

addition of MNPs creates dual-modality imaging probes (Discussed in detail in Chapter 3).

Each sample is then passed separately through an automated high-volume chromatography system to produce our final products. See text for details.

Realizing the qualitative similarities between hydrophobic drugs and hydrophobic nanoparticles, investigators have used similar strategies to entrap multiple nanoparticles on the interior of amphiphilic polymer micelles. While the physical mechanisms of this encapsulation procedure are interesting, in real, practical terms, the approach has

several advantages for biomedical applications. One such advantage is the capability of combining multiple types of nanoparticles into a single probe to create multimodality probes that can include different imaging and therapeutic properties. Another advantage is enhancing probe signal strength through clustering of multiple nanoparticles in a small container, such that each target bound by a probe would have several reporter tags in one area as opposed to one nanoparticle per target, as in the traditional case. Further, by clustering nanoparticles in a larger construct, renal filtration can be avoided while still not encountering a threat from the reticuloendothelial system.

Previous attempts have utilized Fe_2O_3 MNPs [123], gold nanoparticles [124], carbon nanotubes [125], and even QDs [126-128]. In each of these cases, the hydrophilic portion of the block copolymer consisted of PAA, which has advantages in terms of facile functionalization owing to free carboxylic acid groups on the surface of these micelles, but must be crosslinked to ensure probe stability in stringent biological and chemical conditions. Another disadvantage is that carboxyl functional groups on the surface of nanoparticle probes have been shown to contribute to nonspecific uptake by immune cells and protein opsonization, reducing their utility as biomedical imaging probes (Sathe, Kairdolf, Nie, unpublished data). In addition, the QD-based micelles produced in these cases had very low QYs (maximum 5%). Further, despite using magnetic nanomaterials and QDs, no direct assessment of either MRI contrast capabilities or fluorescent imaging in relevant biological systems has been made. Finally, while each of these investigations have demonstrated small-scale synthesis of micellar probes, much larger quantities must be produced and purified before animal studies can be conducted and clinical applications envisioned.

To address the problems in this area, we used the same principles to form clusters of nanomaterials on the interior of amphiphilic block copolymer micelles using

the procedure described in Figure 3.1. However, we used QDs synthesized via high-temperature organic solvent synthesis, and block copolymers containing PEO as the hydrophobic block. Further, we describe a new purification approach that allows scale up to volumes necessary for detailed animal studies. Thus, the synthetic approach and micelles produced here have the following advantages: (1) they are formed from biocompatible polymers with a polyethylene oxide (PEO) surface optimal for biological applications, which we qualitatively demonstrate is more suitable for biological assays than PAA based coatings, (2) using high-QY QD starting materials coated in octadecyl amine produces stable, bright probes with a maximum QY of 40%, 8x brighter than the maximum attainable with other QDs, (3) by using fast protein liquid chromatography (FPLC) to purify our multicomponent micelles, we increase yields and quantities produced dramatically, as opposed to centrifugation methods describe previously, and (4) the probes demonstrate remarkable stability in corrosive biological and chemical conditions, even without crosslinking.

3.3 METHODS

QDs

Cadmium selenide QDs were synthesized in a coordinating solvent following previously published procedures [129]. After purification via precipitations from methanol, the QDs were resuspended in a mixture of ODE and ODA, and then capped with a shell of CdS (2 monolayers) and then ZnS (2 monolayers) at 230°C under argon, using organometallic precursors.[130-132] These ODA-passivated QDs were stored as a crude mixture at 4°C and purified using repeated extractions in hexane/methanol, followed by precipitations with acetone prior to use.

Polymer Preparation

All polymers used in this thesis were received from a variety of suppliers, including Polymersource, JCS biopolymer, Warwick effect, and Rapp Polymre. Typically, polymers were aliquoted as necessary and resuspended in THF or other suitable solvents. Depending on the solvent-polymer pair, sometimes mechanical solubilization methods such as sonication were utilized to create a clear solution.

Dialysis Procedure

Nanoparticles and polymer were dissolved in THF, mixed, and then dialyzed repeatedly against deionized water using a low molecular weight cutoff membrane (2000 MW). Typically, the dialysis procedure was allowed to proceed over 8-12 hours, with 3-4 changes of buffer. Typical volumes used were 2-4 mL of polymer-nanoparticle solution dialyzed against 1-2 L of water. For dual color probes, green and red QDs were mixed in varying ratios determined by their emission intensity at each concentration to achieve the final desired color.

Ultracentrifugation

Initial studies showed that several round of centrifugation and ultracentrifugation could be used to separate the multinanoparticle micelles from excess polymers and ligands. Typically, immediately following dialysis, the resulting solution was centrifuged at 7000 rcf for 20 minutes. The supernatant was collected and ultracentrifuged at 150,000 rcf for 1 hour. The supernatant, which usually contained a cloudy mixture of polymer and excess ligands, was discarded, and the pellet, which contained single nanoparticles and micelles, was resuspended and subjected to another round of centrifugation at 7000 rcf. This procedure was repeated up to 5 times, until no polymer

was visible following ultracentrifugation and the nanoparticles pellet easily resuspended in buffer.

Liquid Chromatography

For separation and purification using liquid chromatography, we used an AKTA Primeplus machine (GE Healthcare). Two different columns were used: Sephacryl 500HR column (bed volume = 45 mL) and Superose 6 (bed volume = 20mls). Fractions were collected using the autofractionater, and corresponded to desired UV absorption peaks. Typical sample volumes were approximately 1-5 mL.

Fluorescent Microscopy

Nanoparticle loaded micelles were typically spread on a L-polylysine coated coverslip and excited with a mercury arc lamp on a conventional inverted microscope. The polylysine coating does not spread with uniform thickness across the coverslip, causing slight haze from micelles that are out of the focal plane, but does allow faster sample processing time. Alternatively, a single drop of the micelle solution can be placed on a coverslip and be allowed to evaporate prior to imaging. Images were captured with a Nikon D100 at 100X magnification. The exposure time is approximately 3 seconds.

Transmission Electron Microscopy

Purified, concentrated samples were dropped onto copper TEM grids with a spacing of 200 and a formvar polymer coating. The sample was allowed to rest on the grid for approximately 10 minutes prior to wicking away excess water using filter paper. Phosphotungstic acid was used to negatively stain the grids by dropping on the grid

for approximately 30 seconds prior to being wicked away. The samples were then imaged using a Hitachi H7500 TEM.

Dynamic Light Scattering

DLS data was typically obtained on a Brookhaven instruments 90 plus particle analyzer. Typically, the experiment was carried out for 3 runs of 2 minutes each, and analyzed using the “number” (first-order) Multimodal Size Distribution.

Spectroscopy

Spectroscopic measurements were obtained using a Jobin Yvon Fluoromax-2. Typically, scans were run from 490 nm to 680 nm with excitation at 475 nm.

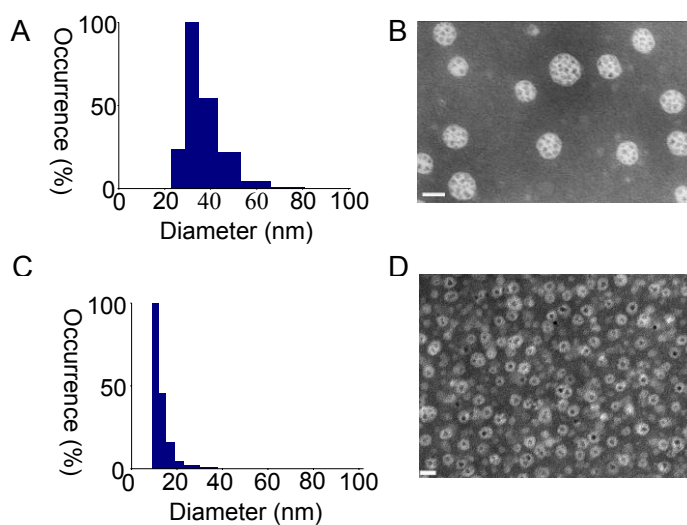


Figure 3.2: TEM and DLS data comparing the size and structure of single and multiple QD micelles. A and B show DLS and TEM data for a sample with a low polymer: QD molar feeding ratio (100:1). C and D show the same data for a higher molar ratio (500:1). The scale bars are 20 nm.

3.4 RESULTS AND DISCUSSION

Our optimized encapsulation and purification procedure was successful in producing single and multinanoparticle micellar probes as demonstrated by the TEM and DLS data presented in Figure 3.2. These data show that the nanoparticle size and composition can be varied by adjusting the starting ratio of QDs to amphiphilic polymer. The data also demonstrate that at very high polymer concentrations, samples tend to be more monodisperse. Control of the size and encapsulation of nanoparticles was obtained by adjusting the molar feeding ratio of amphiphilic polymer: nanoparticles. For example, a ratio of 100 mol polymer: 1 mol nanoparticle produced multinanoparticle micelles with an average diameter of 30 nm. By increasing the feeding ration to 500 mol polymer: 1 mol nanoparticle, we were able to produce singly encapsulated nanoparticles with an average diameter of 13 nm. However, at feeding ratios below 100:1, uncontrollable aggregation occurred, and there were no recoverable micellar probes.

It is interesting to note that increasing the polymer:nanoparticle feeding ratio also increased shell thickness of the polymer coating. The thick PEO is thought to reduce adsorption by blood proteins and uptake by immune cells [133], and is in contrast to the typical “crew cut” polymers with short hydrophilic chains that have been used to create nanoparticle micelles in the past [123, 126, 128]. This range of shell thickness is due to higher density polymer packing in the single nanoparticle case as opposed to the multinanoparticle micelles. Studies of the interactions between nanoparticles and amphiphilic block copolymers have shown similar results (Rhyner and Nie, unpublished data). This observation also offers an explanation as to the uncontrollable aggregation that occurs at low polymer: nanoparticle feeding ratios: the polymer is sterically unable to stabilize large number of nanoparticles because of reduced polymer-polymer interactions at large micelle sizes. This subsequently causes the assembly process to

fail, and rapid nanoparticle-nanoparticle clustering occurs in an attempt to reduce the surface contact area with water.

In general, the size distribution by DLS shows a normal curve with a tail towards larger micelle sizes. There is also a lower limit for micelle size, that of the pure-polymer micelles, 11nm. Since the encapsulation process is fundamentally stochastic, there are always some singly encapsulated QDs produced along with large aggregates. This has an important implication for multimodal nanoparticle based probes: it is nearly impossible to generate completely uniform distributions of two different types of nanoparticles using this system. This same phenomenon has been observed by Taton and coworkers [126]. Further evidence to support this view is given in the Figure 3.6, where we show differential loading between red and green QDs across a micelle field. While this restricts certain applications, such as single-molecule multiplexed detection, it does not hinder end-use goals such as *in vivo* imaging. Further, the problem can be eliminated entirely by creating single-color micellar probes targeted against a variety of proteins. For example, a yellow QD-micelle probe could be targeted against protein A while red QD-micelles could be targeted against protein B. We have previously published results demonstrating the capability to detect multiple QD colors in a single animal with one imaging procedure [36].

As shown in Figure 3.3, the dialysis-based encapsulation procedure preserved many of the spectral properties of hydrophobic QDs, in particular their narrow spectral width, absorption spectra, and emission peak. Fluorescent imaging and other work in our lab demonstrated that the QD-micelles were highly resistant to photobleaching as with other QD coatings. In addition, it is possible to detect QD blinking both in the single-nanoparticle micelle and in the multinanoparticle micelles. However, the blinking is greatly reduced in the multinanoparticle case. This suggests this micelle encapsulation system may also have use for the study of QD-blinking, a phenomenon

which is poorly understood [134-137]. The slight haze in Figure 3.3A is due to micelle based probes outside of the microscope focal plane. This non-uniform coverslip coating

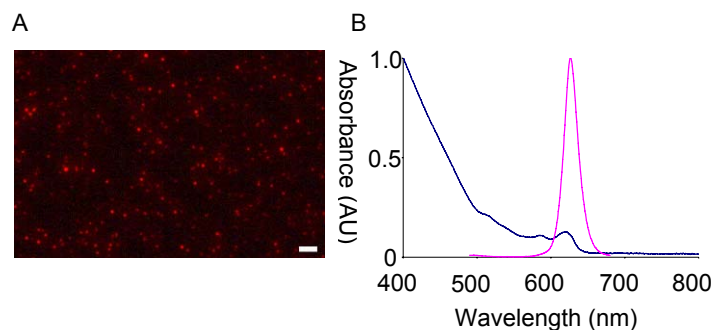


Figure 3.3: Fluorescent images and spectral data of micelle encapsulated QDs (100: 1 feeding ratio). A is a true color image taken on an epifluorescent microscope under excitation with a mercury arc lamp. The scale bar is 10 microns. B shows both the absorption and the emission spectra of these micelle encapsulated QDs.

is due to the poly-L-lysine used to assist in micelle immobilization for rapid image taking. Images can be obtained without this coating, but the process is complex, and often times, the total evaporation of water can cause micelle aggregation due to the surface tension of pure water on the coverslip glass.

There was a loss in QY from 75% to 30% (on average), as measured by comparison with Atto dye 610. We attribute this loss in QY to ligand exchange between the THF solvent and octadecylamine on the QD surface, as evidenced by a total loss in fluorescence after leaving solutions of QDs in THF overnight, and the fact that after exchange of THF for water, no further loss in QY was observed. Further, attempts to perform the entire encapsulation procedure in an oxygen-free environment indicated little or no difference between the open air case and the oxygen free-case, demonstrating

that the loss in fluorescence is not due to oxidation of the QD surface. Others have observed a similar phenomenon, but were unable to determine the cause [126].

It is important to note that high QYs are necessary for QD-micelle based probes to be useful for biological imaging purposes. Several reports have demonstrated that for truly useful biological labels, the lower bound of fluorescence QY should be no lower than 10% [66, 138], which our encapsulation procedure readily provides. It is tempting to suggest changes to the solvent system to enhance QY. However, we conducted extensive studies comparing various polymers and solvents that show only a few combinations of polymer-solvent pairs can create nanoparticle-micelles through dialysis. Specifically, the polymers must form strong hydrophobic interactions with the QD-surface ligands and the solvents used must solubilize all reactants well, including the nanoparticles and polymers. Further, the solvent system must be soluble in water to achieve facile solvent replacement and suspension in biologically useful buffers. For these reasons, THF and the PMMA-PEO polymer are well suited for producing the micellar probes described here.

Our first separation procedure utilized multiple rounds of ultracentrifugation as described in the methods section. Figure 3.4 shows an example from a series of studies conducted to determine optimal conditions for ultracentrifugation. The figure is from only one round of ultracentrifugation, but demonstrates several key points: First, as shown by comparing B and D, it is possible to separate pure polymer from micelles. Secondly, comparison of B and D show that this process is very inefficient as a significant portion of micellar probes are trapped in the discarded supernatant. Finally, Figure 3.4 demonstrates that multiple ultracentrifugation rounds are necessary to generate pure samples.

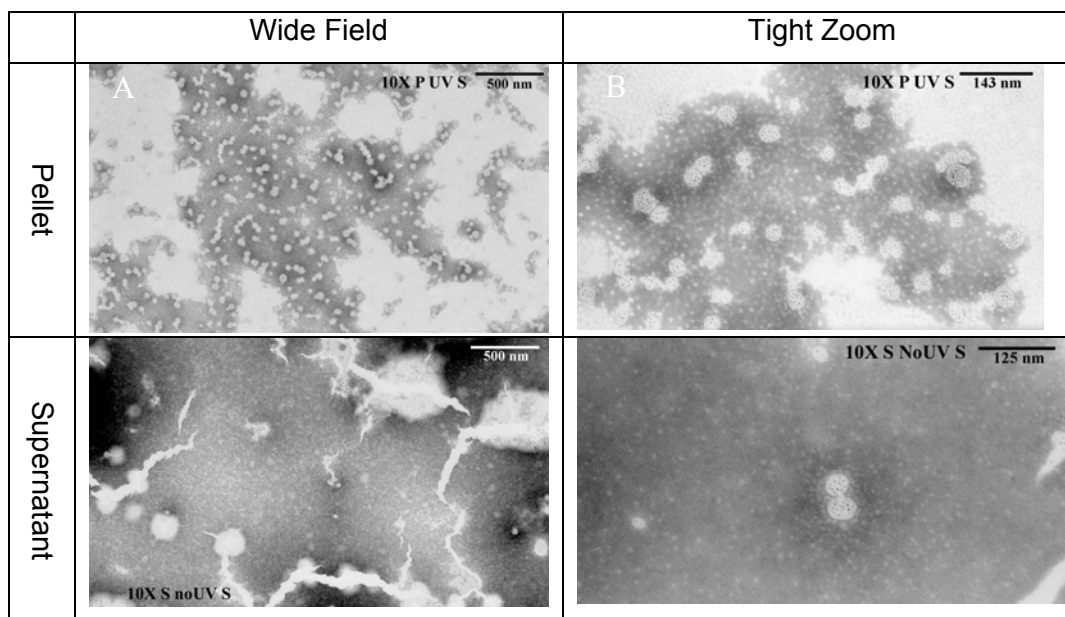


Figure 3.4: TEM micrographs of products from ultracentrifugation. This series of images are taken from a single micelle sample that was subjected to one round of ultracentrifugation at 125,000 rcf for 1 hour. A and C were taken at 25,000 X magnification while B and D were taken at 80,000 X magnification. This result indicated that it was possible to separate micelles from free excess polymer using ultracentrifugation.

Our first separation procedure utilized multiple rounds of ultracentrifugation as described in the methods section. Figure 3.4 shows an example from a series of studies conducted to determine optimal conditions for ultracentrifugation. The figure is from only one round of ultracentrifugation, but demonstrates several key points: First, as shown by comparing B and D, it is possible to separate pure polymer from micelles. Secondly, comparison of B and D show that this process is very inefficient as a significant portion

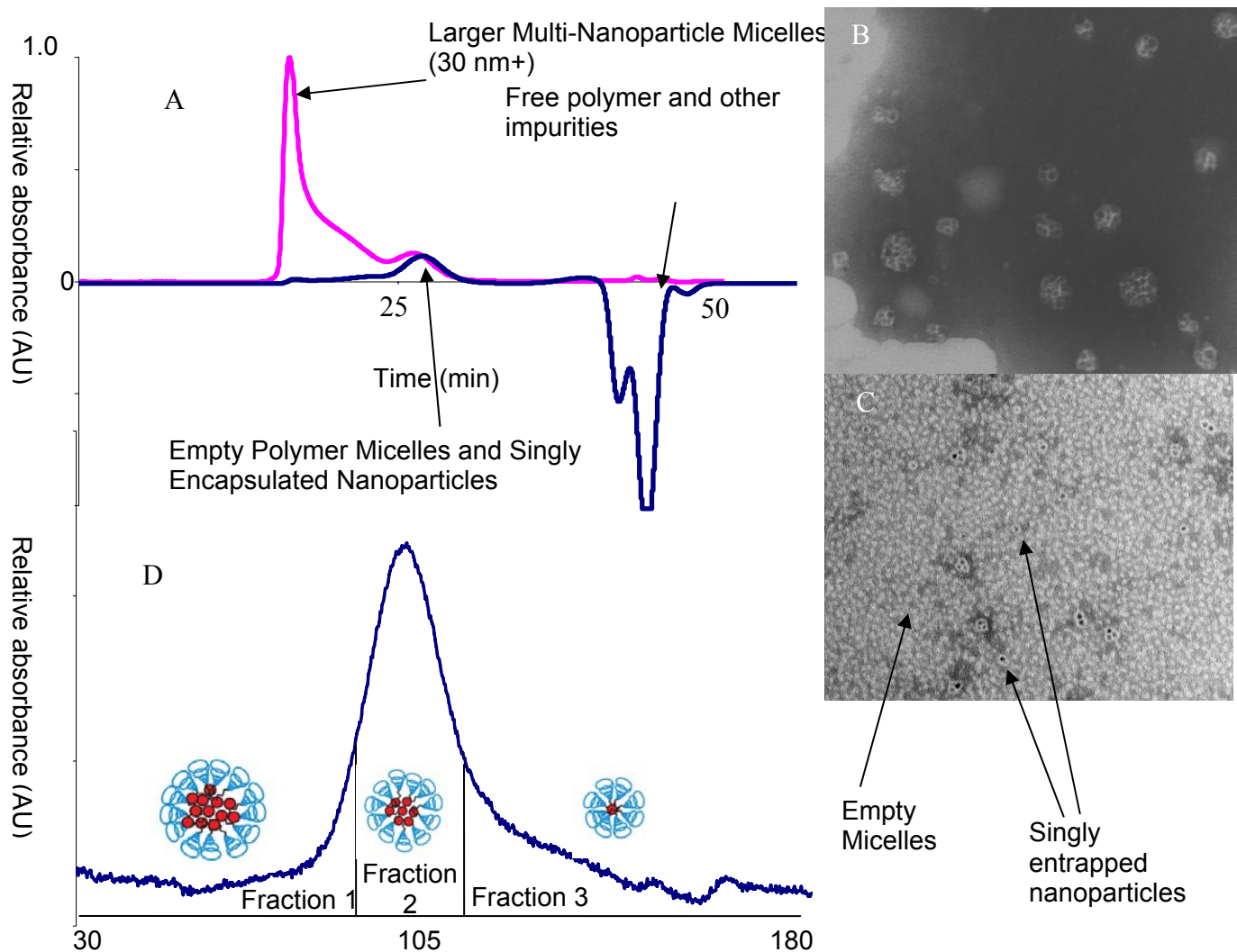


Figure 3.5: Chromatograms and TEMs of micelles separated using FPLC. Figure 3.5 A shows chromatograms of UV (pink) absorbance and refractive index (blue) from a 100:1 Polymer:QD sample separated using Superose 6 packing. B and C show TEMs corresponding to the peaks in A. It is important to note that the UV absorbance peak occurs when the bulk of micelles exit the system while the RI peak occurs when the empty polymeric micelles exit. B is a TEM image of the collected first peak while C shows the collected second peak. Finally, D shows the UV profile for the micelles fed through a column with a larger pore-size (sephadex 500HR).

of micellar probes are trapped in the discarded supernatant. Finally, Figure 3.4 demonstrates that multiple ultracentrifugation rounds are necessary to generate pure samples. Ultracentrifugation also presents several intractable problems: first, sample sizes tend to be small, secondly, it causes significant amounts of aggregation in the pelleted samples, and finally, results can vary widely depending on operator era. These problems combine to make it an inefficient, yet effective purification method.

As demonstrated in Figure 3.4, the centrifugation and ultracentrifugation methods previously used to purify nanoparticle micelles have significant disadvantages: they cause aggregation, are limited to small volumes, are time consuming, and have relatively low yields. To investigate new separation methods that have the advantages of scale-up and robustness while maintaining high separation efficiency, we turned Fast Protein Liquid Chromatography (FPLC), as shown in Figure 3.5. Figures 3.5 A, B, and C demonstrate the capability of FPLC to efficiently and rapidly separate nanoparticle loaded micelles from the surrounding excess polymer using Superose 6 packing. (A) shows the UV-absorbance profile in pink and the refractive index profile in blue. It is important to note that the UV absorbance peak occurs when the bulk of micelles exit the system while the RI peak occurs when the empty polymeric micelles exit, as should be expected. (B) is a TEM image of the collected first peak while (C) shows the collected second peak. Finally, (D) shows the chromatogram for the micelles fed through a column with a larger pore-size and bed volume column packing (Sephadex 500HR), demonstrating that very fine gradients (represented by fractions 1, 2, and 3) can be collected. FPLC has several advantages as compared to ultracentrifugation. First, there is no appreciable aggregation caused by the technique, meaning the final yields are much higher than with centrifugation. Secondly, by choosing different column pore size and elution volumes, fine gradients can be collected and scale up is easy to achieve. Thirdly, by automating the system, operator era is all but eliminated ensuring consistent,

reproducible results. Finally, the process takes much less time and effort than running multiple 1.5 hour rounds of ultracentrifugation and centrifugation. The dialysis procedure can easily produce greater than 10 mL of unpurified nanoparticle-loaded micelles with a final concentration of roughly 5 mg/mL. After multiple rounds of centrifugation and ultracentrifugation, however, it is not uncommon to only produce 500 μ L of pure samples at 2-3 mg/mL. The new FPLC approach can easily produce 10-15 mL of purified product at similar concentrations, and has the added advantage of being able to separate micelles containing many nanoparticles from those containing only a few.

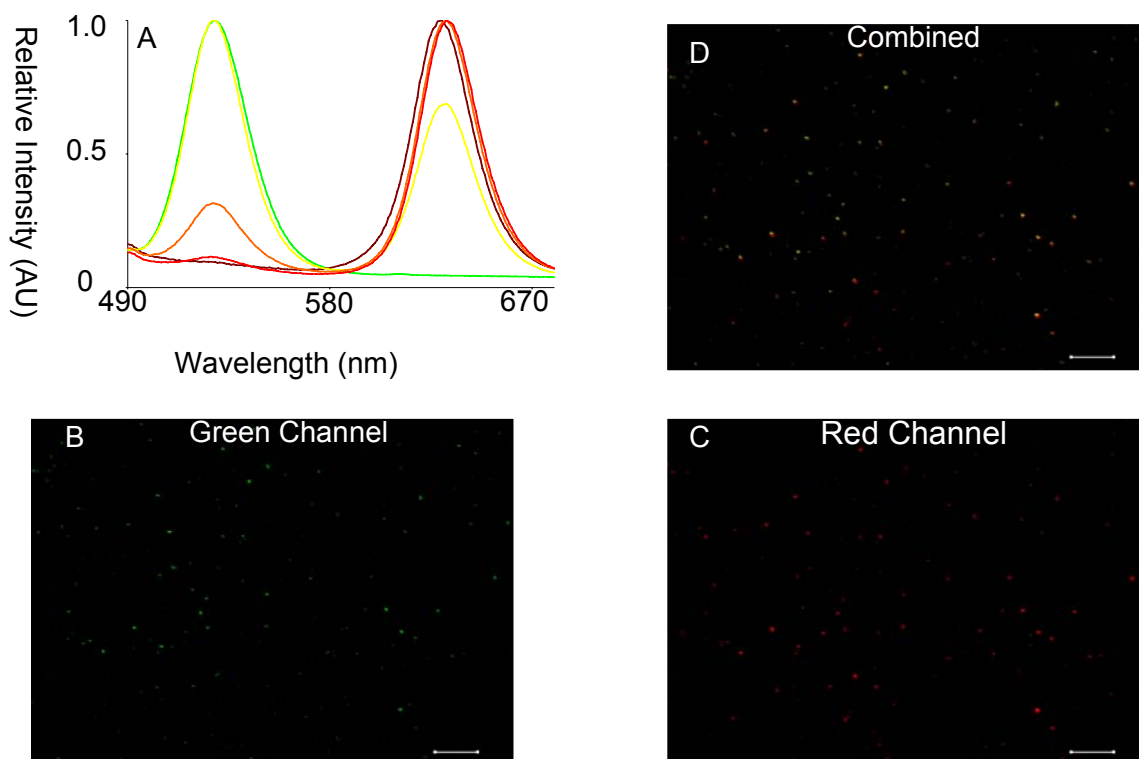


Figure 3.6: Fluorescent spectra and micrographs of multicolor micellar probes. (A) shows bulk fluorescent measurements of several different micelle samples. B-D show green, red, and overlaid images of a single sample. Scale bars are 10 μ m.

Figure 3.6 shows results from experiments considering the encapsulation of two colors of QDs. As shown in Figure 3.6A, the bulk solution color could be tuned very effectively using different feeding ratios of red and green QDs. However, when spread on a coverslip and imaged using a multichannel confocal microscope as shown in B, C, and D, it becomes quickly apparent the loading is not even, and micelles range from pure green to yellow to pure red. As demonstrated, the dialysis procedure was successful in solubilizing both the red and green QDs, but did not result in equal distribution of red and green QDs to micelles. This is most likely due to the fact that the dialysis procedure essentially relies on random entropic processes, and since red and QDs have much different diameters (2 nm compared to 6 nm), polymers behave differently when forced to interact with the two different sizes.

Development of Procedure

Several procedures were examined as possibilities before settling on the dialysis procedure. Figure 3.7 shows in schematic form the various approaches described investigated. As discussed in Chapter 2, each of these approaches has been used with varying degrees of success to encapsulate hydrophobic drugs. However, the adapted single solvent evaporation methods produced either large aggregates in the case of Approach I, or a total loss of fluorescence due to the heat and energy added by sonication, in the case of Approach II. Approach III is useful only when there is a tremendous excess of amphiphiles relative to nanoparticles, and can produce singly encapsulated probes in low quantities. In the multi-nanoparticle micelle case, large aggregates are formed.

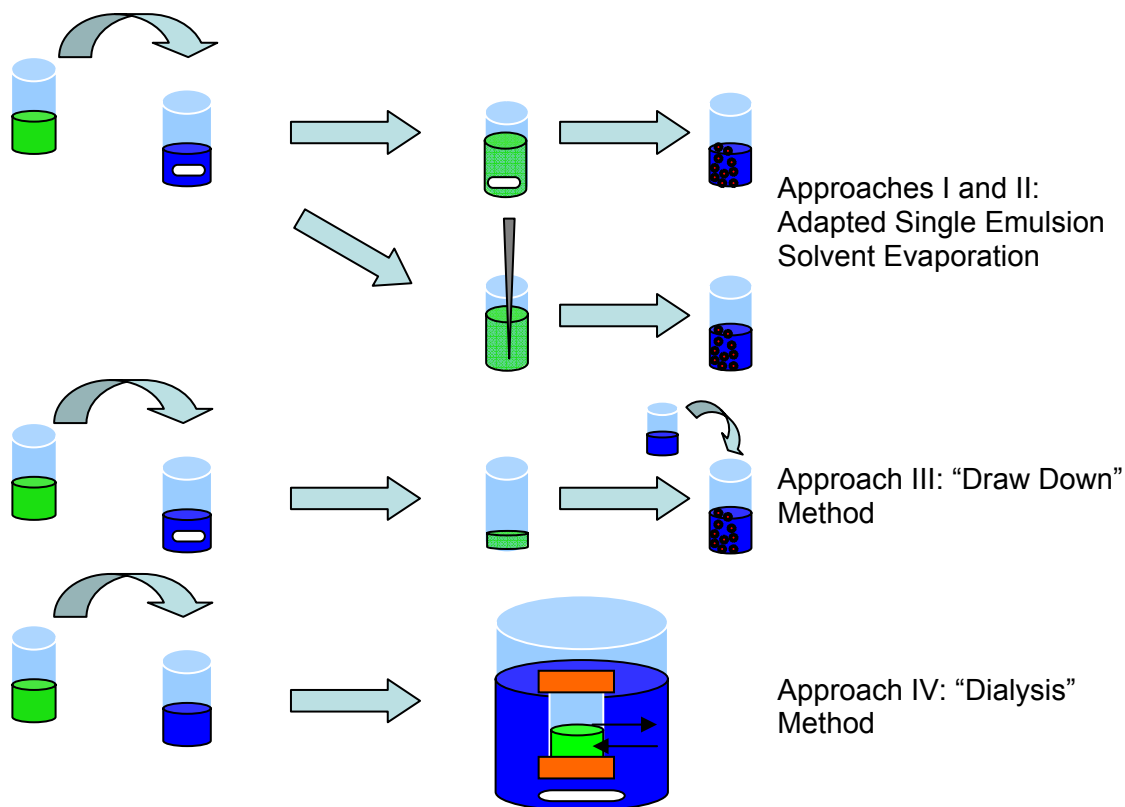


Figure 3.7: Examples of encapsulation methods investigated for this thesis.

We developed approach IV based on the same physical principles as approaches I, II, and III, but optimized the conditions for nanoparticles. There are special considerations when dealing with nanoparticles as opposed to small molecules, which are more commonly used in drug delivery applications. First, nanoparticles are highly sensitive to the solvent used, as demonstrated by the loss of fluorescence caused by tetrahydrofuran (THF). However, this solvent was carefully chosen after a wide-ranging search for other solvents. An ideal solvent for this encapsulation procedure must be able to solubilize the nanoparticles, the amphiphilic polymer, and be water miscible so that it can be easily removed via dialysis, and THF was the only solvent found that met all these criteria. Secondly, the solvent removal must occur relatively

slowly while being well mixed. This allows time for the polymers and hydrophobic capping ligands on the nanoparticle surface to form strong interactions. Finally, as indicated above, the approach must be relatively gentle to preserve the fluorescent properties of QDs. The dialysis procedure we developed meets all these requirements, and has the advantage of producing large quantities of micelles.

Design of Polymers

Similar to the development of the dialysis procedure, we used the drug delivery and nanoparticle encapsulation literature to draw inspiration for the choice of polymers. Figure 3.8 shows some of the polymers from literature that have successfully encapsulated nanoparticles. Figures 3.8 A-E show some structural similarities between the amphiphilic polymers while F shows the PMMA-PEO block copolymer that has been used extensively throughout this thesis. In G, we demonstrate the structure of our “ideal amphiphilic polymer” based on our survey, experimental results with a variety of amphiphilic polymers, and careful studies with polymer F. The polymers we investigated all shared three similarities: first, they contained greater than 50% hydrophilic content to ensure that they would form regular, star-micellar shapes. Polymers with greater than 50% hydrophobic content can form micelles [139-147], but the process is difficult to control and oftentimes, the resulting micelles are irregularly shaped [128, 148]. Secondly, the polymers each contained polyethylene oxide as the hydrophilic segment to reduce nonspecific adsorption and improve biocompatibility. Finally, each polymer had to contain a hydrophobic segment that formed strong non-covalent bonds with the surface ligands on QDS. Using these principles, we investigated a wide range of polymers before discovering the PMMA-PEO block copolymer shown in Figure 3.8F. The PMMA-PEO conjugate shares several similarities with our “ideal” structure: the

hydrophobic block contains linear side chains that interact strongly with the linear hydrophobic

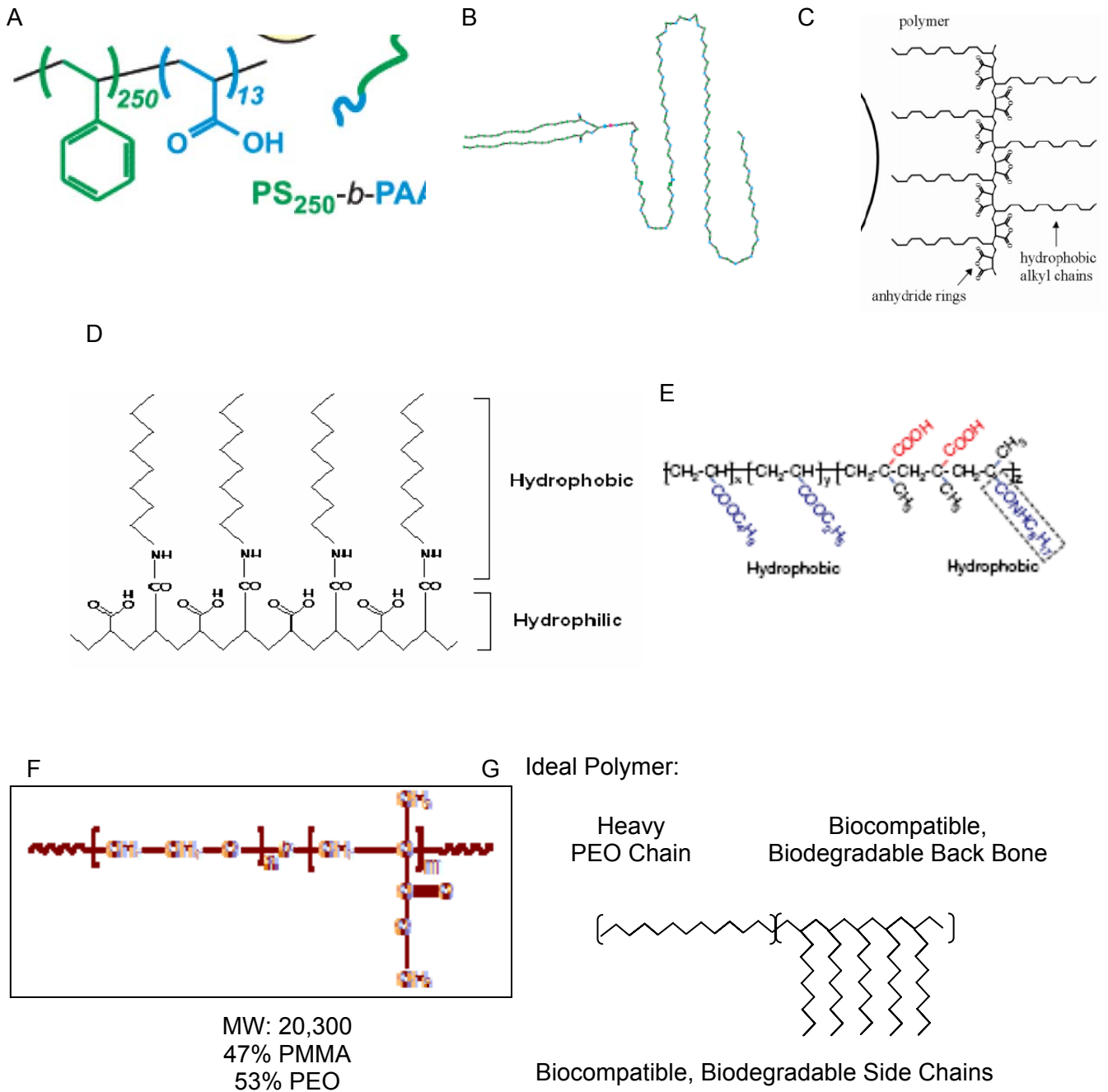


Figure 3.8: Amphiphilic polymers used to encapsulate hydrophobic nanoparticles in literature.

References: A) [123],[149] B) [96] C) [150] D) [151] E) [36]

molecules on the nanoparticle surface, it contains a large PEO block, and both the hydrophobic and hydrophilic segments are FDA approved polymers.

Separations and Scale-up

The dialysis procedure and purification methods presented here can produce large quantities of micelles. While the dialysis procedure requires large excesses of amphiphilic polymers, one could foresee a potential recycling of empty micelles for re-use in industrial applications. It is important to note that the separation and concentrations procedures presented can produce very high quality, high quantity probes as demonstrated in Figure 3.9. This purification and concentration is necessary prior to any conjugation of further derivitization of the probes, otherwise the empty micelles are likely to interfere with any desired reactions. However, for purely passive targeting applications, the empty micelles are unlikely to interfere, as they have no contrast in either optical or magnetic imaging, are small, and induce no biological response.

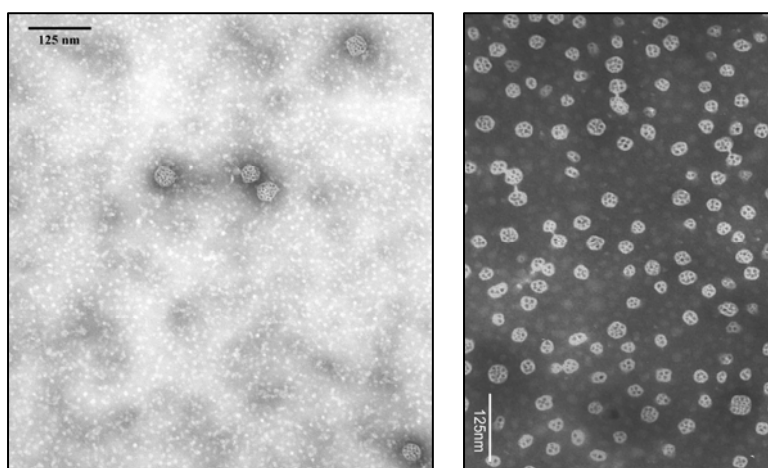


Figure 3.9: TEM images demonstrating the difference between the crude reaction product (A) and purified, concentrated micelles (B).

Multicolor Probes

Finally, it is important to briefly mention the problems with encapsulation multiple colors of QDs and possible solutions. First, as shown in Figure 3.10, there are two primary modes of interaction between the polymers and nanoparticles: interdigitation and coating. The entropic force that drives assembly is the minimization of contact area between the polar water molecules and nonpolar coating ligands on the surface of QDs. However, this process is affected in kinetic way by the ability of the polymers to conform to securely coat QDs. As such, in the case of smaller, green QDs, the polymers can not bend quickly or tightly enough to coat each QD regularly. However, in the case of red QDs (and, as we shall see in Chapter 4, MNPs of roughly the same size, about 6 nm), the polymers can form stable bonds quickly enough to ensure relatively uniform coating and distribution. The QDs used in this thesis consisted solely of traditional, binary QDs (CdSE/ZnS). However, a possible way to achieve uniform color micelles would be to use ternary QDs (CdSE/CdTE/ZnS) which are composition and not size tunable.

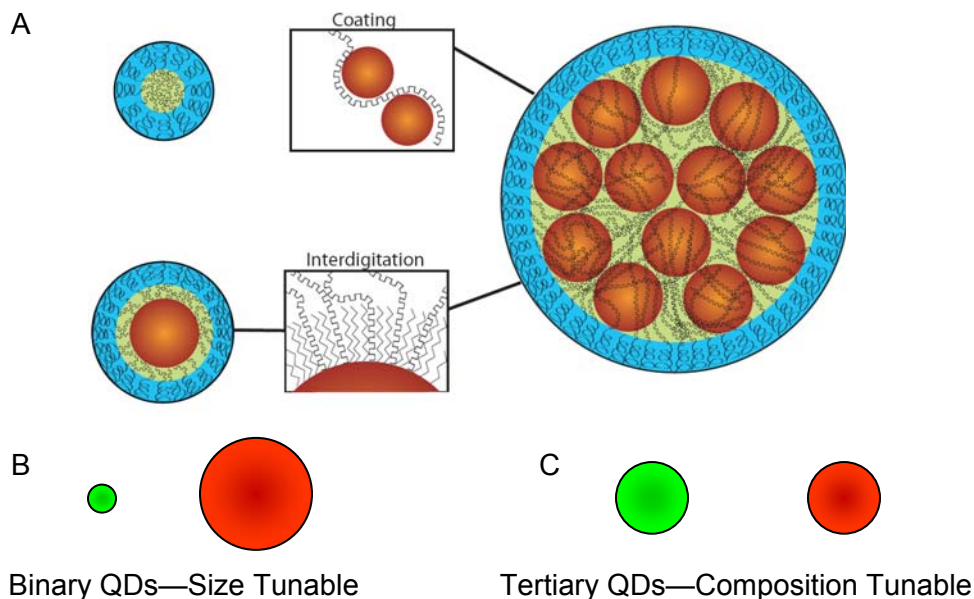


Figure 3.10: The two main interactions that dictate the stable assembly of the micellar probes.

3.6 CONCLUSIONS

In conclusion, we have demonstrated a new approach for the development of bioimaging probes using amphiphilic block copolymers and high quality inorganic nanoparticles. The synthetic approach demonstrated here displays two main advantages: 1) the use of high quality QDs increases QY to a maximum of 40% and 2) the dialysis and purification methods presented are amenable to scale up for future *in vivo* use. Having established these methods as the basis for the rest of this thesis, the coming chapters will explore expansion of the basic passive optical probes and the performance of the surface coating in a variety of environments.

CHAPTER 4

SYNTHESIS AND CHARACTERIZATION OF OPTOMAGNETIC MICELLAR PROBES

4.1 ABSTRACT

The focus of this chapter is on the development of dual modality optomagnetic probes. Dual modality imaging refers to the combination of optical and magnetic imaging capabilities in a single injectable agent. These types of probes are emerging as a focus of biomedical research, and hold promise for many advantages over traditional technologies. Here, we demonstrate the synthesis and characterization of dual modality probes using the dialysis methods presented in Chapter 3. We demonstrate effective T2-weighted MRI enhancement and optical imaging from a single injectable dose. Further, we show that the physical properties of the micelles produced are nearly identical to those of purely optical micelles, in good agreement with our expectations.

4.2 INTRODUCTION

MRI relies on the magnetic moment of protons in strong magnetic fields to create measurable signals as they align with, and then relax from the external field. The magnetic moments of protons are exceedingly small, so that only 3 out of every 1 million protons are actually aligned to the external field at any given moment. However, because there are so many protons in the human body (there are 6.6×10^{19} protons in every mm^3 of water), this realignment of magnetic moments creates an observable signal. By using two magnetic fields, one which aligns protons, and one which is applied perpendicularly as a pulse, the protons are forced to align with one magnetic field, and then suddenly are disrupted and forced to align with the second field. Once the second field pulse is over, the moments relax back to alignment with the primary field. It is this relaxation that creates MRI contrast signals. Figure 4.1 depicts this process graphically.

In Figure 4.1A, a large collection of protons with magnetic moment m are aligned with external magnetic field B_0 . In 4.1B, a pulse has realigned m to be perpendicular to B_0 . In 4.1C,

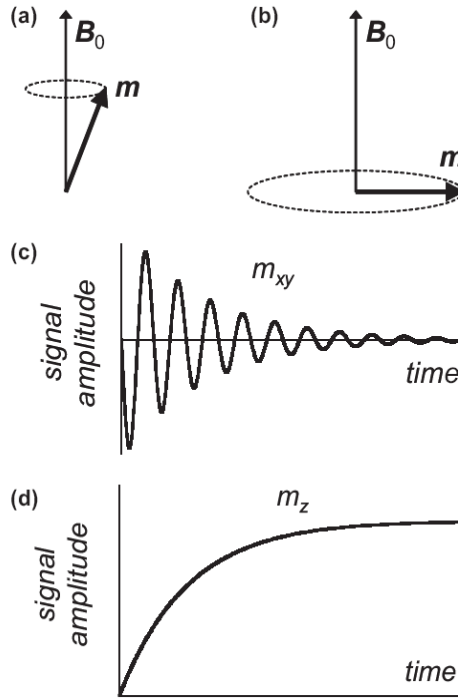


Figure 4.1: Illustration of the creation of MRI signals.. In (A), the net magnetic moment m is aligned with external field B_0 . In (B), a second field is applied as a pulse, perpendicular to field B_0 . (C) shows the relaxation of the in-plane components of vector m , while (D) shows the longitudinal relaxation. Adapted from Pankhurst, et al [152].

after the pulse, m_{xy} oscillates as m precesses around the z axis and relaxes, providing the origination of the T2-weighted MRI contrast. While in 4.1D the signal along the longitudinal axis relaxes in a regular fashion, providing T1-weighted MRI contrast.

While this process can create observable signals solely from water molecules, the speed with which relaxation occurs can be affected by the addition of magnetic

contrast agents that have inducible magnetic moments. There are several types of magnetic material that have been investigated, including ferromagnetic, paramagnetic, and superparamagnetic substances. Ferromagnetic materials have highly ordered magnetic states and are permanently magnetized. Paramagnetic materials can be induced to have magnetic properties by application of a magnetic field. Finally, superparamagnetic materials are a special case of paramagnetism where the magnetic moment of the particle is free to fluctuate in response to thermal energy, as a result of the particles' small size [153].

The most popular contrast agent is a paramagnetic chelate of gadolinium, Gd^{3+} -diethylenetriaminepentaacetate (Gd-DTPA). This compound is very stable, water soluble, and contains seven unpaired electrons, giving it a very strong paramagnetic character. Hydrogen atoms of water in proximity to such chelates experience faster T1 relaxation, thus producing T1-weighted MRI contrast images. These chelates are routinely used for imaging interstitial and vascular space, and are subsequently excreted by the kidneys. Researchers have been studying ways to improve upon the Gd-DTPA chelates in the following ways: enhancing the signal strength by modifying the molecular structure, allowing more water interactions, increasing the plasma half-life beyond the current typical values of 70-100 min, and increasing gadolinium concentrations at the target location [118, 154, 155].

While these enhancements are desirable, several challenges face groups attempting to modify the molecular architecture of Gd-chelates. First, because the Gd ion is highly charged, it can be toxic without proper chelating agents. Secondly, each chelating agent has a dramatic effect on the overall properties of the compound. For instance, several related Gd-chelates are explosive upon mixing with water. Thirdly, it is hard to envision a scenario where Gd-Chelates are conjugated to target ligands in high enough concentrations to bring about true targeted-imaging capabilities [118, 156].

To address these issues, great attention has been given to superparamagnetic materials on the nanoscale. In general, the MNPs consist of iron oxide alloys with the general formula MFe_2O_4 where $M = Co, Ni, Mn, Mg, Fe, Pt, \text{ etc.}$ [116]. However, the most common and widely used nanoparticles are those composed of iron oxides. These superparamagnetic nanoparticles typically shorten T2 relaxation times, thus giving rise to T2-weighted images, as opposed to Gd-DTPA. Fe_2O_3 and Fe_3O_4 iron oxide nanoparticles can be synthesized in the same manner, exhibit similar sizes, shapes, and magnetization characteristics, with the important distinction that Fe_3O_4 bulk materials have an 18% greater magnetic saturation than Fe_2O_3 materials (127.1 emu/g iron vs 108.7 emu/g iron) [37]. To achieve true superparamagnetic behavior, these particles must be below 10 nm in size, and should be highly uniform [153].

Aside from their superparamagnetic behavior, nanoparticle based MRI contrast agents are of interest for many of the same reasons QDs and other nanoparticles are of interest in general. Firstly, their small size allows them to interact closely with cells that are thousands of times larger. Secondly, the ability to tune their surface properties through coatings and conjugations make them a versatile tool for biological applications. Thirdly, they may have significant targeting and multifunctional capabilities as compared to traditional Gd-chelates. In particular, iron oxide nanoparticles benefit from biocompatibility and stability that is clearly a complicating factor in terms of engineering capability of Gd-chelates. For these reasons, we became interested in incorporating iron oxide nanoparticles into our micellar structure to create a novel dual-modality imaging probe.

Dual modality imaging is a subset of both MNP research and QD research. Investigators have realized several advantages of these types of probes for cancer research, including the ability to use MRI functionality prior to surgery to develop surgical plans and then use optical properties intrasurgery to ensure complete removal of cancerous lesions. In addition, other functionalities can be envisioned depending on the exact structure of the dual modality probe. For instance, recent work has shown the

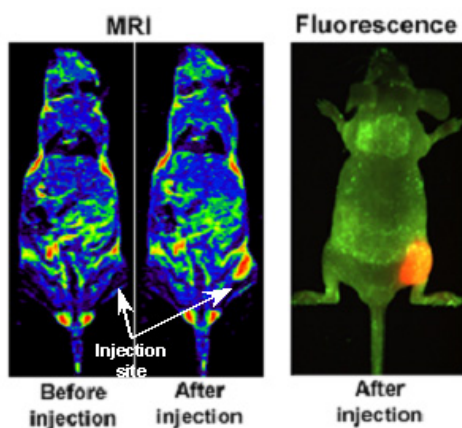


Figure 4.2: Dual-modal imaging using QD-based probes as the fluorescent reagent.

(A) shows a T1-weighted imaging of a GD-coated QD. (B) shows optical images. (Gao and Nie, unpublished data)

ability to combine the spatial resolution of MNP based MRI followed by the functional capability of NIR reactive dyes [157]. Several different combination probes have been attempted, including: incorporating Gd chelates with QDs [113], combining fluorescent molecules with MNPs[158-161], directly synthesizing dual modality compounds [162-164], and various methods for combining MNPs and QDs [165-167].

As shown in Figure 4.2, recent work in our group has demonstrated the feasibility of dual modality imaging using our high quality QDs and a gadolinium chelate. For these probes, Gd-ions were entrapped in a hydrophobic layer coating the QD. While the

probes showed excellent T1 contrast, problems occurred relating to stability and arduous synthetic route. To overcome these hurdles, we decided to use our new encapsulation procedure to create dual modality probes, realizing advantages could be had in terms of stability, synthetic ease, and scale-up.

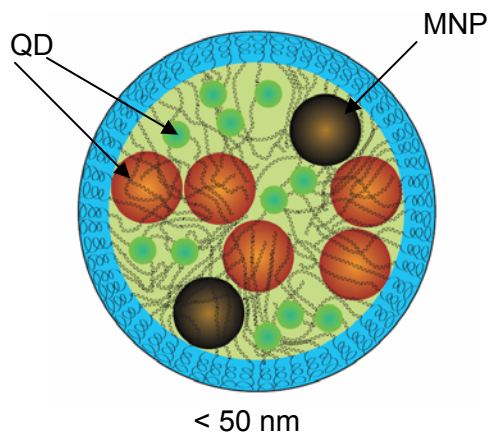


Figure 4.3: Ideal optomagnetic probe. This conceptual figure demonstrates the ideal optomagnetic probe that is the focus of this chapter.

The design for this new probe is shown in Figure 4.4. We hoped to combine multiple types of nanoparticles on the interior of our micelle structure. Our rationale for this process is that superparamagnetic MNPs and QDs are roughly the same size and have very similar surface coatings owing to their similar synthetic methods. Further, based on previous work in our group [168], we expected to retain the excellent optical properties of QDs while adding new MRI contrast capabilities.

4.3 METHODS

Synthesis

The general synthetic methods described in Chapter 3 were followed, with the following modifications:

T1-weighted Optomagnetic Probes

To create T1-weighted optomagnetic probes, we used the gadolinium conjugate Gadolinium tris(2,2,6,6-tetramethyl-3,5-heptanedionate), which is a hydrophobic gadolinium chelate sold under the name Resolve-AI by Sigma Aldrich. The compound was dissolved in THF and added in stoichiometric ratios to the pre-dialysis feeding mixture.

T2-weighted Optomagnetic Probes

Fe₃O₄ MNPs were synthesized in oleic acid coordinating solvent following a procedure developed by Sun [116]. After synthesis, the particles were suspended in hexane. From this hexane solution, the particles were precipitated using methanol and resuspended to desired concentrations in THF. They were then added to the pre-dialysis mixture in desired ratios.

Physical Characterization

We followed the general procedures for TEM, DLS, Fluorescent microscopy, and spectroscopy as described in Chapter 3 without change.

MRI Scanner

A Phillips MRI scanner operating at 1.5 tesla was used to obtain ghost images of micelles in 2.5 mL Eppendorf tubes. Scans of both T1 and T2 relaxivity were taken and data was analyzed using standard techniques.

ICP Spectroscopy

After characterization of purified samples using the MRI Scanner, 3 mL of sample were degraded by adding 1 mL of piranha solution. The mixture was evaporated over night in a desiccator, and sent to UGA Chemical Analysis Lab for ICP spectroscopy. There, the samples were run on a Thermo Jarrell-Ash 965 Inductively Coupled Argon Plasma Spectrometer. Several different sample concentrations were submitted to create a standard curve.

4.4 RESULTS AND DISCUSSION

T1 Imaging

As shown in Figure 4.4, our attempts to create a T1 imaging probe using a hydrophobic gadolinium chelate met with mixed results. The PMMA-PEO clearly solubilized the chelate, as samples containing no polymer precipitated upon dialysis while polymer containing samples formed clear micelle solutions, as in the case with nanoparticles. Prior to purification, the micellar probes exhibited strong T1 signal

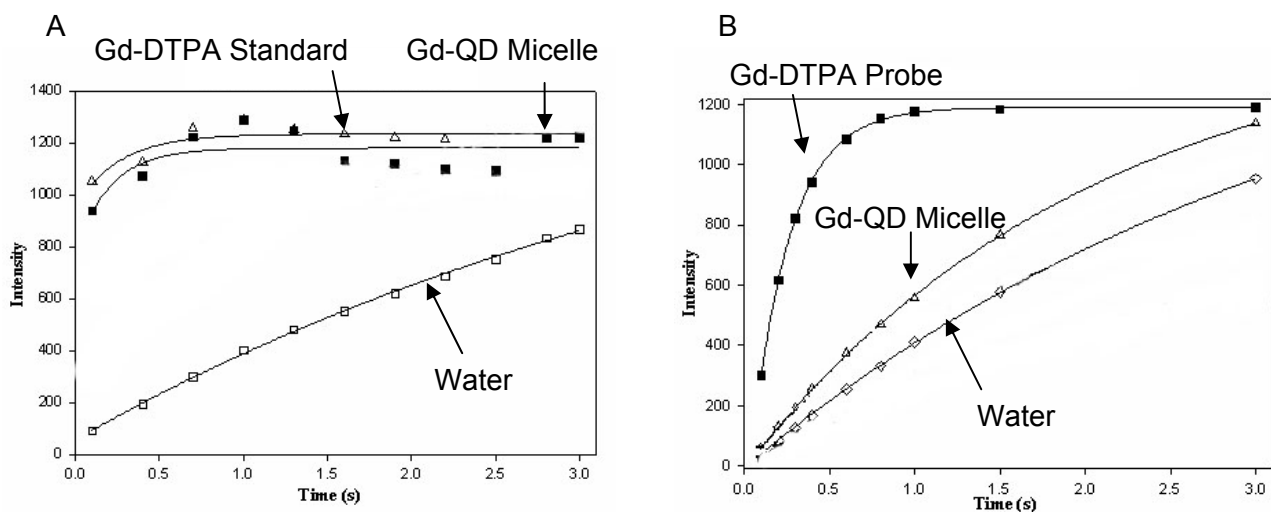


Figure 4.4: MRI scanner results of resolve-AI loaded micelles. (A) before and (B) after purification.

intensity, but after purification, there was little or no signal available. This indicates that the gadolinium is either leached out during the purification process (only ultracentrifugation was utilized as FPLC was unavailable) or the Gd chelate was entrapped in empty micelles. There are several possible solutions to this issue including conjugating Gd ions to either the nanoparticle surface or the polymer itself, or developing a cross-linked polymeric shell that would not leach out entrapped gadolinium. In addition, these samples could be purified using FPLC to determine their true Gd content.

T2 Imaging

As shown in Figure 4.5, we were able to tune the T2 relaxivity of dual modality optomagnetic probes while retaining the exceptional optical properties of QDs by varying the relative ratios of QDs to MNPs in our dialysis feeding ratio. Figure 4.5A shows that even after incorporation of MNPs, the optical properties of QDs are well conserved. As expected, there is some observed loss in QD fluorescence as compared to QD-only micelle probes, which increases with the MNP loading ratio. This loss has been noted previously [168] and is most likely due to the broad optical absorption spectra of mixed valence Fe_3O_4 MNPs. This highlights another advantage of the approach used here: previous attempts to create dual modality micellar probes have focused on use of γ - Fe_2O_3 MNPs, while we have used Fe_3O_4 . Since the saturation magnetization of pure Fe_3O_4 is greater than that of γ - Fe_2O_3 [37], we can use smaller amounts of iron oxide nanoparticles to achieve the same level of T2 contrast. As a result, for biomedical imaging application, moderate MNP:QD ratios would suffice, thus maximizing both the MRI contrast capabilities and optical brightness of these probes.

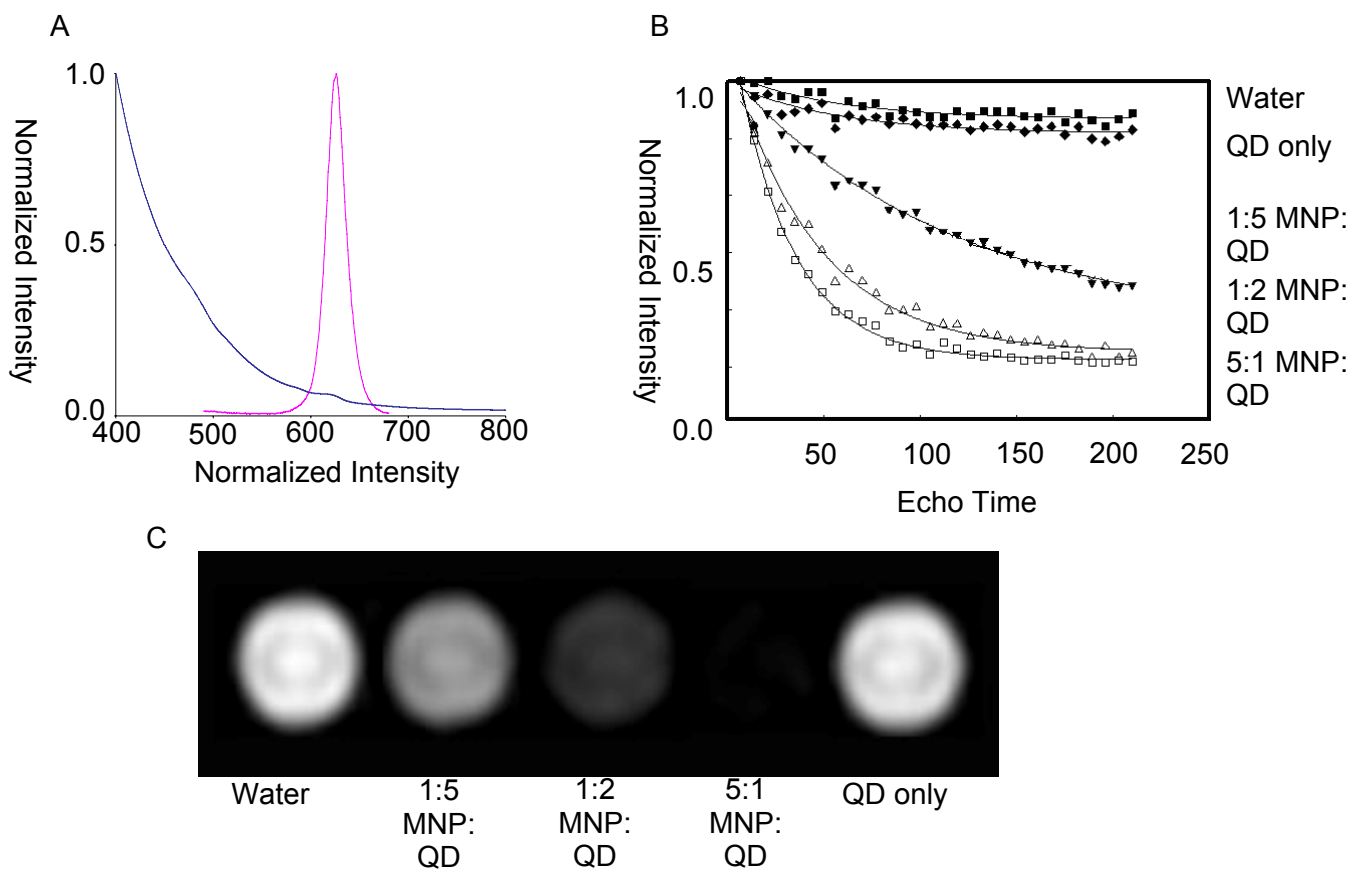


Figure 4.5: Fluorescent and magnetic resonance characterization data for optomagnetic probes. (A) shows fluorescent emission and absorption for the 1:2 MNP:QD feeding ratio micelle sample, while (B) shows normalized T2 relaxivity curves for each of the samples in (C). Images in (C) were taken on a Philips 1.5 Tesla MRI scanner.

Figure 4.6 compares the size and morphology of T2-weighted Optomagnetic micelles and QD-only micelles. The size and shape are nearly identical to QD-only micelles (Figure 3). This uniformity of probes containing similar size nanoparticles is an important property for optimization of future *in vivo* research, and further supports

observations about the dependency of the assembly process on nanoparticle size. It is impossible to accurately distinguish QDs from MNPs in this image owing to their almost identical size. The probes' size and morphology are nearly identical to the QD-only micelles presented in earlier. This is expected, as the size and surface coating of the Fe_3O_4 nanoparticles are nearly identical to that of QDs.

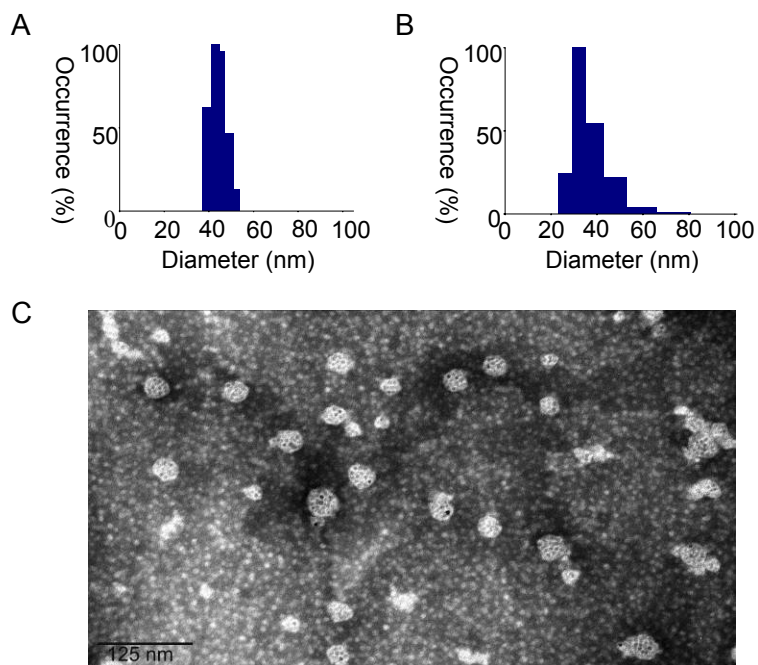


Figure 4.6: DLS and TEM data for optomagnetic probes. (A) DLS size distribution for optomagnetic probes (1:2 MNP:QD ratio) (B) DLS size distribution for QD-only probes. (C) TEM of unpurified optomagnetic probes in (A).

Iron Oxide Nanoparticle Concentration

In order to better understand the final loading ratios of the nanoparticle probes and the effect of MNP absorbance on QD fluorescence, we determined the final MNP:QD ratio per micelle after encapsulation. As such, we degraded the optomagnetic micelles using piranha solution, and then submitted them to the University of Georgia

Chemical Analysis Lab for elemental analysis using ICP spectroscopy. This experiment provided us with information describing the number of iron atoms relative to the number of cadmium atoms, as shown in Table 4.1. We submitted multiple samples to create a standard curve, and determined the average cadmium to iron ratio in each of our samples. For continuity, we have only presented the characterization data for the 1:2 MNP:QD feeding ratio sample described in Figure 4.5.

Table 4.1: Summary of ICP spectroscopy results from UGA Chemical Analysis Lab

Element	Low Micelle Concentration	High Micelle Concentration
Cd	0.143	2.903
Fe	0.346	6.336
Cd/Fe ratio	2.41	2.18

Using this as our starting point, we set out to determine the relative number of QDs and MNPS in the sample. Thus, we calculated the number of Fe atoms per MNP and Cd atoms per QD. To estimate the number Fe atoms per Fe_3O_4 nanoparticle, we used the published bulk density of magnetite (Fe_3O_4) 5175 g/cm^3 , its formula weight, and the volume of a 6 nm nanoparticle. Thus, the number of iron atoms per nanoparticle is:

$$5.175 \frac{\text{g}}{\text{cm}^3} \times \frac{4}{3} \pi 3^3 \text{ nm}^3 \times \frac{1 \text{ cm}^3}{1 \times 10^{21} \text{ nm}^3} \times \frac{1 \text{ mol Fe}_3\text{O}_4}{231.55 \text{ g}} \times N_A \times 3 \frac{\text{mol Fe atoms}}{\text{mol Fe}_3\text{O}_4} \times = 4565 \frac{\text{Fe atoms}}{\text{nanoparticle}} \quad \text{Equation 4.1}$$

Next, we must estimate the number of cadmium atoms per QD using the bulk density of Cadmium Selenide. For this calculation, we assume the QD is 5 nm, subtracting 1 nm to account for the ZnS capping shell that gives the measured diameter of 6 nm.

$$5.655 \frac{\text{g}}{\text{cm}^3} \times \frac{4}{3} \pi 2.5^3 \text{ nm}^3 \times \frac{1 \text{ cm}^3}{1 \times 10^{21} \text{ nm}^3} \times \frac{1 \text{ mol CdSe}}{191.37 \text{ g}} \times N_A \times 1 \frac{\text{mol Cd atoms}}{\text{mol CdSe}} \times = 1164 \frac{\text{Cd atoms}}{\text{nanoparticle}} \quad \text{Equation 4.2}$$

Taking these estimates together with the results from the ICP spectroscopy, we can estimate the ratio of QDs to MNPs to be approximately:

$$\frac{[\text{QD}]}{[\text{MNP}]} = \frac{[\text{Cd atoms}] \left(\frac{\text{nanoparticles}}{\text{Cd atoms}} \right)}{[\text{Fe atoms}] \left(\frac{\text{nanoparticles}}{\text{Fe atoms}} \right)} = 0.43 \left(\frac{4565}{1164} \right) = 1.7 \frac{\text{QDs}}{\text{MNP}} \quad \text{Equation 4.3}$$

In this range, the interference due to MNP absorption should be moderate, as described previously [168]. By adjusting this feeding ratio, it will be possible to tune the optomagnetic probes such that either the fluorescent or magnetic resonance properties can be favored.

4.5 CONCLUSION

We successfully combined MNPs with QDs to create high quality optomagnetic probes that have several potential applications in biomedical diagnostics. Although our synthesis of T1-weighted probes met with mixed results, it is likely that the MNP loaded T2-weighted imaging probes have more utility as a nano-scale MRI contrast agent, because smaller doses of T2 imaging agents are needed to create an observable signal, while much higher concentrations of T1-weighted imaging agents must be localized.

It is important to note that the assembly process was able to create relatively uniform micelles using two nanoparticles of roughly the same size, whereas in the two color micelles described in the previous chapter, significant polydispersity was observed. It is interesting to note that very strong T2 signal was observed even with a relatively moderate ratio of QD:MNP. This shows iron content could be modified to modulate the T2 relaxivity between strong and low, similarly the QD content can be adjusted

depending on how bright the probes must be, within the limitations of an approximately 30 nm particle. However, it is important to note that recent evidence in our lab has implied that iron oxide nanoparticles can interfere with QD fluorescence, both by blocking excitation and emission. Thus, it is likely that there is a non-linear relationship between MNP concentration and resulting fluorescence of the combination probes. On the whole, the dual modality probes presented here represent a new method for combining the superior fluorescent properties of QDs with the T2 imaging capabilities of Fe_3O_4 MNPs.

CHAPTER 5

PERFORMANCE OF MICELLAR PROBES IN CHEMICAL AND BIOLOGICAL CONDITIONS

5.1 ABSTRACT

Here we test the performance properties of our micellar probes in variety of chemical and biological conditions that simulate potential end use applications. We find that, compared to several other nanoparticle coatings, our probes perform well. In particular, their strong stability and low immunogenicity shows promise for these probes to find ultimate end use in *in vivo* research.

5.2 INTRODUCTION

As discussed in Chapter 2, surface coatings are one of the most important aspects of determining the final biocompatibility and utility of the entire nanoparticle construct. Specifically, properties such as charge, coating thickness, uniformity of coating, exposed functional groups, and hydrophobicity are important properties that dramatically effect probe performance. An ideal coating will preserve the nanoparticle's imaging properties, allow conjugation to biological targeting ligands, and prevent opsonization and uptake by immune cells. Further, the coating should be stable in a wide variety of chemical conditions to ensure modifications and survival in the harsher *in vivo* environments. The ability of PEG to stabilize and improve biocompatibility for both injectable reagents and implanted devices has been known for some time, and many approaches have been utilized to incorporate this strategy into these engineering constructs [169-172].

While the general principles affecting nanoparticle biodistribution are well-known, there have been few high-quality, specific studies for QD and MNPs and coating materials in the literature. The earliest work in this area focused on drug delivery

carriers such as liposomes, dendrimers, and other polymeric carriers [173-177]. Early on, investigators found that PEG coating enhanced circulation lifetime. For example, PEGylation was found to increase times for 80% clearance in mice from 1 to 14 hours, and to double the percentage injected dose found in solid tumors [178-180]. These early studies led investigators to hypothesize that the interaction between components in the blood with the surface coatings of drug delivery carriers were the primary factors responsible for blood clearance. Specifically, blood components such as albumin, complement, immunoglobulins, fibronectin, apolipoproteins, c-reactive protein, and beta2-glycoprotein have all been found to interact strongly with drug delivery carriers, and to reduce their circulation times [181, 182]. Further, direct attachment of antibodies in a process known as opsonization can cause immune cells to uptake these same systems. In good agreement with earlier *in vivo* work, investigators found that PEGylated liposomes bound only a small percentage of these blood proteins, as compared to non-PEGylated versions (900 g protein/mol carrier vs. 100 g protein/mol carrier) [183].

Further in depth studies have compared PEO chains of varying lengths for their ability to reduce protein absorption and increase circulation times. In general, these studies have pointed towards larger PEO polymers being important for stable, long-circulating probes [133, 184].

While the literature supports our decision to use large PEO chains as the outer surface of our micellar probes, it is important to note existing comparisons between PEO coatings and PAA-like coatings. PAA coatings expose large numbers of carboxyl groups to the surrounding fluids, and as a result, have a large negative zeta potential [151]. Several groups have conducted comparisons between charged and neutral polymeric coatings. In general, they have found that charged coatings tended to be eliminated from the bloodstream quickly while neutral coatings exhibit longer circulation times [141].

Specifically, PEGylation was shown to reduce the zeta potential of PEI gene delivery vehicles by 10 fold, which led to a dramatic reduction in plasma-induced aggregation and a huge increase in circulation time and gene delivery [185]. Similarly, we have observed that highly charged particles tend to be rapidly taken up by cells in vitro.

While the discussion thus far has focused on organic nanoparticles, studies of inorganic nanoparticle coatings are just beginning. Great interest follows these studies, both from the academic and regulatory communities, as there are many questions surrounding the ultimate biocompatibility of inorganic nanoparticles in general and QDs specifically. Reports demonstrating toxicity of some QD preparations but not others [186, 187] have pointed towards the high importance of surface design for these molecules. For example, PEG coated QDs were not toxic in vitro at high particle concentrations, but QDs coated with charged polymer coatings exhibited cytotoxicity at 40x lower concentrations [187]. Further, coating thickness was shown to play a role in the ability of reactive oxygen species to diffuse away from QD surfaces and harm intracellular machinery [112]. In an important work, Bhatia and coworkers demonstrated that QDs damaged by oxidative environments release Cd ions, and can subsequently demonstrate increased cytotoxicity [111]. Similar results relating cytotoxicity to surface coatings have been observed for MNP preparations [188-190]. However, the design criteria are more flexible since the constituent iron oxide materials are biocompatible, and several similar preparations have already been approved for clinical trials.

With this background in mind, we compared our micellar formulation with 4 other common coatings in chemically and biologically stringent conditions. These included charged and non-charged surface coatings, and were conducted under controlled conditions. For a more applications oriented performance test, we compared the stability of micelles to a model of PAA coating in whole human blood to highlight the

differences between our micellar preparations and those previously used [34, 123-126, 128, 145, 147, 191-193].

5.3 MATERIALS AND METHODS

Nanoparticle Preparation

The micellar nanoparticles were synthesized as described in Chapter 3. All other nanoparticles used in this chapter were prepared according to previously published procedures.

Photooxidation

For photooxidation experiments, QDs were diluted with borate buffer to an optical density of 0.01 at the first exciton peak, and 800 μL was transferred to a 1 mL glass cuvette, resulting in a dead volume of 200 μL of air. Cuvettes were sealed and placed in front of an ultraviolet lamp with 254 nm illumination and spatially homogeneous photon flux, as verified using a power meter.

Acid Etching and Chemical Oxidation

For acid-etching experiments, QDs were diluted with borate buffer to an optical density of 0.05 at the first exciton peak, and 900 μL of this solution was transferred to a cuvette. Then 100 μL of 1 M HCl in water was added. The resulting pH was verified to be 1, and the cuvette was sealed to prevent solvent evaporation. Absorption spectra were obtained periodically. Chemical oxidation was performed similarly, but 100 μL of 3% H_2O_2 (w/v) was added instead of HCl.

Stability in Cell Culture

HeLa cells (ATCC number CCL-2) were cultured in ATCC-modified Eagle's Minimum Essential Medium (EMEM) with 10% fetal bovine serum at 37°C (5% CO_2), and grown in 8-well LabTek chambers (Nalgene Nunc) to achieve 20% confluency. 24 hours after seeding, cells were rinsed with serum-free medium, and QD-containing

serum-free medium (20 nM) was added. After 20 minutes at 37°C, imaging was performed with a spinning disk confocal microscope (Ultraview, Perkin Elmer) using 488 nm laser excitation, a long pass filter, and a high sensitivity CCD camera (ORCA-ER, Hamamatsu).

Fluorescent Imaging

FACS (Fluorescence Assisted Cell Sorting) was used to separate out granulocytes from whole blood. The cells were incubated with QD samples either containing plasma solution or PBS Buffer. Upon incubation in certain specific conditions, such as 4°C or 37°C temperature, the cells were washed twice by centrifugation at 400 x g for 5 minutes followed by removal of the supernatant. The washes were important to remove unbound QDs from the solution as they could increase background interference and make it difficult to image single leukocytes. Following the last washing step, the sample volume was reduced to increase cell concentration. To a clean No. 1 Cover Glass (Corning), 4 µl of cell suspension was added and gently spread uniformly in circular motions. The solution was not spread too thin to prevent quick drying of sample. Images were obtained using a 100 x oil immersion objective (NA 1.35, infinity-corrected), a mercury-arc lamp with bandpass excitation filter (BP460-490) and emission filter (510LP). Images were captured using an Olympus CCD Camera (Model, Olympus, WA) attached to an Olympus IX-71 inverted epifluorescence microscope. Bright field, fluorescence, and combination images (bright field + fluorescence) were obtained by varying exposure settings based on signal intensity. Prior to taking images granulocytes labeled with FITC-anti CD66b antibodies, green signal confirmed positive cell sample. In order to make sure that the samples indeed didn't have any QDs bound or internalized, fluorescence images long exposure times were used.

Gel Mobility Shift Assay

Agarose gel (0.8% w/v) was prepared in 0.5 x TBE Buffer (Tris-HCl + Borate Buffer + EDTA, pH 8.0) and heated for 75 seconds in a microwave at maximum power until a clear solution was obtained. The agarose solution was cast in a refrigerator for 30 minutes and placed into an electrophoresis tray containing 0.5 x TBE Buffer. Upon loading the QD samples, a voltage of 100V was applied for 1 hour. The gel was then imaged using a UV transillumination system (BioRad, Hercules, CA).

FPLC

Samples were incubated for 24 hours with 250 μ l of 30 nM nanoparticles and 250 μ l purified blood plasma and run through a Sephacryl 500HR column at a flow rate of 1 ml/min. The AKTA machine was equipped with a 545 nm filter which dramatically reduced UV absorption signal from blood proteins and allowed viewing of only nanoparticles signal. The pure plasma background chromatogram was subtracted from the micelle-plasma chromatogram.

5.4 RESULTS AND DISCUSSION

Photooxidation

Our photochemical stability assays demonstrated the ability of the polymeric micelle coating to stabilize and protect QDs in a variety of harsh conditions. Figure 5.1 shows the results of a photooxidation experiment where QDs were exposed to a high-intensity UVC light for extended periods of time. In general, QDs that were coated with amphiphilic polymers exhibited longer stability than those that replaced the hydrophobic stabilizing ligands on the QD surface. Specifically, QDs with small molecule coatings such as mercaptopropionic acid and polyethyleneimine experienced severe degradation

after many hours of exposure. MPA QDs precipitated, probably due to oxidation of the thiol ligand [194] while PEI QDs eventually dissolved completely.

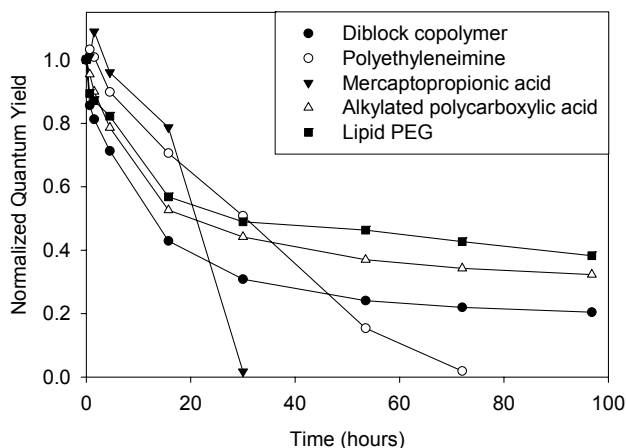


Figure 5.1: Photooxidation of QDs dissolved in borate buffer. All QD solutions were originally the same concentration, and QY was measured periodically during exposure to ultraviolet light. Before plotting, the QY for each QD type was normalized to its initial value. At the 30 hour time point, MPA-coated QDs had precipitated from solution.

It is interesting to note that the lipid PEG, alkylated polycarboxylic acid, and PMMA-PEO all protected QDs from severe photooxidation. These results indicate that the thick polymer shells are important not only for preventing free radicals from diffusing away from the QD surface, as noted previously, but also for preventing their formation in the first place. By protecting the QD for long periods of time, these coatings create the possibility of repeatedly exciting the same QD sample in a patient or animal with no deleterious effects due to the excitation itself. Further, it is important to note that the conditions used for these photooxidation studies far exceed what would be commonly used in biological studies. For instance, the vast majority of *in vivo* and *in vitro* imaging

experiments take place over 1-2 hours at most, and utilize a 124 mW laser excitation at 488 nm. Under these conditions, all QD samples exhibit exceptional stability.

Acid Etching

Figure 5.2 shows the results of acid-etching experiments in 0.1 M hydrochloric acid. MPA and polycarboxylic acid polymer coated QDs aggregated immediately upon addition to the acidic solution. This rapid precipitation can be attributed to attack of the carboxylic acid group by the strong hydrochloric acid, and illustrates one disadvantage of incorporating large numbers of charged functional groups on nanoparticle surfaces. In contrast, PEI coated QDs appeared to be stable indefinitely in these conditions. This phenomenal stability is due to the strong positive charge of the coating helping to buffer hydronium ions near the QD surface, thus increasing the local pH.

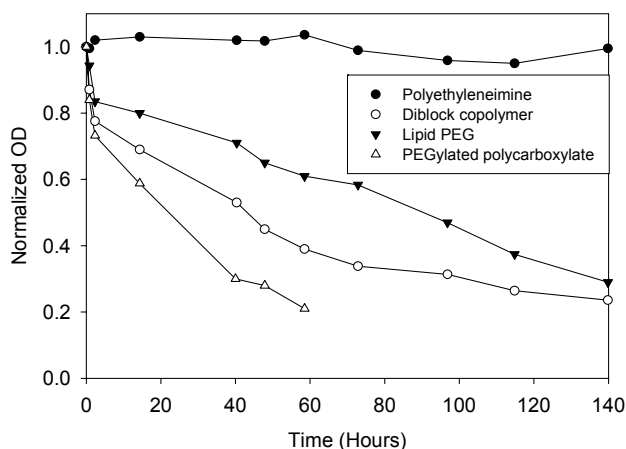


Figure 5.2: Acid-induced etching of QDs. QDs were resuspended in an aqueous solution of pH 1 and monitored via absorption spectrophotometry. QDs coated with MPA or alkylated polycarboxylic acid are not shown because they immediately aggregated. Besides PEI-coated QDs, all samples blue-shifted in absorption. After 60 minutes, PEGylated QDs coated with the amphiphilic polycarboxylate precipitated.

The two neutral coatings with thick polymer shells, PMMA-PEO and lipid-PEG help protect QDs from these strong conditions, but do eventually degrade and lose their fluorescence. The neutral charge and thick coating help to slow the attack of the strong acid, and demonstrate the surprising stability of these coatings, even without crosslinking. The results indicate that PEO based coatings could be used in acidic conditions, potentially even for imaging the gastrointestinal system *in vivo*, while imaging probes with charged polymer coatings are likely to be ineffective in such harsh environments.

Chemical Oxidation

To assess the stability of coated QDs in oxidative environments, we exposed the various QD samples to hydrogen peroxide. This is an important and physiologically

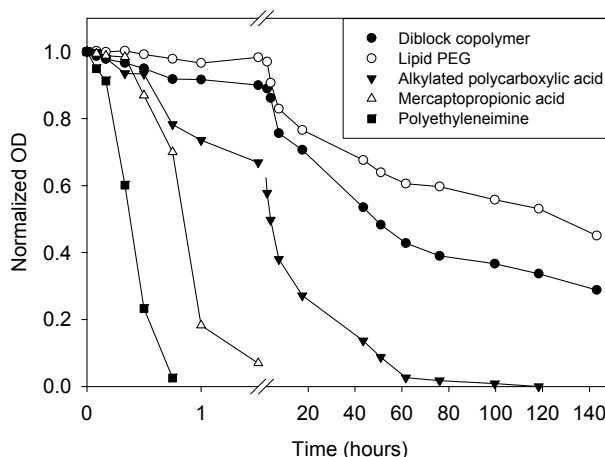


Figure 5.3: Hydrogen peroxide-mediated degradation of QDs in borate buffer. All QDs were originally the same concentration, and optical density was used to determine the stability of the nanoparticle suspensions.

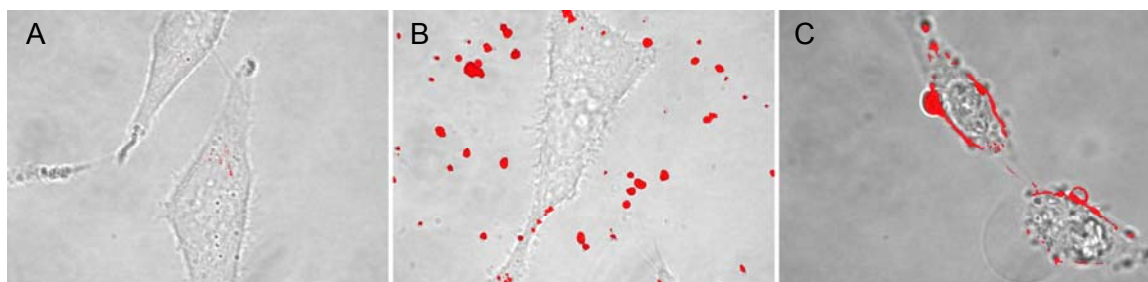
relevant assay, as nanoparticles taken up by phagocytosis will be exposed to oxidative environments intended for the elimination of microorganisms. A recent study has

indicated that this oxidative environment can induce the loss of cadmium ions, a key suspect in the toxicity of QDs [110, 111, 187, 195]. Thus, it is desirable for a biologically relevant coating to prevent chemical oxidation.

Figure 5.3 shows the results of the oxidation experiments. Because MPA and PEI QDs immediately lost fluorescence upon addition to the peroxide solution, we used optical density to measure colloidal stability. While the photooxidation experiments verified colloidal stability of the polycarboxylic acid from light-induced oxidation, the peroxide experiment illustrated this coating is susceptible to oxidation when strong agents are at high concentrations in proximity to the QD surface. Thus, this assay agreed with the other assays presented in this chapter in that QDs coated with small molecules and charged surfaces tended to be less stable owing to the oxidation of the ligands.

Stability in Cell Culture

To test the stability of the 5 coatings in an *in vitro*-imaging application, we incubated the QDs with Hela cells in serum-free media at 37⁰C for 20 minutes. Figure 5.4 shows the results of this experiment. Under these conditions of complex media containing salts and biological molecules, the charged surface coatings precipitated very quickly while neutral, PEGylated coatings were able to stay in soluble. These results are in good agreement with studies of nanoparticle-protein binding [196, 197], and point out an important limitation of charged nanoparticle surface coatings: it can be very difficult to imagine their utility in an *in vivo* environment within the complex milieu of blood. While these coatings could be useful for *in vitro* assays where cellular penetration is an important goal, they are unlikely to find *in vivo* applications, as their circulation lifetimes are short.



HeLa cells exposed to
20 nM QDs for 20 min.
at 37°C

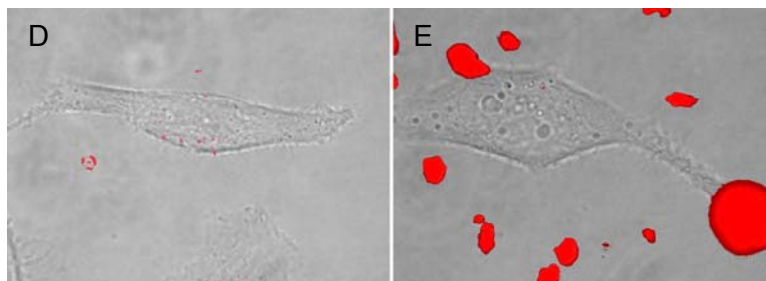


Figure 5.4: Stability of QD coatings in cell culture at 37 °C, visualized via bright field and confocal fluorescence micrograph overlays, focused near the cell centers. The micellar amphiphilic block copolymer (A) and lipid-PEG (D) were stable under these conditions, and showed very little uptake by cells. (B) MPA coated QDs and (E) those coated with the alkylated polycarboxylic acid were unstable and aggregated in solution, yielding insoluble precipitates. (C) QDs coated with PEI were stable in solution and showed rapid association with cellular plasma membranes.

Comparisons of PAAcoatings and PMMA-PEO Micelles

Having verified our coating stability in well controlled in vitro conditions, we decided to test the probe performance in a difficult, application oriented series of assays. For this series of experiments, we compared our PEO micelle coating to a PAA based coating. As mentioned in Chapter 3, PAA-based polymers have been used to create multinanoparticle micellar probes, and have even been suggested for *in vivo* imaging

applications. As such, we decided to test each probe's stability and usefulness in whole human blood and plasma.

Figure 5.5 shows the results of a novel assay using FPLC to detect aggregation in nanoparticle samples incubated with plasma. FPLC was utilized as opposed to DLS for several reasons. First, the vast array of proteins in human plasma make it difficult to analyze DLS data because of strong interference at all size ranges. Secondly, because our micelle probes contain QDs, and QDs absorb strongly in the UV, we hypothesized an UV detector-equipped FPLC could differentiate between micelle-containing probes and human plasma. Finally, the FPLC technique would ultimately allow isolation of micelles bound to blood proteins, and in principal, isolation and identification of the bound proteins. To accomplish this, we used a large pore-size column that (Sephadex 500HR) that can separate proteins up to 400 nm in size.

Figure 5.5c demonstrates that the background absorbance from human plasma is actually quite strong, even when a 545nm excitation filter is used. Despite this strong background, we were able to normalize our samples and subtract the background. As shown in Figures 5.5 A and B, the PMMA-PEO micelle probes clearly elute at longer times as compared to the PAA based coatings. Comparison with controls show that the PAA based coatings tend to shift dramatically from elution times of 165 minutes to only 50 minutes. This dramatic shift in elution time corresponds to a several-fold increase in hydrodynamic radius. In contrast, micelle based QDs elute at 120 minutes in both the plasma samples and in controls.

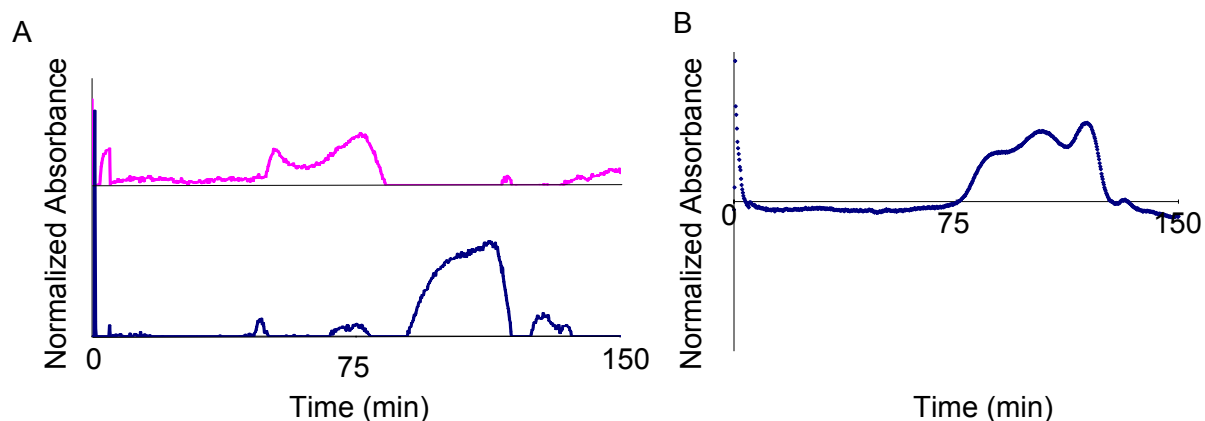


Figure 5.5: FPLC chromatograms comparing various nanoparticle coatings. (A) PAA (pink, top) and PMMA-PEO micelle encapsulated QDs and the chromatogram of pure human plasma (B). The multiple peaks in the micelle samples correspond with a variety of protein-nanoparticle aggregates forming.

The broad, strong background absorbance of plasma interferes with data collection in these assays, but there are several strategies to overcome this issue. First, we used non-diluted plasma while others have used plasma diluted up to 100x for similar assays [184]. Secondly, while UV absorbance is less susceptible to interference than DLS, fluorescence measurements should have no background whatsoever. Unfortunately, most FPLC columns are not equipped with fluorescence detectors, and at the time of writing, none was under development in our laboratory.

These results are further supported by Figure 5.6, which demonstrates fluorescent imaging of PMMA-PEO micelles compared to PAA micelles after incubation

in human plasma for 24 hours. The PMMA-PEO micelles show very little aggregation while the PAA micelles are significantly aggregated. This data is in good agreement with Figure 4.4, which shows charged polymers are quickly aggregated in biological buffers

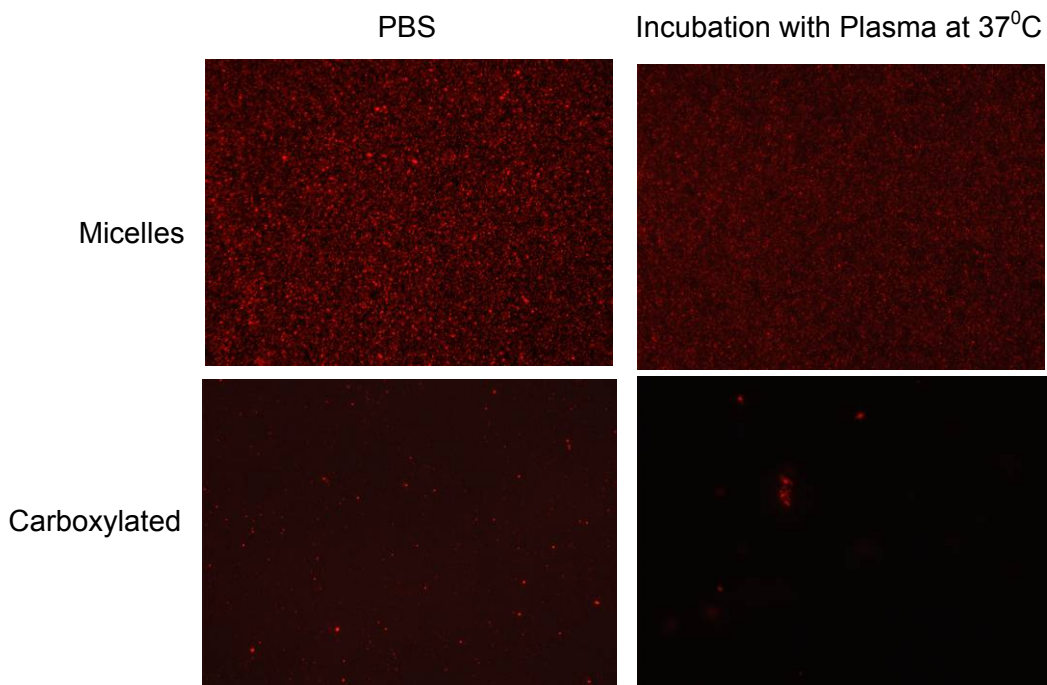


Figure 5.6: Fluorescent micrographs comparing micelle encapsulated QDs with carboxylated QDs. Micelles (A) and QD-COOH (B) both spread uniformly on coverslips without plasma incubation. After incubation for 6 hours with plasma, the micelle encapsulated QDs (C) still spread uniformly while the carboxylated QDs (D) are significantly aggregated.

Having verified that the micelles are not significantly aggregated by blood plasma, we wanted to determine whether or not there were any adsorbed proteins that could create a micelle-protein complex. This type of non-covalent interaction has been observed by others for all nanoparticle coatings. To determine this, we decided to use

agarose gel-electrophoresis. The choice of this technique would allow us to easily visualize differences in electromobility, whereas our FPLC and imaging assays only allowed us to assess hydrodynamic radius. To accomplish this, we incubated several nanoparticle samples with human plasma for 24 hours, and then loaded them into consecutive lanes in an agarose gel. The results in Figure 5.7 highlight several interesting phenomena that were observed. First, the PMMA-PEO micelles do not leave the well appreciably with no plasma incubation while PAA coated nanoparticles show significant mobility, due to their high surface charge. What is interesting is that these behaviors are reversed after incubation with plasma for 24 hours. In the case of the PAA coated QDs, the *lack* of mobility must be due to the aggregation of these QDs, as supported by the results from the FPLC and fluorescent imaging data. However, in the case of the micellar probes, the change in behavior must be solely due to non-covalent interactions with the plasma. These noncovalent interactions then result in charged micelle-protein complexes that can migrate through the gel. These conclusions are supported by several observations. The FPLC and imaging data demonstrate that the micelles exhibit no dramatic increase in aggregation or hydrodynamic radius, which is supported by the fact that the micelles are able to migrate after incubation with plasma, and are not trapped inside the wells, as is the case with PAA QDs. Further, the fact that micelles do not migrate in gels with no plasma indicate they must have gained charge to gain electrophoretic mobility.

Finally, after 24 hours incubation with whole human plasma, some protein adsorption is inevitable for any surface coating, as demonstrated by studies measuring protein binding content [183].

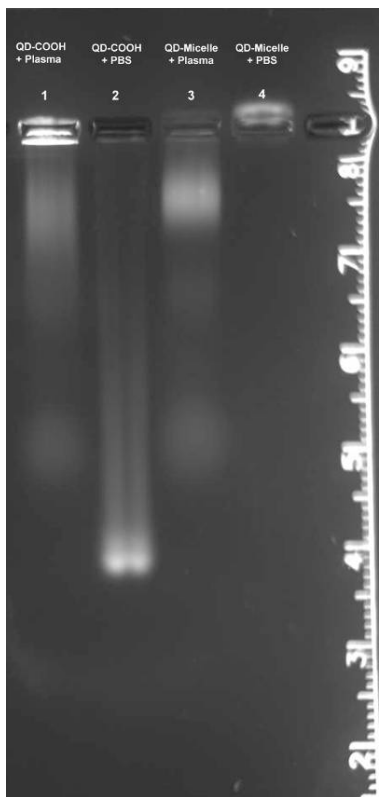


Figure 5.7: Agarose gel electrophoresis of sample with and without incubation with plasma. After incubation with plasma, QD-COOH mobility is all but stopped (lanes 1+2). Micelles do not migrate without plasma because they lack charge (lane 4). However, after incubation, they do exhibit some mobility.

If the probes do not form noncovalent micelle-protein complexes, there is the possibility that the micelles are forced to move due to the overall charge of the plasma, much like a traditional loading buffer. Another possibility is that the proteins interfere with the micelles, and “push” them along through the gel although they are not truly bound together. This would make sense as many the proteins in plasma have similar elution time to micelles in FPLC. Whatever the case, the interaction clearly does not cause the degree of aggregation seen with PAA coated micelles, or any adverse effects to the micelles’ emission properties.

After examining the interaction of PMMA-PEO micelles and PAA in the presence of plasma, we turned our attention to whole blood assays with phagocytic white blood cells present. Specifically, we chose to investigate the interaction with isolated granulocytes. Granulocytes are the scavengers of the immune system, and remove foreign bacteria and toxic substances through phagocytosis. The stages of phagocytosis include opsonization, uptake, release to the granulocyte cytoplasm, and finally, break down by lytic enzymes in the granulocyte. Opsonization and degradation are the two most important processes our design accounts for. Opsonization is the tagging of foreign bodies by blood born proteins, which then trigger uptake by granulocytes. Because our probes are highly resistant to protein binding, they reduce the opsonization process and increase circulation lifetimes. Secondly, during the degradation process, granulocytes use the myeloperoxidase enzyme. This enzyme catalyzes a reaction with hydrogen peroxide which breaks down the foreign substance. As we have demonstrated, not only are our micellar probes stable against opsonization, but they remain stable in hydrogen peroxide environments, which are even more stringent than what is found in a granulocyte.

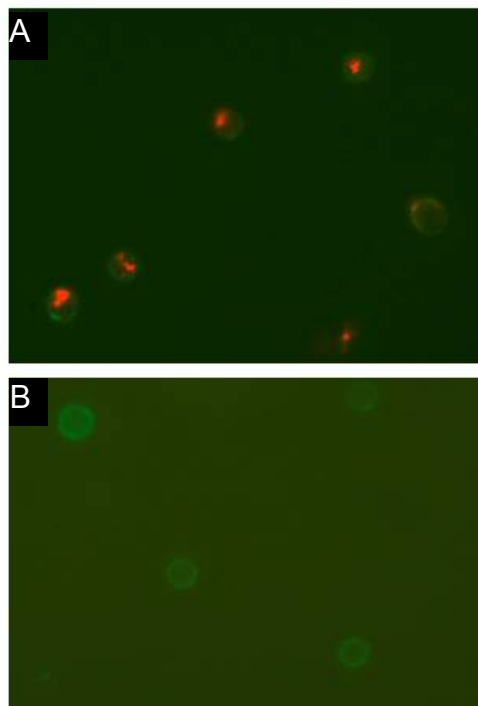


Figure 5.8: Fluorescent micrographs of QD samples incubated with granulocytes for 24 hours. Comparison of PEG coated micelles to carboxy coated QDs. (A) Carboxy coated QDs are rapidly taken up by granulocytes while PEGylated micelles are not internalized (B) – 40x FITC = Granulocyte

These conclusions are supported by the data shown in Figure 5.8. The images demonstrate that the aggregated PAA coated QDs are taken up by granulocytes while the micellar probes are stable even after a 24 hour incubation. These results compare well with all the other data presented in this chapter, and provide further evidence that the micelles are not tightly bound to proteins, as would be the case were they opsonized. This result also is encouraging for the ultimate use of these probes in *in vivo* imaging applications.

5.5 Conclusions

The results presented in this chapter demonstrate some of the main advantages of our PEGylated micellar multi-nanoparticle coating as opposed to carboxylated

coatings used by others. It is not surprising that PEGylation greatly reduces nonspecific adsorption of plasma proteins and uptake by granulocytes. However, the degree to which these micellar probes are stable both in stringent biological and chemical conditions is surprising. The wide range of chemical, photophysical, and other conditions explored here show the wide diversity of these probes, and point towards *in vivo* utility.

CHAPTER 6

ADDITION OF FUNCTIONAL GROUPS ON MICELLAR PROBE SURFACE

6.1 ABSTRACT

Having established the superior biological and chemical stability of our probes, which implies their usefulness to passively target cancer through EPR effect, we turned our attention to the addition of ligands to enable their active cancer targeting capability. The overall strategy presented is to introduce active sites in the micelles' PEO shell with functionalized block copolymers. This chapter explores two different materials that we used to incorporate primary amine groups on our micellar surface.

6.2 INTRODUCTION

The incorporation of active targeting ligands to our micellar probes is a key step in their development towards clinical utility as cancer imaging agents. Actively targeted constructs are desirable for detecting small cancer sites where the EPR effect can not be leveraged. For example, in the case of early metastasis detection, the secondary tumors are so small that they have yet to develop a mature vascularization network, making it dubious to rely on entrapment by the associated blood vessels for targeting [198-200]. However, if high-tumor affinity biological molecules could be attached to the probe surface, they would serve as molecular recognition sites and bind to a greater extent than passively targeted probes.

In general, active targeting has been shown to be effective in certain cases where specific markers are known, such as with the drug Iressa, radioactive iodide and other highly specific therapies [201]. However, as a general tool, there is a significant amount of research to be done. Several groups have pointed towards the possibility of targeting nanoparticles to various tumor markers, both in the tumor vasculature [202]

and on the tumor cell-membrane [203]. While in general, the interest has been on using antibodies and larger biological targeting moieties, recently, focus has shifted to small molecules such as folic acid [50, 173, 175, 204-209].

The active targeting hypothesis is somewhat controversial in the literature, as previous attempts to conjugate antibodies to liposomes and polymeric carriers showed no improvement in therapeutic efficacy compared to non-targeted probes [210]. Further evidence suggests that by incorporating functional groups into a PEO shell, there is a major loss in circulation time, thus indicating that the benefits of the addition of targeting ligands are far outweighed by the decreased circulation capability [20, 204]. Because our micellization procedure offers a high degree of control over the amine content of the PEO shell and we focused on using small molecules such as folic acid or peptides as opposed to antibodies, our design should mitigate some of these pitfalls. Figure 6.1 shows our general design approach and the differences in surface functionality between our standard probe and the targeting-capable probes.

In this chapter two general approaches to incorporate active sites on our probe surface were investigated. In the first, we attempted to synthesize a polymer of roughly the same size and composition as our main constituent polymer, the PMMA-PEO described in Chapter 3. The guiding principle of this approach was based on our experiences with multiple amphiphilic polymers and nanoparticles. We found that the molecular structure and polymer composition were important factors to control for in the development of stable probes. As such, we hypothesized that polymers that were almost identical to the base polymer should be used to introduce functional sites. A polymer of similar size and structure to the base polymer would allow incorporation of high levels of targeted polymer, as the functionalized polymer would be almost interchangeable with the base polymer and be able to form micelles even without the base polymer.

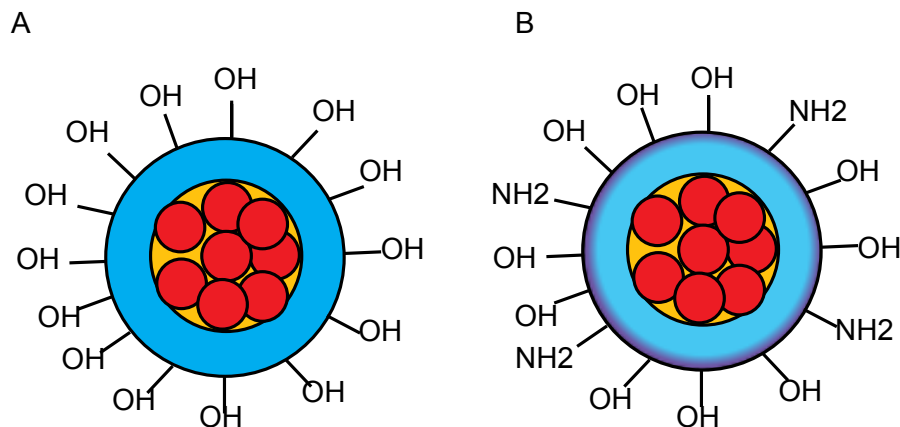


Figure 6.1: Design of targeted micelles developed in this chapter. (A) Our basic micelle described throughout the thesis exposes only hydroxyl groups on the surface. (B) By doping the feeding ratio of the reaction with aminated polymer, we can incorporate active amino groups.

In the second approach, we hypothesized that by doping small amounts of a relatively insoluble amphiphilic polymer into the polymer shell, we would introduce functional groups with a minimal disturbance to the micellar structure. In this approach, the functionalized polymer could never replace the base polymer, as it would not form stable micelles using the dialysis procedure. To accomplish this, we used a smaller M_w polymer with different hydrophobic regimes added in small quantities to the pre-dialysis mixture. Figure 6.2 shows the differences in molecular structure between the polymers used for the first and second approach.

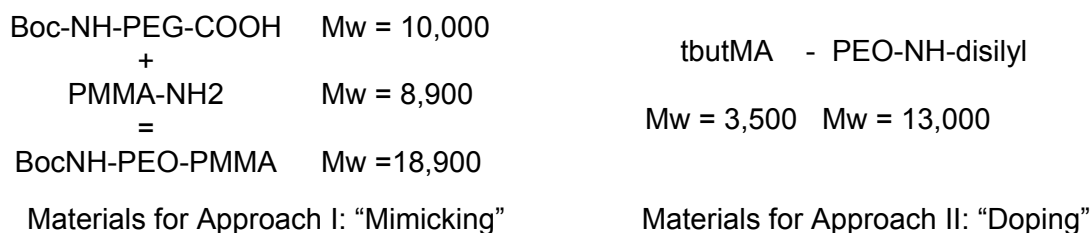


Figure 6.2: Polymers used for the two approaches in this chapter. In Approach I, we synthesized a polymer of similar size and structure to our core PMMA-PEO. In Approach II, we used a very different structure to dope our PEO shell. See text for details.

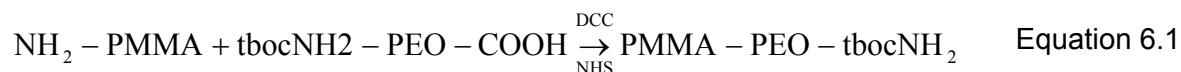
In both these cases, the polymers featured protected primary amines on the PEO tail, which were deprotected after synthesis and evaluated for amine content. To assess our approach, we used the fluorescamine assay [211], which allowed us to assess the active amine content on the micelle surface. Finally, we conjugated folic acid to the active amine sites and observed changes in probe size via size exchange chromatography.

6.3 METHODS

Polymers

NH₂-PEO-t-butylmethacrylate (MW = 16,500; 79% PEO, 21% tBuMA) and polymethylmethacrylate-NH₂ (MW = 9,000, syndiotactic rich) were used as ordered from Polymer Source. tBoc-NH₂-Polymethylmethacrylate-COOH was ordered from Rapp Polymere. Fluorescamine was obtained from Invitrogen. All other chemicals and reagents were used as received from Sigma.

Polymer Synthesis



For a general synthesis, polymethylmethacrylate-NH₂ and tboc-NH₂-Polymethylmethacrylate-COOH or other heterobifunctional PEO were codissolved in either DMF or DCM at concentrations of approximately 1 mg/ml and in about 2 ml total volume. To this mixture were added a 10x excess of DCC and NHS. The reaction was allowed to progress under gentle stirring for several days. After reaction, DCC by-product was filtered off, and the reactants were purified. First, dialysis against pure water was attempted to remove excess small molecules and achieve phase transfer. This process resulted in a significant amount of precipitation owing to the insolubility of the unreacted PMMA-NH₂. Then, products were lyophilized and resuspended in THF for further analysis by standard gel chromatography or FPLC. In another method, the reaction solvent was evaporated off and the resulting film was resuspended in THF followed by filtration again to remove any insoluble products.

Micelle assembly

In the final micelle assembly, either the synthesized polymer or the NH₂-PEO-t-butylmethacrylate was dissolved in THF desired ratios along with the base polymethylmethacrylate-PEO polymer. This mixture was added to nanoparticle-THF solutions and dialysis was performed with the previously described approach. All samples were filtered through 0.2 μm filters prior to further purification to remove insoluble polymer products.

Deprotection

Our deprotection strategy was based on techniques in the literature [212]. After synthesis and purification, the 500 μl of newly functionalized micelles were incubated

with 50 μL of pH 3 TFA. The reaction was allowed to continue for approximately 0.5 hr prior to further characterization.

Fluorescamine assays

Fluorescamine was dissolved to a concentration of 100 mg/ml in DMSO. This solution was then mixed with 200 μL deprotected micelles at a 1:1 ratio. The mixture was allowed to incubate in the dark for about 15 minutes, at which point, fluorescent spectra were taken. Fluorescence spectra were collected on a Photon Technology International spectrometer with a slit width of 0.75 cm. Prior to loading in the cuvette, all samples were filtered through a 0.2 μm syringe filter (Pall).

Folic Acid Conjugation

Briefly, folic acid was solubilized at pH 5.5 and incubated with NHS esters for up to 0.5 hour. Because folic acid was poorly soluble in acidic conditions, careful monitoring of the reaction pH was required to prevent precipitation. This mixture was then added to a solution of EDC and deprotected micelle probes. The conditions were such that folic acid was in at least a 10,000 fold excess compared to the available amines on the micelle surface.

Chromatography

Two different chromatographic methods were used for analyzing the success of the synthesis procedure. For gel permeation chromatography, a Waters HPLC system was used. Samples were dissolved in high-purity DMF and injected using a refractive index detection system.

6.4 RESULTS AND DISCUSSION

To first assess whether the end-to-end coupling of polymers could produce the desired amphiphilic polymer (Approach I), we decided to use a model reaction. In this reaction, we conjugated 3000 MW SH-PEO-COOH with our 8000 Mw PMMA-NH₂.

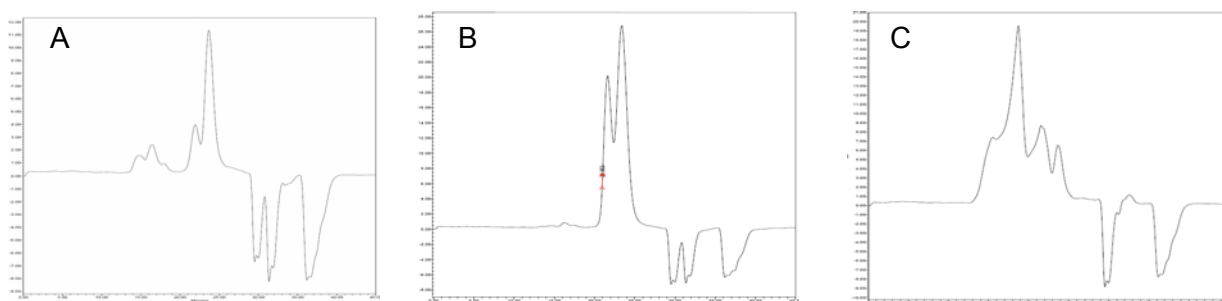


Figure 6.3: GPC data demonstrating the synthesis of PMMA-PEO-SH model polymer. (A) The chromatogram of the model heterobifunctional polymer, SH-PEO-COOH (MW=3000). (B) The chromatogram of the PMMA-NH₂ polymer used throughout this chapter. (C) The chromatogram of the produced polymer, PMAA-PEO-SH.

Figure 6.3 shows the GPC chromatograms of the reactants and final product produced. From comparison of these graphs, it is apparent that a new molecular entity was produced during the DCC coupling reaction. Large new peaks between 15 and 20 minutes are in line with the creation of a larger construct, and probably correspond to some micellization. This synthesis was repeated several times and produced consistent results. However, one major problem with this model system is the existence of the unprotected thiol on the PEO chain. While no direct evidence of cross-reactions or interference from this functional group was readily apparent, it is highly likely that the model polymer behaved differently than the protected amine system. Despite these

concerns, we were encouraged that the DCC reaction did appear to conjugate the two polymers together.

With this experience, we turned towards conjugation of the 10,000 MW PEO to the 8000 MW PMMA-NH₂ using DCC. This reaction appeared to be very inefficient for several reasons. First, after addition of water to the reaction mixture, large amounts of precipitate were quickly created. Some precipitation was expected from DCC by-products, but the large amount visible was most likely due to the insoluble, un-reacted PMMA-NH₂. Secondly, Figure 6.4 shows the results of several FPLC runs in PBS buffer. In general, these runs agree well with the GPC data from the model polymer system in Figure 6.3. The formation of the conjugate itself is demonstrated by the appearance of a unique doublet peak centered around 40 minutes in the conjugate chromatogram. This conclusion is heavily supported by the fact that the PMMA-NH₂ polymer is totally insoluble, and produces no peak in the chromatogram. Careful comparison of the PEO starting material and conjugate chromatograms show corresponding peaks at 50 and 75 min. These peaks show that there is a large amount of heterobifunctional PEO in the purified product and only a small amount of the desired protected amine-PEO-PMMA. Further, there is very little total polymer in the reaction solution after filtration, as observed by the very low absolute signal intensity from the conjugate sample (chromatograms are intensity-normalized). Because of the low yields of this reaction, we decided to focus our efforts on the second approach, using a commercially available functionalized polymer to dope the micellar shell.

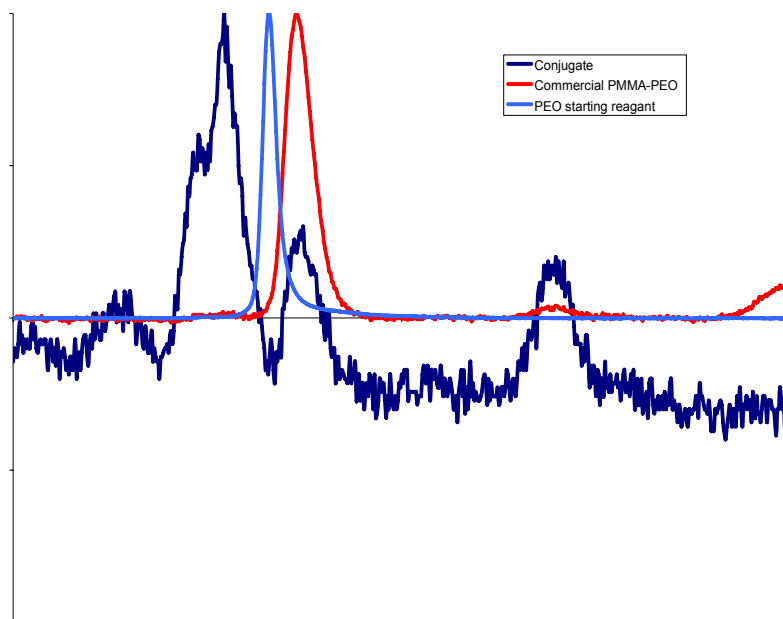


Figure 6.4: FPLC Chromatograms of various polymer samples. UV-vis chromatograms obtained after eluting commercial PMMA-PEO (red), heterobifunctional PEO (light blue) and conjugated PMMA-PEO-NH₂ through a sephacrose 200 column. The intensities of absorbance are normalized

As shown in Figure 6.2, the polymer we used is slightly structurally different from our main PEO-PMMA. It is interesting to note that while conducting our survey of various potential block copolymers described in Chapter 3, we used a tButMA-PEO conjugate, but the polymer caused precipitation in its pure form. However, when used as a doping reagent in the dialysis procedure, the polymer can be incorporated into our micelles. The hypothesis behind this approach is that the micellization process of soluble PMMA-PEO can trap a certain amount of tButMA-PEO and help suspend it. The fluorescamine data in Figure 6.5B supports this hypothesis, as increasing the loading ratio of tButMA-PEO resulted in increased free amine content in purified micelles. Two controls in Figure 6.5A show the fluorescamine signal for pure water and the tButMA-PEO in water. tButMA-PEO has a very low solubility in water, and these samples were

created by adding 10 mg of the polymer to 1 mL of water and vigorously stirring and sonicating the sample. Even after the vigorous mechanical treatment, the polymer still largely remained as a solid. Thus, we were surprised to find any fluorescamine signal in the pure sample. However, given the fact that there are large PEO chains on the polymer, it stands to reason that a certain percentage would be soluble in water. The PEO chains themselves have some polydispersity, so it is likely that the soluble amphiphilic polymers are those with the largest PEO chains. Controls on polymers that were still protected showed no fluorescent signal, which further indicates that the fluorescamine signal was indeed due to the free amine on the polymer and not to any other reason. It is also interesting to note that the absolute fluorescamine signal for these polymer-only samples was significantly stronger than the doped micelle samples. This difference is likely due to a combination scattering and the presence of other polymers that can sterically interfere with the fluorescamine reaction.

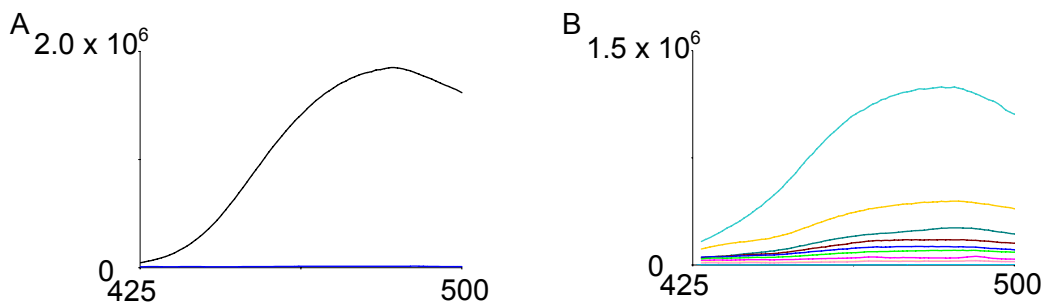


Figure 6.5: Fluorescamine assay demonstrating existence of free amines. (A)

shows fluorescamine signal from deprotected (top) and protected (bottom) NH₂-tba-PEO saturated in pure water while (B) shows micelles incorporating deprotected NH₂-tba-PEO in increasing ratios.

The amount incorporated is a small percentage of the total feeding ratio, as there is a significant amount of suspended tButMA-PEO that is removed during the filtration of

the micelle product. However, the fluorescamine data in Figure 6.5 show that there is still a substantial amount of polymer available for reaction, and this amount can be tuned by adjusting the feeding ratios of the functionalized polymer to the unfunctionalized polymer. It is important to note that because our micelle probes are stable in harsh chemical conditions, the deprotection step can be carried out at pHs below 3.

Conjugation to Folic Acid

Having created a functionalized micelle, we attempted to attach folic acid residues to the deprotected amine groups on the micellar shell. To accomplish this, we added deprotected multianoparticle micelles, NHS-activated folic acid, and EDC in a slightly acidic buffer. We then separated the reactants using FPLC. The results of the first attempt are shown in Figure 6.6. 6.6A shows differences in elution time between conjugated and non-conjugated micelles. The conjugated peak (blue) exhibits an extended elution time as compared to our traditional micellar probes (pink), with very

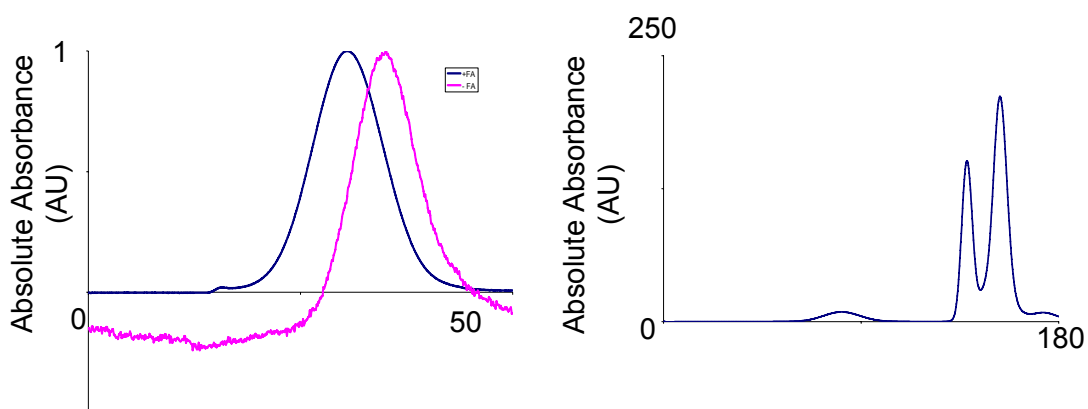


Figure 6.6: Chromatograms of conjugated and non-conjugated micelles.. (A) shows the difference in elution time between folic acid conjugated micelles (blue) and non-conjugated micelles (pink). (B) shows the entire chromatogram for the post-conjugation reaction. The large UV peaks are the characteristic chromatograms for free folic acid.

little increase in peak width. However, because the samples were so dilute, we were unable to recover this peak for further testing and verification. For reference, in 6.4B we show the entire chromatogram with no scaling for the micelle folic acid reaction mixture. The large peak is indicative of free, unreacted folic acid.

There are several factors that can be modified in the future to improve conjugation efficiency. First, the amine content of the micellar probes needs to be optimized. In this instance, it should be increased to the highest content possible without disrupting the dialysis process. Secondly, the pH of the reaction should be modulated to determine the optimal conditions for conjugation. Folic acid has poor solubility in acidic conditions, so running the EDC reaction in more basic conditions should improve yield. Finally, the non-functionalized PEO chains could interfere with the reaction by creating steric interference between the reacting Folic acid and deprotected amine groups [180, 213]. As such, rather than simply keep a protecting group on the tail of the PEO domain; one could envision an alternate approach where targeting ligands were attached to the polymer prior to micellization. We did not attempt this approach based on our experiences with the micellization process. The process is very sensitive to molecular structure and even slightly different hydrophobic block structures can cause uncontrollable aggregation. A pertinent example is the fact that the tButMA-PEO-NH₂ polymer will not form micellar probes when it is in large excess. Rather, it must be doped as described to ensure solubilization and formation of stable probes. Nonetheless, with a small molecule such as folic acid, it may be possible to dope the micelles in a similar fashion to that described in this chapter.

6.5 CONCLUSIONS

Two major conclusions can be drawn from the data presented in this chapter. First, amine coupling two polymers end to end can work as a synthetic strategy, but it is

low yield, and unlikely to produce polymers in sufficient quantity or quality to be useful for further derivitization. Secondly, it is possible and relatively to dope micelles with similar, but not structurally identical amphiphilic polymers. These polymers can have protected end groups that can then be deprotected to yield active functional groups on the micelle surface.

This approach opens up the micelles to further applications, as they can now be conjugated to targeting ligands.

CHAPTER 7

EVALUATION OF NANOPARTICLE BINDING KINETICS USING SURFACE PLASMON RESONANCE

7.1 ABSTRACT

Here we present a new analytical method for studying nanoparticle targeting quantitatively and in real time. We use SPR technology to monitor the specific and non-specific binding of targeted and non-targeted nanoparticles to the important cancer related proteins integrin $\alpha v \beta 3$ and folate binding protein. We show that this method can be used to quantitatively assess probe effectiveness based on the surface design. The approach has several advantages compared to traditional binding assays such as isothermal calorimetry and fluorescence-based imaging, such as: high-throughput capability, high degree of quantification, ease of use, and robustness.

7.2 INTRODUCTION

For nanotechnology to realize its full potential as the next generation approach for cancer diagnosis and therapy, better characterization tools must be developed that will allow a deeper understanding of nanoparticle interactions with cells, proteins, and blood pathogens. As discussed in previous chapters, many studies have demonstrated the importance of surface design to nanoparticle performance in biological applications. Mostly, these experiments incubate nanoparticles either in cell culture or in whole animals and examine the relationship between coating and factors such as circulation lifetime, degree of aggregation or yes/no targeting behavior. While these investigations are relevant because they are excellent models of end-use applications, they obfuscate some of the fundamental kinetic principles that may impact probe performance by examining the coating in highly complex conditions. In other words, these types of

investigations tend to focus on a macroscopic view of probe performance rather than establishing fundamental relationships between factors such as coating, targeting ligand density, charge, and kinetic properties of protein binding. Quantitatively and systematically understanding these relationships will be key to effective nanoparticle design.

There are several well characterized techniques for quantitatively studying binding interactions of biomolecules [214-220]. These include bead based assays, fluorescent polarization, differential scanning calorimetry, isothermal titration calorimetry, and surface plasmon resonance. While the techniques are highly complimentary, in this chapter, we have focused on using surface plasmon resonance as a first step towards quantitatively studying nanoparticle targeting. In the future, using each approach will elucidate new properties of nanoparticle binding and enable the design of better probes. To that end, and to explain our reasons for choosing surface plasmon resonance, here we briefly describe each technique and its strengths and weaknesses. In addition, Table 7.1 summarizes these techniques and highlights the differences between them.

Table 7.1: Comparison of techniques used for assessing biological binding events

Technique	Thermodynamics	Kinetics	Sample Size	Modification	Throughput	Sensitivity	Cost
Bead Based Assays	Indirect	Indirect	Small	High	High	Medium	Low
Fluorescent Polarization	Indirect	Indirect	Small	Some	High	High	Low
DSC	Direct, limited	Indirect	Medium	None	Low	Medium	Medium
ITC	Direct, rich	Indirect	Large	None	Low	Medium	Medium
SPR	Indirect	Direct	Small	Some	Medium	Highest	High

Bead Based Assays

In bead based assays, binding partners are either covalently or indirectly attached to complementary beads where one bead type contains a fluorescent donor and the other is an acceptor. When the binding partners join, the donor-acceptor pair creates a fluorescent signal that can be readily measured. In an alternate configuration, two stable fluorophores of different emission wavelengths can join to create a new optical signal. These assays can occur in solution, and have even been adapted for microplate style readers. The major advantages of this approach are the capabilities for high throughput screening, low background noise, and a large dynamic range. However, the direct observation of binding parameters such as kinetic and thermodynamic constants is quite difficult, as the fluorescent signal yields itself more to yes/no binding observations rather than temporal. Further, because both binding partners must be covalently or indirectly attached to the bead surface, the interaction itself can be greatly affected by this conjugation. However, these assays can be useful for determination for EC50 values and permits fast, effective screening of binding inhibitors [62, 221-224].

Fluorescent Polarization

Fluorescent polarization is based upon the reduced degrees of rotational freedom of a bound molecule as opposed to a molecule free in solution. In this assay, samples are exposed to polarized light and one binding partner must be tagged with a fluorescent molecule. If the tagged binding partner is free in solution, it is rotating freely, and no fluorescent signal can be observed. However, once the tagged molecule binds to its partner, its rotation is hindered, and fluorescent signal is observable as it aligns with the polarized light waves. This technique is useful for observing binding between two highly asymmetric binding partners (molecular weight ratios greater than 1:50). In addition, it can be used as a high throughput screening assay in much the same way as the bead based assays described above. Because the assay minimally modifies the binding partners, it can be used for rapid determination of equilibrium binding constants. However, it does not allow observation of kinetic data, and the fluorescent tagging procedures involved can be difficult to apply generally [225, 226].

Differential Scanning Calorimetry (DSC)

In DSC, equilibrium binding constants are determined by comparing the thermal stability of the target molecule with the stability of the target-binding partner complex. This approach allows for the exploration of very tight binding interactions (K Values in excess of 10^{11} M^{-1}), and is truly label-free (no modification of binding partners necessary). However, it only provides a limited set of thermodynamic data, and is an indirect method of determining binding constants. Further, because of the significant amount of time required for each assay (more than 1 hr per sample), the technique is not applicable for high throughput screening approaches [227, 228].

Isothermal Titration Calorimetry (ITC)

In ITC, repeated additions of the binding partner are made to a solution of the target protein, and the heat necessary to maintain a constant temperature is measured. In this way, full thermodynamic constants can be determined, including changes in enthalpy, entropy, heat capacity, and free energy. The technique can probe tight binding interactions and detect small changes in enthalpy. For example, recently, it was used to detect unexpected anomalies in the binding of small molecules to DNA that were not observable with other techniques. This is a truly “label-free” technique, so measurements are of true binding constant unimpeded by modification. In addition, while the capital expenditures for ITC equipment are significant, they are within the reach of most NIH-funded professors. For these reasons, ITC has become an increasingly popular choice amongst investigators. However, the technique does have some major drawbacks. First, it requires quite large sample concentrations and volume to create observable signal. Secondly, it is impossible to directly determine kinetic information using the technique. Thirdly, the technique is time consuming and does not lend itself to high-throughput applications. Finally, the reaction must always be incomplete and create an observable heat change for an effective assay [229-232].

Surface Plasmon Resonance (SPR)

In SPR assays, a metallic chip is exposed to an incident laser, which, at the correct angle creates electromagnetic waves (plasmons) on the opposite side of the chip while the beam is reflected at an angle. The evanescent plasmons are caused by the electromagnetic portion of the laser light penetrating the chip surface while the photonic portion is reflected. The angle of reflection is dependent upon the refractive index of the material on the plasmon side of the chip. In most SPR experiments, gold is used as the chip material because it has favorable plasmonic properties [233]. While plasmonics

have been studied for decades, the technique was only applied to biological systems about 20 years ago, and has been growing rapidly since. The technique has several unique advantages compared to the other assays described above. First, small sample sizes can be used, which can be important in studying scarce samples such as is often the case with functionalized nanoparticles. Secondly, it allows direct observation of the binding kinetics in real time. Thirdly, the versatility of conjugation chemistry to gold allows a wide variety of experimental designs. Finally, while not a truly high-throughput technique, the relatively short sample processing times (~10 minutes) and development of fully automated SPR systems has allowed rapid, although serial, analysis of large sample sets with relative ease. The major drawbacks of the technique are: its prohibitive cost, the need to modify one binding partner for attachment to gold chips, and a high degree of complexity in experimental optimization [234-237].

SPR for Studying Nanoparticle Binding

While each of the techniques described above could be used for studying nanoparticle probes targeted against biological molecules, the advantages of SPR make it well-suited for these assays. First, the ability to monitor binding in real-time allows assessment of nanoparticle kinetic parameters, which are poorly understood. Secondly, the ability to use small sample size and have a relatively high throughput assay allows multiple surface strategies to be evaluated at once. Finally, because of its high sensitivity, any binding due to nanoparticles should be detected. For these reasons, and because to date, few investigators have studied biofunctionalized nanoparticles using this assay, we chose to focus on SPR to study nanoparticle binding events.

Several excellent reviews exist on the physical basis for SPR assays and their applications to biological systems. As such, we will not recapitulate the information here, but direct the reader to the sources they may find of interest [220, 238-243].

Our ultimate goals for this set of studies were to

1. Demonstrate the feasibility of SPR to measure biofunctionalized QDs binding to cancer targets
2. Draw inferences about the probe design from the binding assay results
3. Use the assay to complement studies of functionalized and non-functionalized micelles from previous chapters

7.3 METHODS

Materials

Alphavbeta3 was used in two forms: presented in triton x and in octyl-beta-d-glucopyranoside. Both were supplied from Millipore. RGD, RGDbiotin, and RGDPEGbiotin were obtained from Peptides International and solubilized according to manufacturer's instructions. QD-streptavidin was obtained from Invitrogen. All buffers were supplied from BIACORE. All other QD probes were synthesized according to procedures described earlier.

Surface Loading

To conjugate target ligand to CM5 chips, the ligand was first washed several times into sodium acetate buffers. In a typical scenario, 2 micrograms of protein were washed 3-5x to a final volume of approximately 1 mL. To determine the appropriate pH for conjugation, standard procedures for running BIACORE preconcentration assays were utilized. In general, the chosen acetate buffers were between pH 4 and 5.

Manufacturer procedures were followed to achieve captured ligand levels. Briefly, while using HBS-P buffer (50 mM HEPES, pH 7.4, 150 mM NaCl, 0.1% PEG 8000) as the running buffer, an EDC/NHS mixture was injected for 7 minutes at a flow rate of 20 μ l/min to activate the carboxylated dextran coating. Next, injections of target ligand in acetate buffer were made either with the INJECT protocol and a pre-

determined volume or by performing manual injections. Once the signal response achieved desired levels, the protein injections were stopped. Finally, ethanolamine was injected for 7 minutes at 20 $\mu\text{L}/\text{min}$ to quench the coupling reaction.

The manufacturer recommends using the following equation to determine appropriate binding levels for quantitative kinetic studies:

$$R_m = \frac{Mw_{\text{analyte}}}{Mw_{\text{ligand}}} (RI)(Sm) \quad \text{Equation 7.1}$$

Where R_m is the maximum response expected, Mw_{analyte} is the molecular weight of the analyte (nanoparticles in our case), Mw_{ligand} is the molecular weight of the bound receptor, RI is the mass of the receptor bound to the chip surface, and Sm is the stoichiometric ratio of the binding. However, because this equation is based on typical proteins, it does not take into account the far heavier density of nanoparticles, thus the predicted levels are not appropriate for most of our assays. Further, because most nanoparticles exhibit multivalent behavior, there is a nonlinear relationship between the amount of mass bound and the stoichiometric ratio of the actual receptor-ligand combination. To compensate, we typically conjugated 5000 RUs of protein to the chip (corresponding to about 5 μg protein). This conjugation level allowed nanoparticle binding to be easily observed.

Binding Assays

Once the chip was prepared with target ligand, injections of analyte were performed. “Analyte” is the BIACORE terminology for the binding partner of the target ligand. Typically, the analyte (nanoparticles, antibodies, and small molecules) were dissolved to a concentration of at most 100 μM . Depending on the purpose of the assay, several different injection techniques were used. For quick assessment of binding-non-binding, INJECT commands were used. To study in detail dissociation, KINJECT with a

3 minute dissociation monitoring phase was used. A typical injection would occur at a flow rate of 20 $\mu\text{l}/\text{min}$, and last for 3 minutes.

Data Evaluation

BIAEvaluation software was used for analyzing the resulting sensograms, and extracting pertinent data. The software allows easy manipulation of several sensograms at once and curve fitting to extract kinetic constants such as K_D , k_{on} , and k_{off} .

7.4 RESULTS AND DISCUSSION

To address the question of whether or not SPR could be used to study bioconjugated QDs, we first consulted the literature to examine ligand-receptor pairs that met three criteria: 1) they could be readily modified with QDs, 2) they were identified as playing an important role in cancer progression, 3) they exhibited multivalent behavior--that is, they were known to bind tighter when multiple ligands were attached to one probe. As discussed in Chapter 2, the ability of nanoparticles to carry multiple targeting ligands is one of the key postulates stimulating research in the area. However, to date, there are very few systematic studies of the phenomena published. A summary of our literature investigation is provided in Table 7.2. Folate and RGD peptides are two of the most widely used nanoparticle-targeting ligands, and have both been studied with SPR. For these reasons, we chose to focus on these two molecules as our targeting ligands of interest.

Table 7.2: Sampling of cancer-related binding partners known to exhibit multivalency.

Ligand	Class	Target	Size	Commercial Availability	Relevance to Cancer
Folate [244]	Sm Molecule	Folate Receptor	0.444 kD	Available Everywhere	Target overexpression in Many Types
EGF [245]	Peptide	EGFR	2.5 kD	Widespread availability	Target overexpression in Many Types
Iressa	Drug	EGFR	0.447 kD	Widespread availability	Cancer Therapeutic
Lewis X/Y [246]	Carbohydrate	E and P selectin	0.530 kD	Widespread availability	E and P selectin are overexpressed during inflammatory processes
RGD Peptides [247]	Sm. Peptide	Integrins	~1 kD	Widespread availability	Integrins involved in angiogenesis
Manno-pyranoside [248]	Carbohydrate	Concanavlin A	~0.200 kD	Widespread availability	Model Receptor--Not directly related

For our first assays, we determined whether or not the target protein could be bound to the SPR chip in a functional format. To do this, we compared the conjugation of our target protein to the model protein provided by the equipment manufacturer. The results of this assay for the integrin $\alpha v \beta 3$ are shown in Figure 7.1. It is important to note that this conjugation is highly dependent on the pH used during the coupling reaction. For example, the rate of ligand binding and RL for equimolar concentrations of $\alpha v \beta 3$ at a pH of 4 was orders of magnitude faster and larger than the at pH 5.5 (RL of 10,000 vs. RL of 200). However, while the faster and tighter conjugation may seem desirable, there was a corresponding loss of activity in the more extreme conditions, owing to protein denaturation at low pH. Thus, intermediate pHs were used for all conjugation reactions, typically around pH 4.8. It is also interesting to note that the success of the immobilization reaction was highly dependent on the formulation of the integrin proteins. For example, two different integrin formulations were available from the manufacturer: one used TritonX-100 to solubilize the protein while the other used

octyl-d-beta glucose. While both formulations were washed several times in sodium acetate buffer prior to conjugation, the TritonX-100 formulation always produced more consistent and uniform binding while the octyl-d-beta glucose typically showed low affinity during the coupling. This anecdote illustrates the sensitivity of the SPR assay to slight difference in the buffers and samples used.

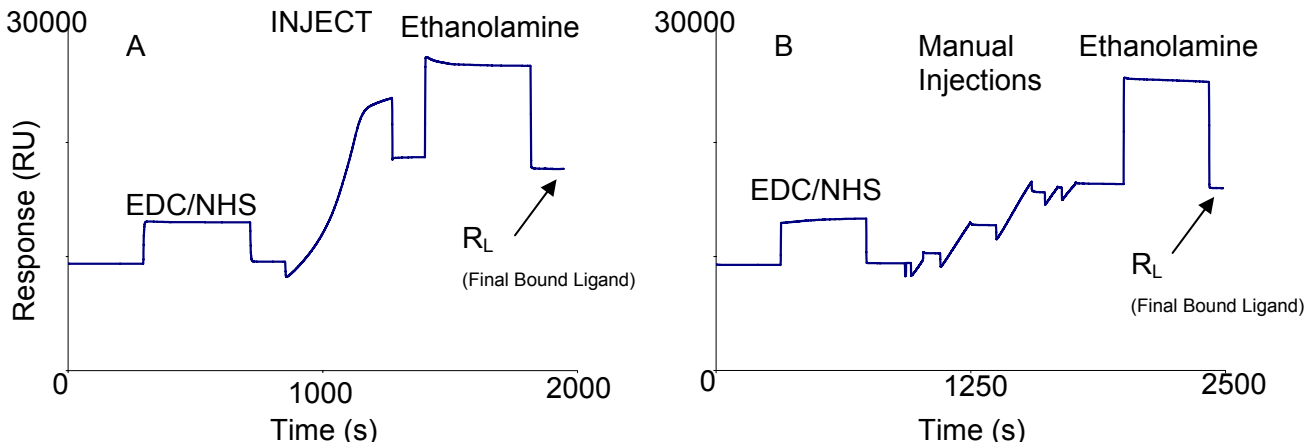


Figure 7.1: Comparison of conjugation of model anti-beta2-microglobulin to CM5. (A) Chip activation and conjugation of Integrin Alpha3beta3 to CM5 (B). Standard INJECT methods were used for anti-beta2-microglobulin conjugation while manual injections were used for integrin alpha3beta3.

Having established that we could successfully conjugate cancer-related proteins to the BIAcore surface, we next attempted to probe the activity of these surfaces. Again, we compared our sample surface to that of a manufacturer-supplied model system. For the first step, we first conducted a sandwich-style assay with the model system. The results from this assay are shown in Figure 7.2. In this instance, beta2-microglobulin was introduced to the flow cell, followed by a secondary antibody injection, followed by a washing step. It is important to note that the beta2-microglobulin signal is relatively weak after binding. While it is clearly observable, stronger signals may be desired for

validation of binding. For instance, one could easily imagine a case where a small molecule binds to a very large antibody and produces a negligible signal response. In such a case, a secondary antibody injection can provide an intense signal boost. The dramatic difference between the signal response for the antibody and the

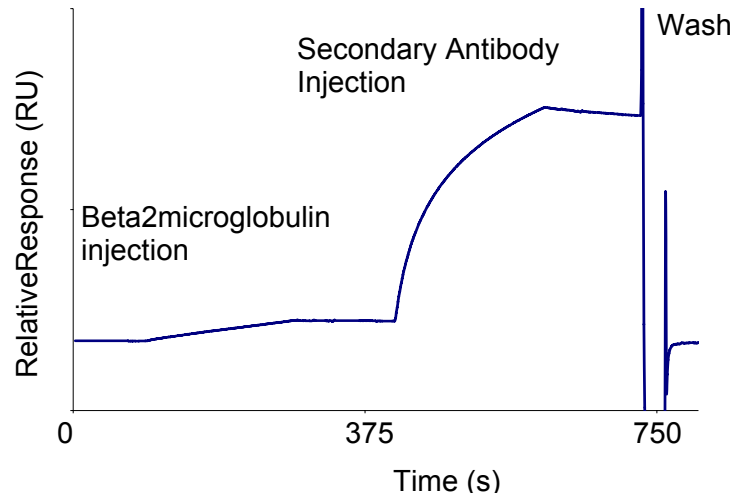


Figure 7.2: Example of sandwich assay using BIACORE.. The first peak is due to the small molecule beta2microglobulin binding to the immobilized anti-beta2 microglobulin model protein. The second peak is the SPR response for a secondary anti-beta2 microglobulin antibody binding to the captured beta2microglobulin.

beta2microglobulin is due primarily to the difference in the molecular weight of each of these molecules. The final important point to note is the importance of the wash step following secondary antibody injection. Because most biological interactions are at least partially reversible, it is possible to create a washing procedure that will allow release of the bound ligands from the surface and regenerate it for future assays. Each wash condition must be determined experimentally and is generally based upon the nature of the binding interaction. For instance, for a binding interaction mediated by charge, it could be desirable to use a high ionic strength buffer to regenerate the surface.

Having successfully demonstrated the activity of our model system, we next turned to our experimental proteins. Our initial probe design was based on using QD-streptavidin bound to anti- α v β 3 antibodies to study the binding of this complex. We chose this probe design for several reasons. First, it is a commonly used approach because of the commercial availability of the probe. Second, SPR's main use has been in the study of antibody binding, and therefore is the most well-characterized. Finally, the streptavidin-biotin linkages make it relatively easy to create probes using this approach. To test our probe design along with the activity of the α v β 3 surface, we conducted two sets of experiments, one using an unmodified anti- α v β 3 antibody, and the other using a biotinylated version of the same antibody. The results from this experiment are shown in Figure 7.3. We were surprised to find an order of magnitude reduction in antibody affinity after biotinylation. This is most likely due to the conjugated biotin molecules interfering with the binding pocket of the protein, and leads to a greatly reduced resonance signal. Because of this great reduction in affinity with no QDs involved, we decided to attempt a different design using peptide based targeting in the hopes that we could avoid some issues involved with random biotinylation of antibodies.

The second probe design we investigated utilized biotinylated cyclic RGD peptides, which have been previously shown to exhibit some multivalent behavior when conjugated to nanoparticles. Cyclic RGDs have demonstrated enhanced affinity as opposed to linear RGDs, which still bind integrins, but at a much lower rate [247, 249, 250]. In a similar fashion to the assay comparing antibodies above, we investigated two different types of biotinylated peptide: one having a PEG spacer between the biotin and

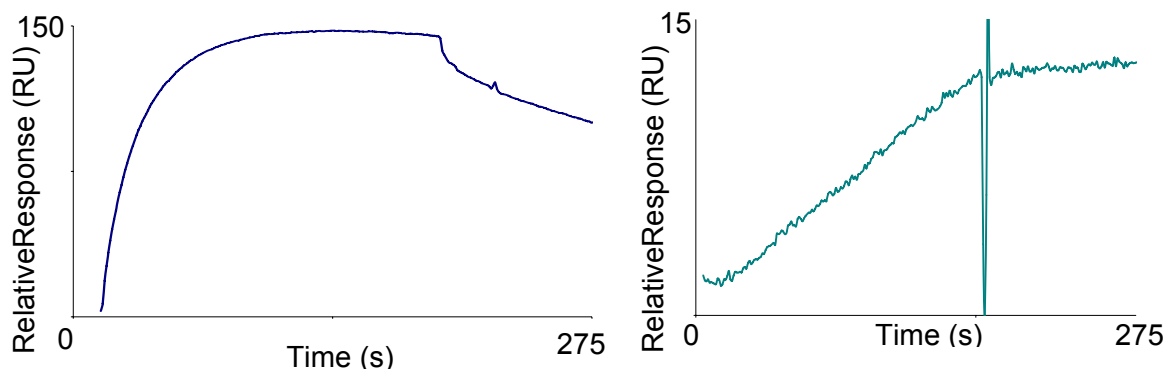


Figure 7.3: Antibodies binding to the alphavbeta3 protein. In (A), non-biotinylated antibody binds to 5000 RUs of immobilized alphavbeta3 with a maximum response of 145. In (B), biotinylated antibody at the same concentration binds with a maximum response of 12.

RGD (RGD-PEG-biotin) and one without a spacer (RGDbiotin). To assess their binding capability, we first conducted a series of injections of increasing concentrations of both types of peptides. The results from these experiments are shown in Figure 7.4. A surprising conclusion from these injections is that the RGDbiotin nonspecifically bound tightly to the conjugated alphavbeta3 while the RGD biotin did not. This is most likely due to solubility problems with the RGDbiotin peptide, which had some difficulty going into solution despite following the manufacturer's recommendations and several attempts to modify the solvent conditions. However, the RGDPEGbiotin performed quite well, and no non-specific binding was observed. This is most likely due to the enhanced hydrophilicity endowed by the PEO linker. In addition to adding water solubility, the design is attractive because the PEO linker helps separate the peptide molecule from

the nanoparticle surface, thus minimizing any steric interference that may be caused by the streptavidin coated QD. For these reasons, we chose to focus on this ligand as the targeting molecule for these studies.

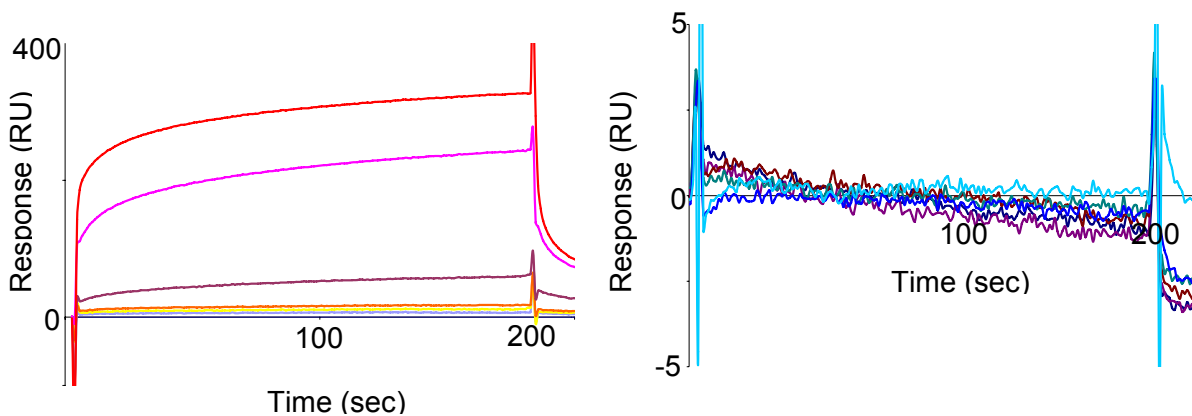


Figure 7.4: RGDs binding to $\alpha 5 \beta 3$ integrin. Each curve represents higher concentrations of peptide from 0.1 μm to 100 μm . RGD Biotin is poorly soluble, and nonspecifically binds to the protein, as evidenced by the sharp rise and drop off the SPR Response. RGD-PEG-biotin shows no response.

Having chosen the RGD targeting ligand of interest, we next aimed to demonstrate its functionality in directing nanoparticles to the integrin. For these experiments, we compared the binding of unmodified QD-streptavidin to the RGD-PEG-biotin bound QDs. We used large excesses of RGD-PEG-biotin to ensure saturated

streptavidin binding. Finally, we sequentially performed 3 injections of the unmodified

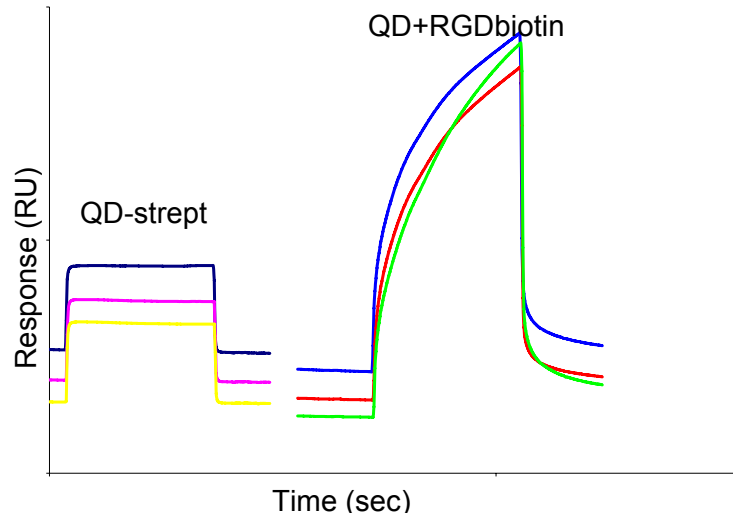


Figure 7.5: Multiple, sequential injections of QD-streptavidin followed by injections of a mixture of RGDbiotin and QD streptavidin.

QD-streptavidin followed by 3 more injections of the QD-RGD-PEG-biotin. The results of these experiments are given in Figure 7.5. In this figure, it is important to note that there is no apparent non-specific binding attributed to the QD-streptavidin, while there appears to be a highly specific binding of the QD-RGD-PEG-biotin complex. Further, it is interesting to note that the complex binding appears to occur very rapidly followed by a precipitous decline in bound complex. These experiments were conducted in buffer having high magnesium concentrations, as it has been demonstrated that the affinity of $\alpha\text{v}\beta\text{3}$ for RGD is highly dependent on this ion concentration. While the experiment proved the principle that RGD-PEG-biotin could target QDstreptavidin to the $\alpha\text{v}\beta\text{3}$ protein, we were surprised to see such fast on and off rates. This high on-off rate behavior is most likely due to competitive binding between the salt ions and the

RGD peptide. Thus, to remove this experimental artifact, we decided to perform another series of experiments with standard BIACORE buffers (no salt addition).

In this new set of experiments, our first task was to determine whether or not we could quantitatively determine the amount of targeted QD probe that would bind to the immobilized protein. In this experiment, we bound 5000 RUs of alphavbeta3 to one flow cell and 10000 RUs to another. The results of multiple injections over these two flow cells are shown in Figure 7.6. In each case, the nanoparticles bind with an appreciably slower rate constant to the protein surface than in Figure 7.5. Once bound, they dissociated much more slowly, because there were no Mg^{2+} ions to compete with RGD binding. Further, we were happy observe a direct correlation between quantity of nanoparticle bound and the strength of the signal response observed. One important feature to note is the step change that is observed after initial binding in the Figure 7.6B. This step change indicates is indicative of a change in the flow rate between the injection phase and dissociation monitoring phase. In the case of the higher-concentration target, this step change is caused by the dramatic increase in material bound to the chip surface. Thus, more mass is affected by the change in flow rate, leading to a larger disturbance in the SPR signal than is the case in the lower concentration assay. These results prove that the SPR can be used to quantitatively assess nanoparticle kinetics by varying the conditions of the buffer solutions, the concentrations of the binding partners, and the surface modifications of the nanoparticles themselves.

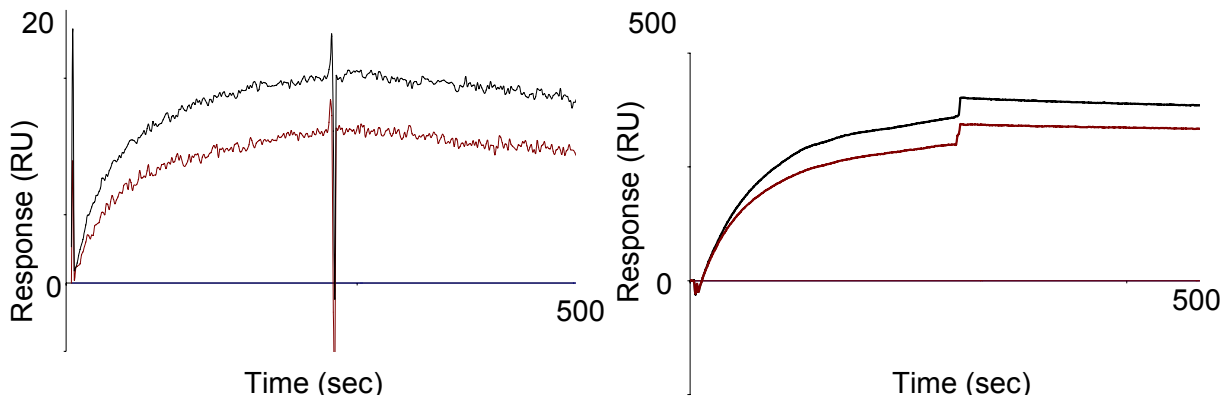


Figure 7.6: Sensitivity of the SPR system to different target ligand immobilization

levels. The response at a low target ligand level (A) is over 20x smaller than the response at high levels (B) for constant QD probe concentrations. The curves occur in pairs of high QD concentration (100 μ M QD + probe, low QD concentration, and controls)

In our next set of experiments, we set out to identify the exact nature of the binding to α v β 3. In Figure 7.7A, we show a series of unmodified RGD injections followed by QD streptavidin injections. There is no appreciable response from this series of injections, indicating that there is no RGD-mediated interaction between the QD streptavidin and the α v β 3. However, in Figure 7.7B, we show sequential injections of the RGD-PEG-biotin followed by injections of the QD streptavidin. In this instance, the RGD specifically binds to the α v β 3, leaving the biotin molecule in the flow path. In the next injections, the QD streptavidin binds tightly to the biotin, and the result is a very similar response to what was observed in Figure 7.6. Thus, it is difficult to tell in many instances whether the QD-RGD binding is due solely to the pre-complexed QD-RGD-PEG-biotin, or whether it is due to the QD streptavidin binding to

biotin molecules that are attached to the $\alpha\text{v}\beta_3$ through RGD linkages. This interference could be mitigated by stringent purification protocols that remove the free RGD-PEG-biotin from solution, but presents significant experimental difficulties, particularly when trying to assess whether or not unsaturated QD-streptavidin-RGD complexes are binding to the sensor chip surface. This is because there will always be a normal distribution of probe-peptide complexes produced, so it is somewhat difficult to accurately assess whether or not there are still unsaturated molecules in solution.

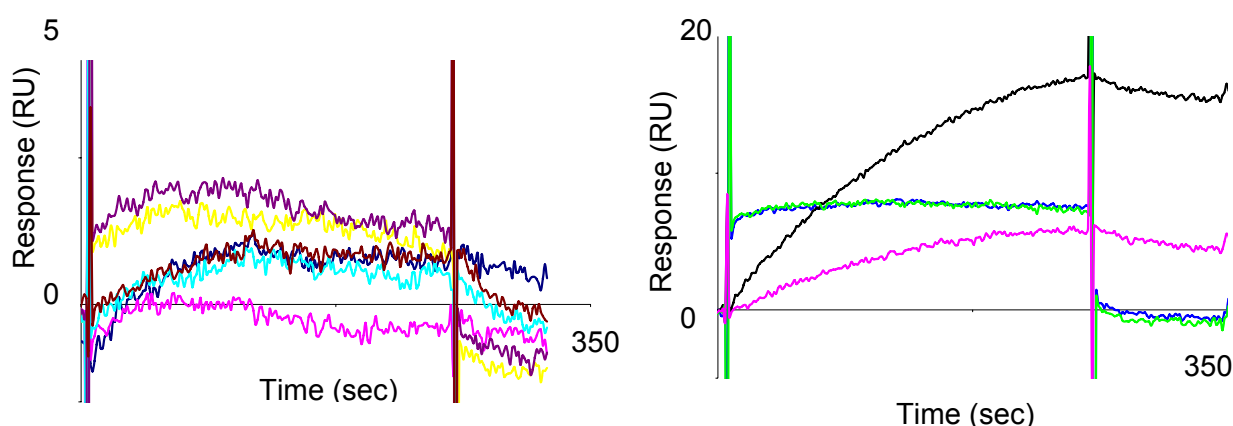


Figure 7.7: Sequential injections of targeting molecule and QD-streptavidin. (A) injections of RGD followed by injections of QD-streptavidin show no response. (B) injections of RGD-PEG-Biotin followed by QD-streptavidin show a strong response that decreases after the second injection.

In the next set of experiments, we attempted to verify the “nonstick” nature of our micellar probes using BIAcore. For this series of experiments, we focused on using folate binding protein as the bound molecule, to correlate with our attempts at functionalizing the micelles discussed in Chapter 6. In this case, we compared the binding of our micellar probes to that of free folic acid. The results of this comparison are shown in Figure 7.8. As supported by all the work presented in previous chapters,

the micellar probes appear to have no non-specific binding to the folate binding protein. This is in dramatic comparison to the free folic acid, which binds folic acid well. This strong binding behavior is in line with literature examples that have examined folate binding protein and folate bound dendrimers. We were encouraged by these results, along with those previously demonstrating that the SPR techniques could be used to detect nanoparticle binding. While beyond the scope of the work presented here, the next logical set of experiments would be to examine folic-acid targeted micelles as they bind to the folate binding protein in the SPR instrument. We would expect there to be a strong correlation between binding affinity and the degree of functionalization. In addition, we would expect some non-linear behavior in the binding affinity curves based on the availability of folic acid molecules in the correct conformation bound on the micelle surface. It is most likely that there are several different conformations of the bound targeting ligand at any given time on the surface, and each conformation will display a significantly different binding behavior.

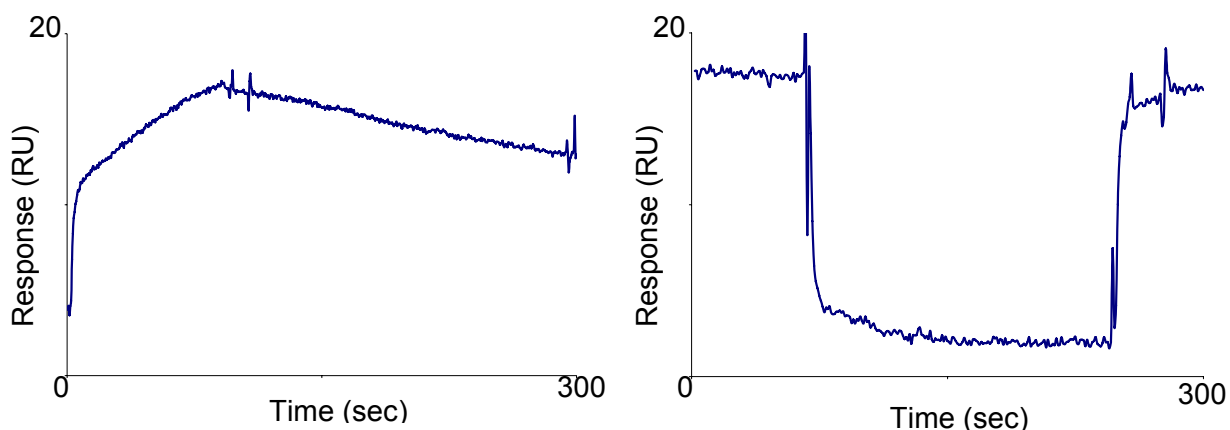


Figure 7.8: Folic acid binding to the folate binding protein shows a strong, reproducible, and reversible response while non-targeted micelles exhibit no non-specific binding to the folate binding protein.

7.5 CONCLUSIONS

The purpose of this chapter was to explore the feasibility of SPR to characterize the binding of functionalized nanoparticles to cancer related proteins. The results presented here indicated that SPR can be used for this application, and could lead to a deeper understanding of the relationship between nanoparticle surface design and the functionality of nanoparticles in their end-use applications. In the future, further study of this approach should lead to improved bioprobe design and better engineering models for nanotechnology.

CHAPTER 8

FUTURE DIRECTIONS

8.1 ABSTRACT

In this chapter, we first summarize the work presented in the previous chapters and the contributions made to the field of cancer nanotechnology. Next, we examine future applications of the micellar probes specifically, and finally, future directions for cancer nanotechnology in general.

8.2 SUMMARY

This dissertation has focused on the development of a novel and robust procedure for encapsulating hydrophobic nanoparticles while conferring water solubility and biocompatibility. In the first chapter, we described the field of cancer nanotechnology generally to give the reader an understanding of where this dissertation fits in the broader struggle against metastatic disease. Cancer is a deadly and difficult disease, and has many molecular and physiological factors that make nanoparticles attractive vehicles for therapy and diagnosis. From the applications discussed in Chapter 1, it is apparent that cancer nanotechnology is a burgeoning field that is ripe with potential.

In the second chapter, we reviewed the use of QDs in biology and medicine, focusing specifically on the surface modification strategies that have been used, and how these modifications affected the end application. Two main functionalization strategies exist: the first replaces the ligands on the surface of QDs with amphiphilic molecules, and the second coats the QDs with macromolecular solubilization agents. While each approach has unique benefits and drawbacks, coating procedures seem

more applicable to *in vivo* imaging, and thus were chosen as the main focus of this thesis.

The third chapter presented the development of our encapsulation procedure. Here, we described the physical properties necessary to form stable, noncovalent interactions between amphiphilic block copolymers and hydrophobic nanoparticles. We presented TEM, DLS, spectroscopic, and fluorescence imaging data to characterize the procedure and our resulting probes. We found the procedure to be robust, flexible, and capable of producing large quantities of the micellar probes.

In the fourth chapter, we explored extensions of this encapsulation procedure to create optomagnetic probes. We demonstrated high quality T2-weighted contrast agents could be synthesized using Fe₃O₄ iron oxide nanoparticles and our encapsulation procedure. We also explored T1 weighted agents using gadolinium chelates, but found that these molecules were not easily amenable to entrapment via our procedures.

The fifth chapter presented a host of chemical and biological assays that demonstrated the stability and versatility of our probes. In direct comparisons with coatings from other work, we showed that our probes were more stable in almost every scenario. Of particular interest were assays where our probes were incubated in whole human blood for 24 hours at 37⁰C. This points towards the utility of these micellar probes for *in vivo* imaging or solution based assays where performance in complex biological systems is required.

In chapter six, we presented strategies for functionalizing the micelle coating by incorporating protected amine groups. The most successful strategy used a structurally distinct polymer to dope the micellar shell during assembly. In this case, the constituent polymer also helped to solubilize the activated molecule along with the nanoparticles. We presented fluorescamine assay data and preliminary results of folic acid conjugation assays to demonstrate the activity of these surface amino groups.

Finally, the seventh chapter discussed our efforts in understanding the detailed kinetics of nanoparticle binding using SPR. We presented a series of proof of principle assays showing that functionalized nanoparticle binding could be detected using these systems. We used the important cancer related proteins integrin α v β 3 and folate binding protein for these assays.

In sum, this dissertation made contributions to the field by providing a new route of functionalizing nanoparticles, exploring the fundamental interactions between amphiphilic polymers and nanoparticle coatings, and also by providing a new method for quantitatively exploring the binding kinetics of various surface functionalization strategies.

8.3 FUTURE DIRECTIONS FOR DISSERTATION TECHNOLOGY

The work presented in this thesis has focused mostly on proof-of-principle studies. While the synthesis procedure of optical, optomagnetic, and functionalized micellar probes has been demonstrated conclusively, there still remains a large amount of further development and optimization to be completed. These studies fall under three main areas: fundamental physical studies, engineering of the synthetic procedure, and end use bioapplications. Here, we discuss each area in turn and suggest specific studies to be undertaken.

Fundamental Physical Studies

The work presented suggests several interesting avenues for exploring the fundamental properties of nanomaterials and their interactions with polymer systems. For example, an interesting phenomenon we noted in Chapter 3 was the occurrence of blinking in the micellar probes, and the differences between singly encapsulated (more blinking on average) and multiple entrapped (less blinking) nanoparticle containing

micelles. This observation suggests the capability of the micelle system to be used as a way of systematically studying the blinking behavior of QDs. A second important area proposed by the synthesis procedure is that of the basic physical interactions between amphiphilic polymers and nanoparticle surface coatings. Because synthetic amphiphilic polymers are relatively new and poorly understood materials, few accurate models exist that are able to predict their behavior in complex solutions. In particular, little work exists studying the basic molecular interactions of amphiphilic polymers with other materials, and even less exists on the behavior of these polymers as they interact with nanomaterials. We attempted to take a systematic approach to this topic, as discussed with our survey of literature polymer structures, but there is ample opportunity to conduct fruitful research in this area. Finally, a complete thermodynamic description of the complex solutions would be useful for further design and engineering in this area. That is, if one could predict the conformation and behavior of the amphiphilic + nanoparticle + solvent system, one could better design the encapsulation procedure and resulting micellar probes.

Engineering of the Synthetic Procedure

Another area of study that deserves further attention is the optimization and scale up of the encapsulation procedure developed in this thesis. While we have demonstrated some scale-up ability and capability to entrap a wide variety of nanoparticles on the interior of our probes, there remains room for significant improvement. It is not difficult to imagine that these procedures could be used to produce up to gram quantities of micellar probes, and perhaps one day in a continuous process. Thus, studies on the optimal dialysis and separations conditions could be conducted to design large scale synthesis procedures. Further, optimization of the functionalization procedure should be pursued, as we have only developed one method

for introducing functional groups. Further work could explore a variety of doping polymers, and could be built upon the results of some of the fundamental studies described above. Also, one could explore options such as crosslinking the amphiphilic polymer shell, although we have observed no adverse effects from a lack of crosslinking agents.

Bioapplication Studies

Finally, further biological studies should be pursued with the micellar probes. We have presented some exciting preliminary results demonstrating their applicability in an array of environments, but there remains many other scenarios to explore. One major area not addressed by the work here is that of *in vivo* animal imaging. Studies detailing the ability of the micelles to be imaged in mice would be a very important step towards their ultimate clinical utility. Further applications may be found outside of pure imaging could also be envisioned. For example, the optomagnetic micelles may have utility in applications aimed at isolating circulating tumor cells, by relying on the magnetic characteristics of the nanomaterials: one could “pull-down” cells using magnetism and then image them using the fluorescent characteristics of the probes. Finally, an exciting future area could be combining therapeutics in the micellar structure and studying the benefits of this combined therapeutic-diagnostic probe in animal models.

8.4 FUTURE DIRECTIONS FOR CANCER NANOTECHNOLOGY

Cancer nanotechnology is an promising and attractive field. It holds the potential to change the way in which one of our most deadly diseases is diagnosed and treated. However, the field faces several significant challenges that are sometimes forgotten in the excitement to push towards commercialization and clinical applications. In particular, the field suffers from a dearth of truly fundamental, systematic studies that explore in a

rigorous way all the many factors that impact nanoparticles' behavior in biological systems. In this thesis, we have focused on a thorough examination of one coating procedure, but there are literally hundreds of other coating approaches that could be used. A major problem with designing systematic studies is that a minority of the researchers in the field truly understand both the biological systems and nanomaterials involved. Thus, many studies suffer from poorly characterized nanomaterials, which calls into doubt the bold conclusions and dramatic biological results. In the future, studies which address both the fundamental material questions along with the biological application will be invaluable for advancing the field as a whole.

A related area is the final metabolism and clearance of nanoparticles once they are injected into the body. This is perhaps the greatest single barrier to their clinical application, and deserves a thorough and prolonged investigation. The two main concerns regarding nanoparticles are the effect of small particles if they are trapped in the body and the fact that some toxic component may be introduced by the nanoparticle system. To date, there has been no conclusive evidence one way or the other regarding the toxicity of these particles. Speculations are made in favor of and opposed to biocompatibility. For example, many worry that QDs contain Cd in their cores, and that this will prevent any use in the clinic. On the other hand, the amount of Cd introduced by a QD injection is small, and the Cd is in the form of CdSe, which is not toxic (the only toxicity could be from the ionic form of Cd). There have been some studies in the literature exploring this topic, but like many of the application-focused efforts mentioned above, they tend to lack in a fundamental characterization of the nanomaterials itself.

This problem is also compounded by the amount of excitement and press that cancer nanotechnology received in 2004 with the advent of the NCI's alliance for cancer nanotechnology. The expectations ran high that within 5 years, several nanoparticle based methods would be available in the clinic. While there is still hope that some

systems may start to enter the clinic in this time frame, this goal created somewhat unrealistic expectations both within the scientific community and from outside observers. Realistically, these systems need much more characterization and engineering before they can be truly clinically relevant. However, this means that there are years of fruitful and exciting research ahead!

8.5 CONCLUSIONS

In this chapter, we have summarized the work completed in the course of this dissertation and pointed towards several important future research questions. In sum, this thesis has made contributions in the design and understanding of nanoparticle based probes, and laid the groundwork for future systematic explorations in the area. These systematic explorations of surface coatings and biological behavior of nanoparticles will prove vitally important to the field of cancer nanotechnology as it progresses from an academic to an applied science.

APPENDIX A

TIGON NANOSTRATEGIES EXECUTIVE SUMMARY

A.1 ABSTRACT

As part of my graduate school career, I had the opportunity and fortune to participate in the Technological Innovation: Generating Economic Results program. This is an National Science Foundation sponsored program that brings together two law students and an MBA student to explore the commercialization process. As part of this program, my team and I developed a business plan based on my dissertation. The plan did quite well: we won the Georgia Tech Business Plan Competition, and were able to compete internationally at the Nanochallenge in Padua, Italy. I have included the Executive Summary for the plan as an appendix because it was a very important part of my graduate career, and helped shape my plans for the future.

A.2 EXECUTIVE SUMMARY

Business Concept

TIGON Nanostrategies will provide the next generation of clinical imaging agents to doctors around the world. Our nanotechnology-based probes will locate cancer and other diseases in their earliest stages, making disease management easier, cheaper, and more successful. The extremely small size of our probes will enable clinicians to find metastatic cancer months, if not years, sooner than any current techniques, leading to better cancer treatment options and survival rates. While we are honing our technology for human use, we will sell to researchers who will use our probes in their labs, allowing us to form a profitable company before gaining regulatory approval. Using this strategy, our company will realize cash flow almost immediately (within 6 months of establishing a production facility), and be ready to seek FDA approval for clinical applications by Year 5. To demonstrate the utility of our products, Figure 1 shows how our fluorescent probes can make tumors visible to the naked eye. TIGON probes could one day guide a surgeon's tools to exact disease sites, rather than crudely removing large chunks of tissue. Our Probes offer a host of technical and practical advantages over currently used imaging agents. ***In short, TIGON probes will save lives, time, and money.***



Figure B1 TIGON's technology can create dramatic images in living animals. This image shows an example of the intensity and sharpness of our probe technology.

Target Market and Customers

When fully developed, TIGON will operate in the \$3.26 billion (€2.53 B) clinical imaging agent market, which is expected to grow 20% by 2009. Using our multiphase strategy, we will generate revenue from two additional markets as we grow. Our **Phase I market, in vivo fluorescent imaging probes for researchers, is conservatively estimated to be about \$21 million (€16.3 million) per year, and is growing at approximately 10% per year.** Our **Phase II market, in vivo magnetic resonance imaging (MRI) probes, is approximately \$575 million (€446 million) annually with about 5% growth.** We will quickly realize revenue from these two markets helping us to enter **Phase III, the clinical imaging agent marketplace.** In addition, by bringing new technical capabilities to all three market segments, we expect to drive growth in a collaborative fashion by allowing new types of investigations to take place.

TIGON's two segments of target customers are **researchers** (Phase I & II products) and **clinicians** (Phase III products) at well funded research institutes. These customers are likely to have received a grant from the National Institutes of Health ("NIH") in the U.S., and considered leaders in their fields. We understand these customers due to our strong connections within the academic and clinical communities and our extensive interviews with potential customers. **We have found that researchers are attracted by TIGON's versatility, quality, and ease of use. Clinicians are excited about TIGON technology's life-saving potential.**

Our Competitive Advantage and Barriers to Entry

Our primary competitive advantage is the superior technical properties of our probes as compared to traditional dyes. We are solidifying this advantage by building intellectual property (IP) barriers and will maintain the advantage through a strong product pipeline. Our technology was invented in Dr. Shuming Nie's laboratory at Emory University. We are currently in negotiations with Emory's technology licensing office to finalize protection of our core technologies, and to establish TIGON as a conduit for commercialization for Dr. Nie's laboratory. Dr. Nie is a world famous nanotechnologist who has received over \$40 million in federal research grants, has a thriving laboratory, and over 18 patents and applications on file with the US patent and technology office. Thus, we will establish and maintain competitive advantage through a solid IP position and rapid market entry, and establishing a loyal customer base.

Estimated Technical Challenges to Overcome

TIGON will ultimately offer probes with several color combinations and magnetic properties. In addition, we will offer a handful of different chemical functionalities. These combinations will allow researchers and clinicians to study virtually any disease in the manner they see fit. Thus, a major technical challenge will be to retain the ability to manufacture truly customized probes at a reasonable cost. With strategic process engineering, we will be able to offer probes with a short turnaround time (2 days max). In addition, we will roll out new chemical functionalities through partnerships with beta-testing customers. **Our beta customers will receive our product at no cost during an introductory period. In exchange, TIGON will receive guidance in product development, and must be mentioned in any publication/proceeding that our collaboration produces.**

Estimated Time to Commercialization, Profitability, and Future Funding

TIGON's strategy is rapid entry. Given the level of technical development, our Phase I product will be ready for market within six months of establishing our production line. We are seeking an initial seed funding level of \$2,500,000 (€1,939,000). This level of funding will allow us to break even late in Year 3, gives us a \$500,000 cushion on top of our estimates, and drives rapid profit growth, as detailed in Table 1. If desired, the investment could be traunched into an initial outlay of \$1,500,000, to establish the facility, launch Phase I, and prepare Phase II products for market. The subsequent \$1,000,000 will enable the launch of Phase II products and sustain the company until profitability. We anticipate no additional funding requirements to achieve profitability. Comparable comparisons to public companies suggest a firm value of approximately \$70M in Year 5, including a 30% "liquidity discount". The investor could expect a 50% annual return with a 30% ownership stake in the business for the initial, \$2,500,000 investment.

Table A.1. TIGON Nanostrategies Revenues and Profits Through Year 5 (\$)

	Year 1	Year 2	Year 3	Year 4	Year 5
Revenue	\$40,800	\$806,000	\$2,600,000	\$8,475,000	\$23,150,000
Profit (pre-tax)	-\$1,135,000	\$-774,000	\$277,000	\$3,465,000	\$12,927,000

TIGON's Team Strength

One of our greatest assets is our well-diversified team and experienced advisory board. TIGON's principals currently include an MBA candidate, two JD candidates, and a PhD level engineer. We are actively seeking an experienced CEO. We have already assembled a scientific advisory board consisting of world class physical and biological scientists and clinicians. Our management advisory board contains successful entrepreneurs, with expertise in start-ups and in depth knowledge of companies who target markets such as ours. ***With this multidisciplinary, experienced, and highly qualified team, TIGON has the breadth and depth of knowledge necessary to be successful in executing this business plan.***

Exit Strategy

Our diverse nanobiotechnology product line will enable TIGON to be a competitive independent company for quite some time. Our initial preference is to keep the company private and independent with only a few key investors. However, we are open to acquisition by a large pharmaceutical firm, initial public offering, or management buyout, as our investors see fit.

Key Success Factors for TIGON Nanostrategies:

- **Provide easy to use, customizable, versatile probes that have unique *in vivo* imaging capabilities.**
- **Enter into development partnerships with world-class research laboratories to stimulate product use.**
- **Increase visibility and reputation through strategic placement of our products in journals, conferences, and a strong web presence.**

REFERENCES

1. Service, R.F., *Nanotechnology takes aim at cancer*. Science, 2005. 310(5751): p. 1132-1134.
2. *National Cancer Institute Office of Technology and Industrial Relations Cancer Nanotechnology Plan*. 2004, NIH.
3. *NSF-NCI joint nano program targets cancer*. Chemical & Engineering News, 2005. 83(39): p. 30-30.
4. *American Cancer Society Cancer Facts and Figures 2007*.
5. Ferrari, M., *Cancer nanotechnology: Opportunities and challenges*. Nature Reviews Cancer, 2005. 5(3): p. 161-171.
6. Cuenca, A.G., et al., *Emerging implications of nanotechnology on cancer diagnostics and therapeutics*. Cancer, 2006. 107(3): p. 459-466.
7. Peters, G.a.V., K.H. , *Oncogenes and Tumor Suppressors*. 1997: IRL Press, Oxford. .
8. Hanahan, D. and R. Weinberg, *The Hallmarks of Cancer*. Cell (Cambridge, Massachusetts), 2000. 100: p. 57-70.
9. Voldborg, B.R., et al., *Epidermal growth factor receptor (EGFR) and EGFR mutations, function and possible role in clinical trials*. Annals of Oncology, 1997. 8(12): p. 1197-1206.
10. Chakravarti, A., J.S. Loeffler, and N.J. Dyson, *Insulin-like growth factor receptor I mediates resistance to anti-epidermal growth factor receptor therapy in primary human glioblastoma cells through continued activation of phosphoinositide 3-kinase signaling*. Cancer Research, 2002. 62(1): p. 200-207.
11. Aaronson, S., *Growth Factors and Cancer*. Science (Washington, D. C., 1883-), 1991. 254: p. 1146-1153.
12. Powers, C., S. Mcleskey, and A. wellstein, *Fibroblast growth factors, their receptors, and signaling*. Endocrine-Related Cancer, 2000. 3: p. 165-197.
13. Paweletz, C.P., et al., *Reverse phase protein microarrays which capture disease progression show activation of pro-survival pathways at the cancer invasion front*. Oncogene, 2001. 20(16): p. 1981-1989.
14. Takahashi, Y., et al., *Expression of Vascular Endothelial Growth-Factor and Its Receptor, Kdr, Correlates with Vascularity, Metastasis, and Proliferation of Human Colon-Cancer*. Cancer Research, 1995. 55(18): p. 3964-3968.
15. Ribatti, et al., *The history of the angiogenic switch concept*. Leukimia, 2007. 21: p. 44-52.

16. Gerard, E. and K. Vousden, *Proliferation, cell cycle, and apoptosis in Cancer*. Nature (London), 2001. 411: p. 342-348.
17. Vogelstein, B., D. Lane, and A.J. Levine, *Surfing the p53 network*. Nature, 2000. 408(6810): p. 307-310.
18. Giannakakou, P., et al., *Enhanced microtubule-dependent trafficking and p53 nuclear accumulation by suppression of microtubule dynamics*. Proceedings of the National Academy of Sciences of the United States of America, 2002. 99(16): p. 10855-10860.
19. Blasco, M.A., et al., *Telomere shortening and tumor formation by mouse cells lacking telomerase RNA*. Cell, 1997. 91(1): p. 25-34.
20. Moghimi, S.M., A.C. Hunter, and J.C. Murray, *Long-circulating and target-specific nanoparticles: Theory to practice*. Pharmacological Reviews, 2001. 53(2): p. 283-318.
21. Brigger, I., et al., *Nanoparticles in cancer therapy and diagnosis*. Advanced Drug Delivery Reviews, 2002. 54(5): p. 631-651.
22. Carmeliet, P. and R.K. Jain, *Angiogenesis in cancer and other diseases*. Nature, 2000. 407(6801): p. 249-257.
23. Hoffman, R.M., *Green fluorescent protein imaging of tumour growth, metastasis, and angiogenesis in mouse models*. Lancet Oncology, 2002. 3(9): p. 546-556.
24. Satchi-Fainaro, R., et al., *Targeting angiogenesis with a conjugate of HPMA copolymer and TNP-470*. Nature Medicine, 2004. 10(3): p. 255-261.
25. Mundy, G.R., *Mechanisms of bone metastasis*. Cancer, 1997. 80(8): p. 1546-1556.
26. Weigelt, B., J.L. Peterse, and L.J. van't Veer, *Breast cancer metastasis: Markers and models*. Nature Reviews Cancer, 2005. 5(8): p. 591-602.
27. Roodman, G.D., *Mechanisms of disease: Mechanisms of bone metastasis*. New England Journal Of Medicine, 2004. 350(16): p. 1655-1664.
28. Mundy, G.R., *Metastasis to bone: Causes, consequences and therapeutic opportunities*. Nature Reviews Cancer, 2002. 2(8): p. 584-593.
29. Muller, A., et al., *Involvement of chemokine receptors in breast cancer metastasis*. Nature, 2001. 410(6824): p. 50-56.
30. Yoneda, T., et al., *Inhibition of osteolytic bone metastasis of breast cancer by combined treatment with the bisphosphonate ibandronate and tissue inhibitor of the matrix metalloproteinase-2*. Journal Of Clinical Investigation, 1997. 99(10): p. 2509-2517.

31.

http://www.isrec.ch/research/groups/research_groups_detail_eid_1682_lid_2.htm. Date Accessed: 09/2007
32. Swartz, M.A., *The physiology of the lymphatic system*. Advanced Drug Delivery Reviews, 2001. 50(1-2): p. 3-20.
33. Trubetskoy, V.S., V.P. Torchilin, and A.D.D. Reviews, *Use of Polyoxyethylene-Lipid Conjugates as Long-Circulating Carriers for Delivery of Therapeutic and Diagnostic Agents*. Advanced Drug Delivery Reviews, 1995. 16(2-3): p. 311-320.
34. Park, S.J., T.A. Taton, and C.A. Mirkin, *Array-based electrical detection of DNA with nanoparticle probes*. Science (Washington, D. C., 1883-), 2002. 295(5559): p. 1503-1506.
35. Georganopoulou, D.G., et al., *Nanoparticle-based detection in cerebral spinal fluid of a soluble pathogenic biomarker for Alzheimer's disease*. Proceedings of the National Academy of Sciences of the United States of America, 2005. 102(7): p. 2273-2276.
36. Gao, X.H., et al., *In vivo cancer targeting and imaging with semiconductor quantum dots*. Nature Biotechnology, 2004. 22(8): p. 969-976.
37. Bulte, J.W.M., et al., *Magnetodendrimers allow endosomal magnetic labeling and in vivo tracking of stem cells*. Nature Biotechnology, 2001. 19(12): p. 1141-1147.
38. Akerman, M.E., et al., *Nanocrystal targeting in vivo*. Proceedings of the National Academy of Sciences of the United States of America, 2002. 99(20): p. 12617-12621.
39. Lewin, M., et al., *Tat peptide-derivatized magnetic nanoparticles allow in vivo tracking and recovery of progenitor cells*. Nature Biotechnology, 2000. 18(4): p. 410-414.
40. Duncan, R. and N.R.D. Discovery, *The dawning era of polymer therapeutics*. Nature Reviews Drug Discovery, 2003. 2(5): p. 347-360.
41. Hirsch, L.R., et al., *Nanoshell-mediated near-infrared thermal therapy of tumors under magnetic resonance guidance*. Proceedings of the National Academy of Sciences of the United States of America, 2003. 100(23): p. 13549-13554.
42. West, J.L. and N.J. Halas, *Engineered nanomaterials for biophotonics applications: Improving sensing, imaging, and therapeutics*. Annual Review of Biomedical Engineering, 2003. 5: p. 285-292.
43. Soma, C.E., et al., *Reversion of multidrug resistance by co-encapsulation of doxorubicin and cyclosporin A in polyalkylcyanoacrylate nanoparticles*. Biomaterials, 2000. 21(1): p. 1-7.
44. Powis, G. and M.P. Hacker, *The Toxicity of anticancer drugs*. 1991, New York: Pergamon Press. ix, 228.

45. Kohori, F., et al., *Process design for efficient and controlled drug incorporation into polymeric micelle carrier systems*. Journal of Controlled Release, 2002. 78(1-3): p. 155-163.
46. Niwa, T., et al., *Preparations of Biodegradable Nanospheres of Water-Soluble and Insoluble Drugs with D,L-Lactide Glycolide Copolymer by a Novel Spontaneous Emulsification Solvent Diffusion Method, and the Drug Release Behavior*. Journal of Controlled Release, 1993. 25(1-2): p. 89-98.
47. Liu, J.B., Y.H. Xiao, and C. Allen, *Polymer-drug compatibility: A guide to the development of delivery systems for the anticancer agent, Ellipticine*. Journal of Pharmaceutical Sciences, 2004. 93(1): p. 132-143.
48. Conference, P. *Nanomedicine and Drug Delivery*. 2004. Brooklyn Polytechnic
49. Jain, R.A., *The manufacturing techniques of various drug loaded biodegradable poly(lactide-co-glycolide) (PLGA) devices*. Biomaterials, 2000. 21(23): p. 2475-2490.
50. Stella, B., et al., *Design of folic acid-conjugated nanoparticles for drug targeting*. Journal of Pharmaceutical Sciences, 2000. 89(11): p. 1452-1464.
51. Kwon, G.S., et al., *Biodistribution of Micelle-Forming Polymer Drug Conjugates*. Pharmaceutical Research, 1993. 10(7): p. 970-974.
52. Smith, A.M., X.H. Gao, and S.M. Nie, *Quantum dot nanocrystals for in vivo molecular and cellular imaging*. Photochemistry And Photobiology, 2004. 80(3): p. 377-385.
53. Alivisatos, A.P., *Semiconductor clusters, nanocrystals, and quantum dots*. Science, 1996. 271(5251): p. 933-937.
54. Gao, X.H., et al., *In vivo molecular and cellular imaging with quantum dots*. Current Opinion in Biotechnology, 2005. 16(1): p. 63-72.
55. Smith, A., Ruan, G, Rhyner, MN, Nie, SM, *Engineering Luminescent Quantum Dots for In Vivo Molecular and Cellular Imaging*. Annals of Biomedical Engineering, 2006. 34(1): p. 1 - 12.
56. Pinaud, F., et al, *Advances in fluorescence imaging with quantum dot bio-probes*. Biomaterials, 2006. 27: p. 1679-1687.
57. Weller, H., *Colloidal Semiconductor Q-Particles - Chemistry in the Transition Region between Solid-State and Molecules*. Angewandte Chemie-International Edition in English, 1993. 32(1): p. 41-53.
58. Lemon, B.I. and R.M. Crooks, *Preparation and characterization of dendrimer-encapsulated CdS semiconductor quantum dots*. Journal of the American Chemical Society, 2000. 122(51): p. 12886-12887.

59. Murray, C.B., et al., *Colloidal synthesis of nanocrystals and nanocrystal superlattices*. IBM Journal of Research and Development, 2001. 45(1): p. 47-56.
60. Rogach, A., et al., *Colloidally prepared HgTe nanocrystals with strong room-temperature infrared luminescence*. Advanced Materials (Weinheim, Federal Republic of Germany), 1999. 11(7): p. 552-+.
61. Gao, X.H. and S.M. Nie, *Doping mesoporous materials with multicolor quantum dots*. Journal of Physical Chemistry B, 2003. 107(42): p. 11575-11578.
62. Han, M.Y., et al., *Quantum-dot-tagged microbeads for multiplexed optical coding of biomolecules*. Nature Biotechnology, 2001. 19(7): p. 631-635.
63. Chan, W.C.W. and S.M. Nie, *Quantum dot bioconjugates for ultrasensitive nonisotopic detection*. Science, 1998. 281(5385): p. 2016-2018.
64. Yu, W.W., et al., *Experimental determination of the extinction coefficient of CdTe, CdSe, and CdS nanocrystals*. Chemistry Of Materials, 2003. 15(14): p. 2854-2860.
65. Kim, S.W., et al., *Engineering InAs_xP_{1-x}/InP/ZnSe III-V alloyed core/shell quantum dots for the near-infrared*. Journal Of The American Chemical Society, 2005. 127(30): p. 10526-10532.
66. Bruchez, M., et al., *Semiconductor nanocrystals as fluorescent biological labels*. Science, 1998. 281(5385): p. 2013-2016.
67. Agrawal, A.Z., C.; Byassee, T.; Tripp, R. A.; Nie, S., *Counting Single Native Biomolecules and Intact Viruses with Color-Coded Nanoparticles* Analytical Chemistry 2006. 78(4): p. 1061-1070.
68. Pellegrino, T., et al., *Hydrophobic nanocrystals coated with an amphiphilic polymer shell: A general route to water soluble nanocrystals*. Nano Letters, 2004. 4(4): p. 703-707.
69. Mattoussi, H., et al., *Self-assembly of CdSe-ZnS quantum dot bioconjugates using an engineered recombinant protein*. Journal of the American Chemical Society, 2000. 122(49): p. 12142-12150.
70. Goldman, E.R., et al., *A hybrid quantum dot-antibody fragment fluorescence resonance energy transfer-based TNT sensor*. Journal Of The American Chemical Society, 2005. 127(18): p. 6744-6751.
71. Goldman, E.R., et al., *Multiplexed toxin analysis using four colors of quantum dot fluororeagents*. Analytical Chemistry, 2004. 76(3): p. 684-688.
72. Goldman, E.R., et al., *Conjugation of luminescent quantum dots with antibodies using an engineered adaptor protein to provide new reagents for fluoroimmunoassays*. Analytical Chemistry, 2002. 74(4): p. 841-847.

73. Clapp, A.R., et al., *Fluorescence resonance energy transfer between quantum dot donors and dye-labeled protein acceptors*. Journal of the American Chemical Society, 2004. 126(1): p. 301-310.
74. Goldman, E.R., et al., *Avidin: A natural bridge for quantum dot-antibody conjugates*. Journal of the American Chemical Society, 2002. 124(22): p. 6378-6382.
75. Lingerfelt, B.M., et al., *Preparation of quantum dot-biotin conjugates and their use in immunochromatography assays*. Analytical Chemistry, 2003. 75(16): p. 4043-4049.
76. Patolsky, F., et al., *Lighting-up the dynamics of telomerization and DNA replication by CdSe-ZnS quantum dots*. Journal of the American Chemical Society, 2003. 125(46): p. 13918-13919.
77. Samia, A.C.S., X.B. Chen, and C. Burda, *Semiconductor quantum dots for photodynamic therapy*. Journal of the American Chemical Society, 2003. 125(51): p. 15736-15737.
78. Guo, W.Z., et al., *Conjugation chemistry and bioapplications of semiconductor box nanocrystals prepared via dendrimer bridging*. Chemistry of Materials, 2003. 15(16): p. 3125-3133.
79. Dutch, R.E.J., S. B.; Lamb, R. A, *Membrane fusion promoted by increasing surface densities of the paramyxovirus F and HN proteins: Comparison of fusion reactions mediated by simian virus 5 F, human parainfluenza virus type 3 F, and influenza virus HA* Journal of Virology, 1998. 72: p. 7745-7753.
80. Wertz, G.W.M., R. M., *Antigenic and genetic variation in human respiratory syncytial virus* PEDIATRIC INFECTIOUS DISEASE JOURNAL, 2004. 23: p. S19-S24.
81. Ho, Y.P., et al., *Multiplexed hybridization detection with multicolor colocalization of quantum dot nanoprobles*. Nano Letters, 2005. 5(9): p. 1693-1697.
82. Mansson, A., et al., *In vitro sliding of actin filaments labelled with single quantum dots*. Biochemical and Biophysical Research Communications, 2004. 314(2): p. 529-534.
83. Seitz, A. and T. Surrey, *Processive movement of single kinesins on crowded microtubules visualized using quantum dots*. Embo Journal, 2006. 25(2): p. 267-277.
84. Bakalova, R., et al., *Quantum dot-conjugated hybridization probes for preliminary screening of siRNA sequences*. Journal of the American Chemical Society, 2005. 127(32): p. 11328-11335.
85. Ornberg, R., Harper, TH, Liu, H, *Western blot analysis with quantum dot fluorescence technology: a sensitive and quantitative method for multiplexed proteomics*. Nature Methods, 2005. 2(1): p. 79-81.

86. Bakalova, R., et al., *Quantum dot-based western blot technology for ultrasensitive detection of tracer proteins*. Journal Of The American Chemical Society, 2005. 127(26): p. 9328-9329.
87. Pathak, S., et al., *Hydroxylated quantum dots as luminescent probes for in situ hybridization*. Journal of the American Chemical Society, 2001. 123(17): p. 4103-4104.
88. Rosenthal, S.J., et al., *Targeting cell surface receptors with ligand-conjugated nanocrystals*. Journal of the American Chemical Society, 2002. 124(17): p. 4586-4594.
89. Jaiswal, J.K., et al., *Long-term multiple color imaging of live cells using quantum dot bioconjugates*. Nature Biotechnology, 2003. 21(1): p. 47-51.
90. Pinaud, F., et al., *Bioactivation and cell targeting of semiconductor CdSe/ZnS nanocrystals with phytochelatin-related peptides*. Journal of the American Chemical Society, 2004. 126(19): p. 6115-6123.
91. Sukhanova, A., et al., *Biocompatible fluorescent nanocrystals for immunolabeling of membrane proteins and cells*. Analytical Biochemistry, 2004. 324(1): p. 60-67.
92. Lagerholm, B.C., et al., *Multicolor coding of cells with cationic peptide coated quantum dots*. Nano Letters, 2004. 4(10): p. 2019-2022.
93. Osaki, F., et al., *A quantum dot conjugated sugar ball and its cellular uptake on the size effects of endocytosis in the subviral region*. Journal of the American Chemical Society, 2004. 126(21): p. 6520-6521.
94. Vu, T.Q., et al., *Peptide-conjugated quantum dots activate neuronal receptors and initiate downstream signaling of neurite growth*. Nano Letters, 2005. 5(4): p. 603-607.
95. Silver, J. and W. Ou, *Photoactivation of quantum dot fluorescence following endocytosis*. Nano Letters, 2005. 5(7): p. 1445-1449.
96. Dubertret, B., et al., *In vivo imaging of quantum dots encapsulated in phospholipid micelles*. Science, 2002. 298(5599): p. 1759-1762.
97. Dahan, M., et al., *Diffusion dynamics of glycine receptors revealed by single-quantum dot tracking*. Science, 2003. 302(5644): p. 442-445.
98. Mattheakis, L.C., et al., *Optical coding of mammalian cells using semiconductor quantum dots*. Analytical Biochemistry, 2004. 327(2): p. 200-208.
99. Ferrara, D.E., et al., *Quantitative 3D fluorescence technique for the analysis of en face preparations of arterial walls using quantum dot nanocrystals and two-photon excitation laser scanning microscopy*. American Journal of Physiology-Regulatory Integrative and Comparative Physiology, 2006. 290(1): p. R114-R123.

100. Lidke, D.S., et al., *Quantum dot ligands provide new insights into erbB/HER receptor-mediated signal transduction*. Nature Biotechnology, 2004. 22(2): p. 198-203.
101. Wu, X.Y., et al., *Immunofluorescent labeling of cancer marker Her2 and other cellular targets with semiconductor quantum dots*. Nature Biotechnology, 2003. 21(1): p. 41-46.
102. Parak, W.J., et al., *Cell motility and metastatic potential studies based on quantum dot imaging of phagokinetic tracks*. Advanced Materials, 2002. 14(12): p. 882-885.
103. Nan, X.S., P. A.; Chen, P.; Xie, X. S., *Observation of Individual Microtubule Motor Steps in Living Cells with Endocytosed Quantum Dots* Journal of Physical Chemistry B, 2005. 109(51): p. 24220-24224.
104. Kim, S., et al., *Near-infrared fluorescent type II quantum dots for sentinel lymph node mapping*. Nature Biotechnology, 2004. 22(1): p. 93-97.
105. Soltesz, E.G., et al., *Intraoperative sentinel lymph node mapping of the lung using near-infrared fluorescent quantum dots*. Annals Of Thoracic Surgery, 2005. 79(1): p. 269-277.
106. Voura, E.B., et al., *Tracking metastatic tumor cell extravasation with quantum dot nanocrystals and fluorescence emission-scanning microscopy*. Nature Medicine, 2004. 10(9): p. 993-998.
107. Larson, D.R., et al., *Water-soluble quantum dots for multiphoton fluorescence imaging in vivo*. Science, 2003. 300(5624): p. 1434-1436.
108. Hoshino, A., et al., *Applications of T-lymphoma labeled with fluorescent quantum dots to cell tracing markers in mouse body*. Biochemical and Biophysical Research Communications, 2004. 314(1): p. 46-53.
109. Stroh, M., et al., *Quantum dots spectrally distinguish multiple species within the tumor milieu in vivo*. Nature Medicine, 2005. 11(6): p. 678-682.
110. Hoshino, A., et al., *Physicochemical properties and cellular toxicity of nanocrystal quantum dots depend on their surface modification*. Nanoletters, 2004. 4(11): p. 2163-2169.
111. Derfus, A.M., W.C.W. Chan, and S.N. Bhatia, *Probing the cytotoxicity of semiconductor quantum dots*. Nano Letters, 2004. 4(1): p. 11-18.
112. Ipe, B.I., M. Lehnig, and C.M. Niemeyer, *On the generation of free radical species from quantum dots*. Small, 2005. 1(7): p. 706-709.
113. Mulder, W.J.M.K., R.; Brandwijk, R. J.; Storm, G.; Chin, P. T. K.; Strijkers, G. J.; de Mello Donega, C.; Nicolay, K.; Griffioen, A. W., *Quantum Dots with a Paramagnetic Coating as a Bimodal Molecular Imaging Probe*. Nano Letters, 2006. 6(1): p. 1-6.

114. Murray, C.B., D.J. Norris, and M.G. Bawendi, *Synthesis And Characterization Of Nearly Monodisperse Cde (E = S, Se, Te) Semiconductor Nanocrystallites*. Journal of the American Chemical Society, 1993. 115(19): p. 8706-8715.
115. Sun, S.H., et al., *Controlled synthesis and assembly of FePt nanoparticles*. Journal of Physical Chemistry B, 2003. 107(23): p. 5419-5425.
116. Sun, S.H., et al., *Monodisperse MFe₂O₄ (M = Fe, Co, Mn) nanoparticles*. Journal of the American Chemical Society, 2004. 126(1): p. 273-279.
117. Erwin, S.C., et al., *Doping semiconductor nanocrystals*. Nature, 2005. 436(7047): p. 91-94.
118. Mornet, S., et al., *Magnetic nanoparticle design for medical diagnosis and therapy*. Journal of Materials Chemistry, 2004. 14(14): p. 2161-2175.
119. Bulte, J.W.M. and D.L. Kraitchman, *Iron oxide MR contrast agents for molecular and cellular imaging*. NMR in Biomedicine, 2004. 17(7): p. 484-499.
120. Jain, R.K., *Delivery of molecular medicine to solid tumors*. Science, 1996. 271(5252): p. 1079-1080.
121. Zhang, X.C., J.K. Jackson, and H.M. Burt, *Development of amphiphilic diblock copolymers as micellar carriers of taxol*. International Journal Of Pharmaceutics, 1996. 132(1-2): p. 195-206.
122. Gref, R., et al., *Biodegradable Long-Circulating Polymeric Nanospheres*. Science (Washington, D. C., 1883-), 1994. 263(5153): p. 1600-1603.
123. Kim, B., et al., *Magentomicelles: Composite Nanostructures from Magnetic Nanoparticles and Cross-Linked Amphiphilic Block Copolymers*. Nano Letters, 2005. 5(10): p. 1987-1991.
124. Kang, Y.J. and T.A. Taton, *Core/shell gold nanoparticles by self-assembly and crosslinking of micellar, block-copolymer shells*. Angewandte Chemie-International Edition, 2005. 44(3): p. 409-412.
125. Kang, Y.J. and T.A. Taton, *Micelle-encapsulated carbon nanotubes: A route to nanotube composites*. Journal Of The American Chemical Society, 2003. 125(19): p. 5650-5651.
126. Kim, B.S. and T.A. Taton, *Multicomponent nanoparticles via self-assembly with cross-linked block copolymer surfactants*. Langmuir, 2007. 23(4): p. 2198-2202.
127. Moffitt, M. and A. Eisenberg, *Size Control Of Nanoparticles In Semiconductor-Polymer Composites .1. Control Via Multiplet Aggregation Numbers In Styrene-Based Random Ionomers*. Chemistry Of Materials, 1995. 7(6): p. 1178-1184.
128. Duxin, N., et al., *Cadmium sulphide quantum dots in morphologically tunable triblock copolymer aggregates*. Journal Of The American Chemical Society, 2005. 127(28): p. 10063-10069.

129. Qu, L.H. and X.G. Peng, *Control of photoluminescence properties of CdSe nanocrystals in growth*. Journal Of The American Chemical Society, 2002. 124(9): p. 2049-2055.
130. Talapin, D.V., et al., *CdSe/CdS/ZnS and CdSe/ZnSe/ZnS core-shell-shell nanocrystals*. Journal of Physical Chemistry B, 2004. 108(49): p. 18826-18831.
131. Xie, R.G., et al., *Synthesis and characterization of highly luminescent CdSe-Core CdS/Zn_{0.5}Cd_{0.5}S/ZnS multishell nanocrystals*. Journal Of The American Chemical Society, 2005. 127(20): p. 7480-7488.
132. Li, J.J., et al., *Large-scale synthesis of nearly monodisperse CdSe/CdS core/shell nanocrystals using air-stable reagents via successive ion layer adsorption and reaction*. Journal of the American Chemical Society, 2003. 125(41): p. 12567-12575.
133. Ballou, B., et al., *Noninvasive imaging of quantum dots in mice*. Bioconjugate Chemistry, 2004. 15(1): p. 79-86.
134. Stefani, F.D., et al., *Memory in quantum-dot photoluminescence blinking*. New Journal Of Physics, 2005. 7.
135. Yao, J., et al., *Blinking and nonradiant dark fraction of water-soluble quantum dots in aqueous solution*. Proceedings Of The National Academy Of Sciences Of The United States Of America, 2005. 102(40): p. 14284-14289.
136. Stefani, F.D., et al., *Quantification of photoinduced and spontaneous quantum-dot luminescence blinking*. Physical Review B, 2005. 72(12).
137. Kuno, M., et al., *Nonexponential "blinking" kinetics of single CdSe quantum dots: A universal power law behavior*. Journal Of Chemical Physics, 2000. 112(7): p. 3117-3120.
138. Ntziachristos, V., C. Bremer, and R. Weissleder, *Fluorescence imaging with near-infrared light: new technological advances that enable in vivo molecular imaging*. European Radiology, 2003. 13(1): p. 195-208.
139. Choucair, A., C. Lavigueur, and A. Eisenberg, *Polystyrene-b-poly(acrylic acid) vesicle size control using solution properties and hydrophilic block length*. Langmuir, 2004. 20(10): p. 3894-3900.
140. Soo, P.L. and A. Eisenberg, *Preparation of block copolymer vesicles in solution*. Journal of Polymer Science, Part B: Polymer Physics, 2004. 42(6): p. 923-938.
141. Discher, D.E. and A. Eisenberg, *Polymer vesicles*. Science (Washington, D. C., 1883-), 2002. 297(5583): p. 967-973.
142. Shen, H.W. and A. Eisenberg, *Morphological phase diagram for a ternary system of block copolymer PS₃₁₀-b-PAA(52)/dioxane/H₂O*. Journal of Physical Chemistry B, 1999. 103(44): p. 9473-9487.

143. Cox, J.K., et al., *Polystyrene-poly(ethylene oxide) diblock copolymers form well-defined surface aggregates at the air/water interface*. Langmuir, 1999. 15(22): p. 7714-7718.
144. Cameron, N.S., M.K. Corbierre, and A. Eisenberg, *1998 E.W.R. Steacie Award Lecture Asymmetric amphiphilic block copolymers in solution: a morphological wonderland*. Canadian Journal of Chemistry, 1999. 77(8): p. 1311-1326.
145. Zhang, L.F. and A. Eisenberg, *Multiple Morphologies Of Crew-Cut Aggregates Of Polystyrene-B-Poly(Acrylic Acid) Block-Copolymers*. Science (Washington, D. C., 1883-), 1995. 268(5218): p. 1728-1731.
146. Terreau, O., C. Bartels, and A. Eisenberg, *Effect of poly(acrylic acid) block length distribution on polystyrene-b-poly(acrylic acid) block copolymer aggregates in solution. 2. A partial phase diagram*. Langmuir, 2004. 20(3): p. 637-645.
147. Terreau, O., L.B. Luo, and A. Eisenberg, *Effect of poly(acrylic acid) block length distribution on polystyrene-b-poly(acrylic acid) aggregates in solution. 1. Vesicles*. Langmuir, 2003. 19(14): p. 5601-5607.
148. Allen, C., D. Maysinger, and A. Eisenberg, *Nano-engineering block copolymer aggregates for drug delivery*. Colloids And Surfaces B-Biointerfaces, 1999. 16(1-4): p. 3-27.
149. Kang, H.S., et al., *Effects of grafted alkyl groups on aggregation behavior of amphiphilic poly(aspartic acid)*. Langmuir, 2001. 17(24): p. 7501-7506.
150. Pellegrino, T., et al., *On the development of colloidal nanoparticles towards multifunctional structures and their possible use for biological applications*. Small, 2005. 1(1): p. 48-63.
151. Smith, A.M., et al., *A systematic examination of surface coatings on the optical and chemical properties of semiconductor quantum dots*. Physical Chemistry Chemical Physics, 2006. 8(33): p. 3895-3903.
152. Pankhurst, Q.A., et al., *Applications of magnetic nanoparticles in biomedicine*. Journal of Physical Chemistry D: Applied Physics, 2003. 36(13): p. R167-R181.
153. LesliePelecky, D.L. and R.D. Rieke, *Magnetic properties of nanostructured materials*. Chemistry of Materials, 1996. 8(8): p. 1770-1783.
154. Parac-Vogt, T.N., et al., *Godolinium DTPA-monoamide complexes incorporated into mixed micelles as possible MRI contrast agents*. European Journal of Inorganic Chemistry, 2004(17): p. 3538-3543.
155. Mohs, A.M., et al., *PEG-g-poly(GdDTPA-co-L-cystine): Effect of PEG chain length on in vivo contrast enhancement in MRI*. Biomacromolecules, 2005. 6(4): p. 2305-2311.

156. Morales, M.P., et al., *Contrast agents for MRI based on iron oxide nanoparticles prepared by laser pyrolysis*. Journal of Magnetism and Magnetic Materials, 2003. 266(1-2): p. 102-109.
157. Josephson, L., et al., *Near-infrared fluorescent nanoparticles as combined MR/optical imaging probes*. Bioconjugate Chemistry, 2002. 13(3): p. 554-560.
158. Kircher, M.F., et al., *A multimodal nanoparticle for preoperative magnetic resonance imaging and intraoperative optical brain tumor detection*. Cancer Research, 2003. 63: p. 8122-8125.
159. Kelly, K.A., et al., *Detection of vascular adhesion molecule-1 expression using a novel multimodal nanoparticle*. Circulation Research, 2005. 96(3): p. 327-336.
160. Weissleder, R., et al., *Cell-specific targeting of nanoparticles by multivalent attachment of small molecules*. Nature Biotechnology, 2005. 23(11): p. 1418-1423.
161. Sosnovik, D.E., et al., *Magnetic resonance imaging of cardiomyocyte apoptosis with a novel magneto-optical nanoparticle*. Magnetic Resonance in Medicine, 2005. 54(3): p. 718-724.
162. Redl, F.X., et al., *Three-dimensional binary superlattices of magnetic nanocrystals and semiconductor quantum dots*. Nature, 2003. 423(6943): p. 968-971.
163. Santra, S., et al., *Synthesis of water-dispersible fluorescent, radio-opaque, and paramagnetic CdS : Mn/ZnS quantum dots: A multifunctional probe for bioimaging*. Journal of the American Chemical Society, 2005. 127(6): p. 1656-1657.
164. Gu, H.W., et al., *Facile one-pot synthesis of bifunctional heterodimers of nanoparticles: A conjugate of quantum dot and magnetic nanoparticles*. Journal of the American Chemical Society, 2004. 126(18): p. 5664-5665.
165. Wang, D.S., et al., *Superparamagnetic Fe₂O₃ Beads-CdSe/ZnS quantum dots core-shell nanocomposite particles for cell separation*. Nano Letters, 2004. 4(3): p. 409-413.
166. Xie, H.Y., et al., *Cell-targeting multifunctional nanospheres with both fluorescence and magnetism*. Small, 2005. 1(5): p. 506-509.
167. Mandal, S.K., et al., *Encapsulation of magnetic and fluorescent nanoparticles in emulsion droplets*. Langmuir, 2005. 21(9): p. 4175-4179.
168. Sathe, T.R., A. Agrawal, and S.M. Nie, *Mesoporous silica beads embedded with semiconductor quantum dots and iron oxide nanocrystals: Dual-function microcarriers for optical encoding and magnetic separation*. Analytical Chemistry, 2006. 78(16): p. 5627-5632.

169. Vail, D.M., et al., *STEALTH liposome-encapsulated cisplatin (SPI-77) versus carboplatin as adjuvant therapy for spontaneously arising osteosarcoma (OSA) in the dog: a randomized multicenter clinical trial*. *Cancer Chemotherapy and Pharmacology*, 2002. 50(2): p. 131-136.
170. Gregoriadis, G. and B. McCormack, *Targeting of Drugs 6: Strategies for Stealth Therapeutic Systems*. Vol. ix, 302. 1998, New York: Plenum Press.
171. Shi, B., et al., *Stealth MePEG-PCL micelles: effects of polymer composition on micelle physicochemical characteristics, in vitro drug release, in vivo pharmacokinetics in rats and biodistribution in S-180 tumor bearing mice*. *Colloid And Polymer Science*, 2005. 283(9): p. 954-967.
172. Couvreur, P., et al., *Nanocapsule technology: A review*. *Critical Reviews in Therapeutic Drug Carrier Systems*, 2002. 19(2): p. 99-134.
173. Lee, R.J. and P.S. Low, *Delivery Of Liposomes Into Cultured Kb Cells Via Folate Receptor-Mediated Endocytosis*. *The Journal of Biological Chemistry*, 1994. 269(5): p. 3198-3204.
174. Torchilin, V.P., et al., *Targeted Delivery of Diagnostic Agents by Surface-Modified Liposomes*. *Journal of Controlled Release*, 1994. 28(1-3): p. 45-58.
175. Vogel, K., et al., *Peptide-mediated release of folate-targeted liposome contents from endosomal compartments*. *Journal Of The American Chemical Society*, 1996. 118(7): p. 1581-1586.
176. Torchilin, V., J. Babich, and V. Weissig, *Liposomes and micelles to target the blood pool for imaging purposes*. *Journal of Liposome Research*, 2000. 10(4): p. 483-499.
177. Park, J.W., et al., *Tumor targeting using anti-her2 immunoliposomes*. *Journal of Controlled Release*, 2001. 74(1-3): p. 95-113.
178. Kabanov, A.V., et al., *The Neuroleptic Activity of Haloperidol Increases after Its Solubilization in Surfactant Micelles - Micelles as Microcontainers for Drug Targeting*. *Febs Letters*, 1989. 258(2): p. 343-345.
179. Maruyama, K., et al., *Immunoliposomes bearing polyethyleneglycol-coupled Fab' fragment show prolonged circulation time and high extravasation into targeted solid tumors in vivo*. *Febs Letters*, 1997. 413(1): p. 177-180.
180. Mori, A., et al., *Influence of the Steric Barrier Activity of Amphipathic Poly(Ethyleneglycol) and Ganglioside Gm1 on the Circulation Time of Liposomes and on the Target Binding of Immunoliposomes In vivo*. *Febs Letters*, 1991. 284(2): p. 263-266.
181. Chambers, E. and S. Mitragotri, *Long circulating nanoparticles via adhesion on red blood cells: Mechanism and extended circulation*. *Experimental Biology and Medicine*, 2007. 232(7): p. 958-966.

182. Chambers, E. and S. Mitragotri, *Prolonged circulation of large polymeric nanoparticles by non-covalent adsorption on erythrocytes*. Journal of Controlled Release, 2004. 100(1): p. 111-119.
183. Semple, S.C., A. Chonn, and P.R. Cullis, *Interactions of liposomes and lipid-based carrier systems with blood proteins: Relation to clearance behaviour in vivo*. Advanced Drug Delivery Reviews, 1998. 32(1-2): p. 3-17.
184. Choi, H.S., et al., *Renal clearance of quantum dots*. Nature Biotechnology, 2007. 25(10): p. 1165-1170.
185. Ogris, M., et al., *PEGylated DNA/transferrin-PEI complexes: reduced interaction with blood components, extended circulation in blood and potential for systemic gene delivery*. Gene Therapy, 1999. 6(4): p. 595-605.
186. Kirchner, C., et al., *Cytotoxicity of nanoparticle-loaded polymer capsules*. Talanta, 2005. 67(3): p. 486-491.
187. Kirchner, C., et al., *Cytotoxicity of colloidal CdSe and CdSe/ZnS nanoparticles*. Nano Letters, 2005. 5(2): p. 331-338.
188. Gupta, A.K. and S. Wells, *Surface-modified superparamagnetic nanoparticles for drug delivery: Preparation, characterization, and cytotoxicity studies*. IEEE Transactions on Nanobioscience, 2004. 3(1): p. 66-73.
189. Gupta, A.K. and A.S.G. Curtis, *Surface modified superparamagnetic nanoparticles for drug delivery: Interaction studies with human fibroblasts in culture*. Journal of Materials Science-Materials in Medicine, 2004. 15(4): p. 493-496.
190. Gupta, A.K. and M. Gupta, *Synthesis and surface engineering of iron oxide nanoparticles for biomedical applications*. Biomaterials, 2005. 26(18): p. 3995-4021.
191. Kang, Y.J. and T.A. Taton, *Controlling shell thickness in core-shell gold nanoparticles via surface-templated adsorption of block copolymer surfactants*. Macromolecules, 2005. 38(14): p. 6115-6121.
192. Moffitt, M., H. Vali, and A. Eisenberg, *Spherical assemblies of semiconductor nanoparticles in water-soluble block copolymer aggregates*. Chemistry of Materials, 1998. 10(4): p. 1021-1028.
193. Zhang, L.F., K. Yu, and A. Eisenberg, *Ion-induced morphological changes in "crew-cut" aggregates of amphiphilic block copolymers*. Science (Washington, D. C., 1883-), 1996. 272(5269): p. 1777-1779.
194. Bleuse, J., S. Carayon, and P. Reiss, *Optical properties of core/multishell CdSe/Zn(S,Se) nanocrystals* Physica E, 2004. 21: p. 331-335.

195. Lovric, J., et al., *Differences in subcellular distribution and toxicity of green and red emitting CdTe quantum dots*. Journal Of Molecular Medicine-Jmm, 2005. 83(5): p. 377-385.
196. Sathe, T., et al., *Examining the Behavior of Quantum Dots in Human Blood as a Function of Surface Coatings*. In Preparation, 2007.
197. McNeeley, K.M., A. Annapragada, and R.V. Bellamkonda, *Decreased circulation time offsets increased efficacy of PEGylated nanocarriers targeting folate receptors of glioma*. Nanotechnology, 2007. 18(38).
198. Sengupta, S., et al., *Temporal targeting of tumour cells and neovasculature with a nanoscale delivery system*. Nature, 2005. 436(7050): p. 568-572.
199. Schiffelers, R.M., et al., *Anti-tumor efficacy of tumor vasculature-targeted liposomal doxorubicin*. Journal of Controlled Release, 2003. 91(1-2): p. 115-122.
200. Shukla, R., et al., *Tumor angiogenic vasculature targeting with PAMAM dendrimer-RGD conjugates*. Chemical Communications, 2005(46): p. 5739-5741.
201. Konan, Y.N., R. Gurny, and E. Allemann, *State of the art in the delivery of photosensitizers for photodynamic therapy*. Journal of Photochemistry and Photobiology B-Biology, 2002. 66(2): p. 89-106.
202. Neri, D. and R. Bicknell, *Tumour vascular targeting*. Nature Reviews Cancer, 2005. 5(6): p. 436-446.
203. Loo, C., et al., *Immunotargeted nanoshells for integrated cancer imaging and therapy*. Nano Letters, 2005. 5(4): p. 709-711.
204. McNeeley, K., A. Annapragada, and R. Bellamkonda, *Decreased circulation time offsets increased efficacy of PEGylated nanocarriers targeting folate receptors of glioma*. Nanotechnology, 2007. 18: p. 395101.
205. Moon, W.K., et al., *Enhanced tumor detection using a folate receptor-targeted near-infrared fluorochrome conjugate*. Bioconjugate Chemistry, 2003. 14(3): p. 539-545.
206. van Steenis, J.H., et al., *Preparation and characterization of folate-targeted pEG-coated pDMAEMA-based polyplexes*. Journal of Controlled Release, 2003. 87(1-3): p. 167-176.
207. Quintana, A., et al., *Design and function of a dendrimer-based therapeutic nanodevice targeted to tumor cells through the folate receptor*. Pharmaceutical Research, 2002. 19(9): p. 1310-1316.
208. Nayak, S., et al., *Folate-mediated cell targeting and cytotoxicity using thermoresponsive microgels*. Journal of the American Chemical Society, 2004. 126(33): p. 10258-10259.

209. Lu, Y.J. and P.S. Low, *Folate-mediated delivery of macromolecular anticancer therapeutic agents*. *Advanced Drug Delivery Reviews*, 2002. 54(5): p. 675-693.
210. Goren, D., et al., *Targeting of Stealth liposomes to erB2 (Her2) receptor: in vitro and in vivo studies*. *British Journal of Cancer*, 1996. 74: p. 1749-1756.
211. Garesse, R., et al., *A Fluorescamine-Based Sensitive Method for the assay of proteinases, capable of detecting the initial cleavage steps of a protein*. *Eur J Biochem*, 1979. 99: p. 253-259.
212. Srinivasan, N., A. Yurek-George, and A. Ganesan, *Rapid deprotection of N-Boc amines by TFA combined with freebase generation using basic ion-exchange resins*. *Molecular Diversity*, 2005. 9: p. 291-293.
213. Hansen, C., et al., *Attachment of antibodies to sterically stabilized liposomes: evaluation, comparison, and optimization of coupling procedures*. *Biochim Biophys Acta*, 1995. 1239: p. 133-144.
214. Hitt, E., *Label-Free Methods are not Problem Free*. *Drug Discovery and Development*, 2004.
215. Karlsson, R., et al., *Practical aspects concerning direct detection of low molecular weight analytes using BIAcore 2000*. *BIA journal*, 1997(Special Issue): p. 18-21.
216. Moll, D., et al., *Biomolecular interaction analysis in functional proteomics*. *Journal of Neural Transmission*, 2006. 113(8): p. 1015-1032.
217. Mukhopadhyay, R., *Surface plasmon resonance instruments diversify*. *Analytical Chemistry*, 2005. 77(15): p. 313A-317A.
218. Piehler, J., *New methodologies for measuring protein interactions in vivo and in vitro*. *Current Opinion in Structural Biology*, 2005. 15(1): p. 4-14.
219. Gauglitz, G., *Direct optical sensors: principles and selected applications*. *Analytical and Bioanalytical Chemistry*, 2005. 381(1): p. 141-155.
220. Guilbault, G.G., et al., *Biosensors - 42 years and counting*. *Analytical Letters*, 2004. 37(8): p. 1481-1496.
221. Stsiapura, V., et al., *Functionalized nanocrystal-tagged fluorescent polymer beads: synthesis, physicochemical characterization, and immunolabeling application*. *Analytical Biochemistry*, 2004. 334(2): p. 257-265.
222. Tan, W.B. and Y. Zhang, *Multifunctional quantum-dot-based magnetic chitosan nanobeads*. *Advanced Materials*, 2005. 17(19): p. 2375-+.
223. Xu HX, S.M., Wong EY, et al., *Multiplexed SNP genotyping using the Qbead (TM) system: a quantum dot-encoded microsphere-based assay* *NUCLEIC ACIDS RESEARCH* 2003. 31(8): p. e43.

224. Agrawal, A., T. Sathe, and S.M. Nie, *Single-bead immunoassays using magnetic microparticles and spectral-shifting quantum dots*. Journal of Agricultural and Food Chemistry, 2007. 55(10): p. 3778-3782.
225. Cooper, M.A., *Label-free screening of bio-molecular interactions*. Analytical and Bioanalytical Chemistry, 2003. 377(5): p. 834-842.
226. Forkey, J.N., et al., *Three-dimensional structural dynamics of myosin V by single-molecule fluorescence polarization*. Nature, 2003. 422(6930): p. 399-404.
227. Truneh, A., et al., *Temperature-sensitive differential affinity of TRAIL for its receptors - DR5 is the highest affinity receptor*. Journal of Biological Chemistry, 2000. 275(30): p. 23319-23325.
228. Homola, J., S.S. Yee, and G. Gauglitz, *Surface plasmon resonance sensors: review*. Sensors and Actuators B-Chemical, 1999. 54(1-2): p. 3-15.
229. Bolger, R., et al., *Rapid screening of environmental chemicals for estrogen receptor binding capacity*. Environmental Health Perspectives, 1998. 106(9): p. 551-557.
230. Gonzalez, M., et al., *Interaction of biotin with streptavidin - Thermostability and conformational changes upon binding*. Journal of Biological Chemistry, 1997. 272(17): p. 11288-11294.
231. Wu, J.G., et al., *The receptor binding site for the methyltransferase of bacterial chemotaxis is distinct from the sites of methylation*. Biochemistry, 1996. 35(15): p. 4984-4993.
232. Spivakkroizman, T., et al., *Heparin-Induced Oligomerization of Fgf Molecules Is Responsible for Fgf Receptor Dimerization, Activation, and Cell-Proliferation*. Cell, 1994. 79(6): p. 1015-1024.
233. Mulvaney, P., *Surface plasmon spectroscopy of nanosized metal particles*. Langmuir, 1996. 12(3): p. 788-800.
234. Jule, E., Y. Nagasaki, and K. Kataoka, *Lactose-installed poly(ethylene glycol)-poly(D,L-lactide) block copolymer micelles exhibit fast-rate binding and high affinity toward a protein bed simulating a cell surface. A surface plasmon resonance study*. Bioconjugate Chemistry, 2003. 14(1): p. 177-186.
235. Jule, E., Y. Nagasaki, and K. Kataoka, *Surface plasmon resonance study on the interaction between lactose-installed poly(ethylene glycol)-poly(D,L-lactide) block copolymer micelles and lectins immobilized on a gold surface*. Langmuir, 2002. 18(26): p. 10334-10339.
236. Murthy, B.N., N.H. Voelcker, and N. Jayaraman, *Evaluation of alpha-D-mannopyranoside glycolipid micelles-lectin interactions by surface plasmon resonance method*. Glycobiology, 2006. 16(9): p. 822-832.

237. Gestwicki, J.E., H.V. Hsieh, and J.B. Pitner, *Using receptor conformational change to detect low molecular weight analytes by surface plasmon resonance*. Analytical Chemistry, 2001. 73(23): p. 5732-5737.
238. Rich, R.L. and D.G. Myszka, *Survey of the year 2000 commercial optical biosensor literature*. Journal of Molecular Recognition, 2001. 14(5): p. 273-294.
239. Rich, R.L. and D.G. Myszka, *Survey of the year 2001 commercial optical biosensor literature*. Journal of Molecular Recognition, 2002. 15(6): p. 352-376.
240. Rich, R.L. and D.G. Myszka, *A survey of the year 2002 commercial optical biosensor literature*. Journal of Molecular Recognition, 2003. 16(6): p. 351-382.
241. Rich, R.L. and D.G. Myszka, *Survey of the year 2004 commercial optical biosensor literature*. Journal of Molecular Recognition, 2005. 18(6): p. 431-478.
242. Rich, R.L. and D.G. Myszka, *Survey of the year 2003 commercial optical biosensor literature*. Journal of Molecular Recognition, 2005. 18(1): p. 1-39.
243. Rich, R.L. and D.G. Myszka, *Survey of the year 2005 commercial optical biosensor literature*. Journal of Molecular Recognition, 2006. 19(6): p. 478-534.
244. Gabizon, A., et al., *Targeting folate receptor with folate linked to extremities of poly(ethylene glycol)-grafted liposomes: In vitro studies*. Bioconjugate Chemistry, 1999. 10(2): p. 289-298.
245. Larocca, D., et al., *Receptor-targeted gene delivery using multivalent phagemid particles*. Molecular Therapy, 2001. 3(4): p. 476-484.
246. DeFrees, S.A., et al., *Sialyl Lewis x liposomes as a multivalent ligand and inhibitor of E-selectin mediated cellular adhesion*. Journal of the American Chemical Society, 1996. 118(26): p. 6101-6104.
247. Boturyn, D., et al., *Template assembled cyclopeptides as multimeric system for integrin targeting and endocytosis*. Journal of the American Chemical Society, 2004. 126(18): p. 5730-5739.
248. Dam, T.K., et al., *Negative cooperativity associated with binding of multivalent carbohydrates to lectins. thermodynamic analysis of the "multivalency effect"*. Biochemistry, 2002. 41(4): p. 1351-1358.
249. Ruoslahti, E., *RGD and other recognition sequences for integrins*. Annual Review of Cell and Developmental Biology, 1996. 12: p. 697-715.
250. Aumailley, M., et al., *Arg-Gly-Asp Constrained within Cyclic Pentapeptides - Strong and Selective Inhibitors of Cell-Adhesion to Vitronectin and Laminin Fragment-P1*. Febs Letters, 1991. 291(1): p. 50-54.

CURRICULUM VITAE

MATTHEW NEVIN RHYNER

Education

Georgia Institute of Technology and Emory University Expected Dec '07
Joint PhD Program in Biomedical Engineering
Advisor: Dr. Shuming Nie

Georgia Institute of Technology Aug '98 – May '02
BS in Chemical Engineering with Highest Honor

University College of London; London, England Jun '01 – Jul '01
-Chemical engineering study abroad program that combined a variety of cultural and engineering education

Academic Research

Thesis Research, Advisor: Dr. Shuming Nie May '03 – Present
"Development of Cancer Diagnostics Using Nanoparticles and Amphiphilic Polymers"

Graduate Lab Rotation, Advisor: Dr. Gang Bao Jan '03 – May '03
"Magnetic Nanoparticles for Conjugation to Molecular Beacons"

Teaching

Undergraduate Physiological Systems, Chief TA Jan '03 – Dec '04
Advisor: Dr. Barbara Boyan

- Coordinated activities of 3 TAs, the laboratory manager, and 2 undergraduate assistants
- Responsible for laboratory implementation, grading system, and exam proctoring
- Organized weekly training/planning sessions for TAs and lab manager
- Course involved well over 60 undergraduates in 3 lab sections
- Advised on major re-design of course structure after identifying several problem areas

St. Paul's School; Concord, NH Jun '02 – Aug '02

- Taught astronomy and cross training at prestigious summer program for top 10% of high school juniors in New Hampshire
- Responsibilities included lecturing, organizing social events, and supervising students 24 hours
- Gave a morning address to entire 300+ faculty, students, and interns

Policy

BME Policy Forum, Founding Planning Committee Chair May '04 – August '06

- Led a student group to implement a policy seminar series for our department (8 talks annually)
- Coordinated with several professors to establish and invite contacts outside of Georgia Tech and Emory in accordance with our own syllabus
- Received funding from two different organizations at Georgia Tech (Georgia Tech Policy Research Initiative and the Parker H. Petit Institute for Bioengineering and Biosciences)

Business

Technological Innovation: Generating Economic Results Aug '05 – May '07
-Won fellowship in competitive program that teams law students (Emory University), MBAs (Georgia Tech), and PhDs (Georgia Tech/Emory) for two years to develop a business plan based on the PhD's research

Vehicle Monitoring Technology; Atlanta, GA Jun '06 – Dec '06
-Leading a team of consultants to address this start-up's needs in several strategic areas: intellectual property, initial product deployment, identification of outside executives to take charge, and funding approach

Industrial Experience

Solvay Polymers; Houston, TX May '00 – Aug '00
Anheuser-Busch; Merrimack, NH May '99 – Dec '99

Awards

NSF IGERT Fellowship:
Technological Innovation: Generating Economic Results Aug '05 – May '07
GAANN Drug Delivery Fellowship Aug '03 – Aug '04
University of New Hampshire Presidential Fellowship Aug '98 – Dec '99

Publications

MN Rhyner, AM Smith, SM Nie. *Controlled Assembly of Quantum Dot Clusters in Biocompatible Block Copolymer Micelles*. **Journal of the Physical Chemistry C**. In preparation.

TR Sathe, WC Harris, MN Rhyner, BA Kairdolf, J Maberly, E Waller, SM Nie. *Examining the Behavior of Quantum Dots in Human Blood as a Function of Surface Coatings*. **NanoLetters**. In preparation.

MN Rhyner, AM Smith, X Gao, H Mao, L Yang, and SM Nie. *Quantum Dots and Targeted Nanoparticle Probes for In-vivo Tumor Imaging*. **Springer Book Chapter**. In press. 2007

AM Smith, G Ruan, MN Rhyner, SM Nie. *Engineering Luminescent Quantum Dots for In Vivo Molecular and Cellular Imaging*. **Annals of Biomedical Engineering**. 34, 1, 1-12. 2006.

MN Rhyner, AM Smith, X Gao, H Mao, L Yang, and SM Nie. *Quantum Dots and Multifunctional Nanoparticles: New Contrast Agents for Tumor Imaging*. **Nanomedicine**. Vol. 1, No. 2, Pages 189-199. 2006.

AM Smith, H Duan, MN Rhyner, G Ruan, SM Nie. *A Systematic Examination of Surface Coatings on the Optical and Chemical Properties of Semiconductor Quantum Dots*. **Physical Chemistry Chemical Physics** 8 (33) 3895-3903. 2006.

Patents

MN Rhyner, SM Nie, AM Smith. *Micellar Structures, Methods of Making Micellar Structures, Methods of Imaging, and Methods of Delivering Agents*. Provisional Patent in

Preparation with Emory Office of Tech Transfer and the Law Firm Thomas, Kayden, Horstemeyer, and Risely.

Posters

Frontiers in Cancer Nanotechnology *Braselton, GA Mar '06*
MN Rhyner, HW Duan, BA Kairdolf, and SM Nie. *Development of Diagnostic and Therapeutic Nanoparticle Agents Using Amphiphilic Polymers.*

Winship Cancer Institute Symposium *Atlanta, GA Sept '03*
MN Rhyner, AM Smith, A Agrawal, D Ansari, X Gao, T Sathe, G Ruan, YK Li, SM Nie.
Biomolecular Engineering and Nanotechnology for Translational Cancer Research.

Conferences

Georgia Life Science Summit *Atlanta, GA Sept '07*
Plenary Session: TIGON Nanostrategies

Controlled Release Society Conference *Long Beach, CA Jul '07*
Bioconjugated Nanoparticles for Molecular Imaging and Drug Delivery

Biomedical Engineering Society Annual Meeting. *Chicago, IL Oct '06*
Self Assembly of Hydrophobic Nanoparticles and Amphiphilic Polymers for Disease Diagnostics

Nanomedicine And Drug Delivery *Brooklyn, NY Aug '04*

Business Plan Competitions

Idea to Product International Competition *Austin, TX Nov '06*
Team captured 2nd place

Nanochallenge *Padua, Italy Nov '06*
Team captured 2nd place

Georgia Bowl *Kennesaw, GA Feb '07*
Team finished 3rd

Georgia Tech Business Plan Competition *Atlanta, GA Feb '07*
Team won 1st prize

Nanonexus Idea to Product Competition *Oak Ridge, TN Mar '07*
Finalists

Professional Organizations ***American Academy for the Advancement of Science**